UPPER MIDDLE TO UPPER MIOCENE SEISMIC SEQUENCES, NEW JERSEY MIDDLE TO OUTER CONTINENTAL SHELF

By

TUCE DEGIRMENCI

A thesis submitted to the

Graduate School-New Brunswick

Rutgers, The State University of New Jersey

in partial fulfillment of the requirements

for the degree of

Master of Science

Graduate Program in Geological Sciences

written under the direction of

Dr. Gregory S. Mountain

and approved by

_____

_____

_____

New Brunswick, New Jersey

[May, 2014]

ABSTRACT OF THE THESIS

Upper Middle to Upper Miocene Seismic Sequences,

New Jersey Middle to Outer Continental Shelf

by

TUCE DEGIRMENCI

Thesis Director:

Dr. Gregory S. Mountain

The Miocene stratigraphic succession on the middle to outer continental shelf off New Jersey, immediately south of the Hudson Canyon, is examined using high-resolution 2D multichannel seismic (MCS) and log data to evaluate sequence stratigraphic models, aided by results of Integrated Ocean Drilling Program (IODP) Expedition 313. High sedimentation, associated with extensive progradation and aggradation, provides a higher resolution record in this region than elsewhere on the shelf. The study of 29 MCS profiles and 4 gamma-ray logs identified and loop-correlated 14 Miocene sequences. Based on log interpretations, highstand systems tracts are associated with most of these 14 sequences; only 3 (sequences A, C, D) exhibit lowstand and transgressive systems tracts.

Topset and foreset deposits on the middle to outer continental shelf are thicker than those on the inner shelf due to pronounced aggradation and

progradation. This pattern is attributed to middle to late Miocene deltaic progradation and migration combined with sediment compaction and loading that created the accommodation space for these especially thick shallow-marine deposits.

Seismic profiles provide a means of anticipating sedimentary facies based on the vertical and lateral arrangement of reflectors within sequences, even in the absence of geologic samples and wireline log measurements. This study evaluates models of sequence stratigraphic evolution by utilizing high sedimentation rates, gamma-ray logs and seismic profiles available in this area. Sequence A shows the importance of drill site data. Using cores and logs, IODP Exp313 showed the maximum flooding surface is the first major downlap surface within sequence A, implying this interval is dominated by thick highstand deposits. By contrast, the widely cited Exxon model predicts that this and all sequences have thick lowstand units containing multiple flooding surfaces, overlain by comparatively thin highstand deposits. Furthermore, the present study showed not all sequences are alike. Shell-632 gamma-ray data reveals thick lowstand and transgressive strata in sequence D, and thin highstand strata consistent with the Exxon model. In contrast, many other sequences examined here have thin lowstand and transgressive systems tracts either below seismic resolution or absent, and thick highstand systems tracts that agree with the model built on Expedition 313 studies.

To my beloved Devin

Acknowledgement

I would like to express my special appreciation and thanks to my advisor Prof. Dr. Gregory Mountain for his tremendous help, encouragement, and support throughout my thesis with his patience and knowledge. I could not wish for a friendlier advisor and I am very grateful to be one of his students. I would also like to thank my committee members Prof. Dr. Kenneth Miller and Dr. Donald Monteverde who have offered much advice, invaluable comments and suggestions throughout my work. A special thanks to Dr. James Browning for providing me the necessary data whatever I needed. Furthermore I would like to thank to all faculty members, all technical and academic staff, especially to Jason Pappas and Jovani Reaves who solved my problems instantly.

I am thankful to the TPAO (Turkish Petroleum Corporation) for giving me the opportunity of studying in the U.S. and having a great experience in my life.

I would like to thank my beloved Ali Devin Sezer for his crucial and lovely impact on my life, his precious companion and constant support throughout years.

I would like to thank my dear friend Selen Esmeray Senlet who has helped me whenever I needed, and I am grateful for my dear friends Turan Iscimen, Masha Makarova, Christian Putra, Cesar Sequeira, Gulsad Kucuk, and Kubra Kamisoglu for their great friendship. I would also like to thank my friends in Turkey who has always supported me: Ceren Coskuner Toper, Meryem Arslan, Elif Seyhan, and Mine Ozcan. Last but not least, I would like to thank to my family: my parents (Gulnihal & Hayrettin Degirmenci), my grand mother (Hatice Balkaya), my sister and brother-in-law (Muge Degirmenci & Alper Camci), my cousins (especially to Ayfer Balkaya), my aunts, my uncle, and my 7 cats (especially to my precious Sakiz).

Table of Contents

List of Tables

List of Figures

1 Introduction

Tectonics (subsidence and uplift), sea-level changes, and climate are the primary controls on shallow marine sedimentary rocks in terms of forming their stratigraphic properties and stratal patterns (Van Wagoner et al., 1987; Emery and Myers, 1996). The interaction among these three mechanisms control the rate, volume, and composition of sediment supply, while tectonics and sea-level changes control the amount of accommodation, which is "the space available for sediment deposition" (Emery and Myers, 1996; and references therein).

Sequence stratigraphy studies packages of sedimentary deposits by analyzing facies changes, geometric relationships of strata and identifying key bounding surfaces and therefore builds a chronostratigraphic framework (Van Wagoner et al., 1988). Because of the inapplicability of radiometric methods to determine directly the age of long-term continental margin records, it is necessary to rely on available biostratigraphic (using fossils), magnetostratigraphic (using the Earth's magnetic polarity reversals), and geochemical records (using variations in $^{87/86}Sr$, $^{18/16}O$, $^{13/12}C$ ratios) as ties to the geologic time-scale derived elsewhere. Outcrop and core data are used in these dating methods. Biostratigraphy and Sr-isotopic records were used to date chronostratigraphically significant surfaces of Tertiary deposits of New Jersey where samples were available in both the coastal plain and the adjacent continental shelf and slope (Miller et al., 1998).

Sequence stratigraphy is used to analyze sedimentary processes in a basin's geological history, to evaluate local and global changes controlling these processes, and to seek natural resources such as the petroleum, coal, gas and mineral resources (Catuneanu et al., 2009). Various data sets including seismic profiles, outcrops, well-logs, and coreholes form the database of sequence stratigraphy (Van Wagoner et al., 1987; Catuneanu et al., 2009). The data used in this study is based on seismic profiles and geophysical logs (see the Data section for details).

Sequence stratigraphy has gained great importance first with exploration in the petroleum industry, and then with scientific studies in academia (Nystuen, 1998). The Baltimore Canyon Trough, located offshore New Jersey, is one of the major sedimentary basins on the mid-Atlantic margin of the United States (Poag, 1984). Industry and academic studies in this region have revealed that Neogene deposits in this basin are very thick (as thick as 12 km) (Poag, 1984; Greenlee et al., 1992) and sequences have characteristic clinothem shape (Greenlee and Moore, 1988; Greenlee et al., 1992) (see the following section for the explanation of the term "clinothem"). Furthermore, stable tectonics and an unusually complete sedimentary record provide the opportunity to carry out sequence stratigraphic studies in this region based on the abundant corehole, seismic and well-log data that are available (Greenlee et al., 1992).

Previous studies have focused on Neogene clinothems beneath the New Jersey continental shelf (e.g., Greenlee and Moore, 1988; Greenlee et al., 1992; Miller and Mountain, 1994; Poulsen et al., 1998; Monteverde, 2008; Monteverde et al., 2008; Mountain et al., 2010; Miller et al., 2013). This thesis focuses on an approximately 10,000 km^2 area of the New Jersey continental margin that has not been examined in

detail in these previous studies: the middle to outer continental shelf immediately south of where the Hudson Canyon has cut across the continental shelf. Only Poulsen et al. (1998) have analyzed limited seismic data traversing this region (Fig. 1). High sedimentation, associated with extensive progradation and aggradation, provides a higher resolution record in this region compared with elsewhere on the shelf. This study incorporates drilling results of the Integrated Ocean Drilling Program (IODP) Expedition 313 that examined the clinothems on the inner to middle New Jersey continental shelf landward of the main area of this study. I traced seismic sequences from the Expedition 313 area to the study area. The objectives of this thesis are to evaluate sequence stratigraphic models by analyzing seismic profiles of strata that accumulated at high sedimentation rate tied to nearby drilling and logging results.

2 Background

2.1 Sequence Stratigraphy

The history of sequence stratigraphy is "as old as the science of stratigraphy" (Nystuen, 1998) and despite debates over nomenclature and methodology, the fundamental principles and concepts of sequence stratigraphy are widely agreed upon (Catuneanu et al., 2009). Mitchum et al. (1977) originally defined the fundamental unit of sequence stratigraphy, a sequence, as "a relatively conformable succession of genetically related strata bounded at its top and base by unconformities or their correlative conformities". These unconformities and their correlative conformities have great importance in providing the relative time of events (Mitchum et al., 1977) based on the assumption that these hiatuses are not generally time-transgressive (see Christie-Blick et

al., 1990 for special exceptions). This means that sequence boundaries divide the strata of a depositional basin in such a way that all sediments above a given sequence boundary are younger than all sediments below that same sequence boundary everywhere in that basin. Significant hiatuses are usually associated with sequence boundaries as a result of erosion or nondeposition (Mitchum et al., 1977) (Fig. 2A).

Correlation of seismic data with log and core data enhances sequence stratigraphic analysis. Seismic stratigraphic terminations such as onlap, downlap, toplap and erosional truncation are the seismic criteria used for recognizing the sequence boundaries on seismic data (Mitchum et al., 1977). The terms "onlap, downlap, toplap, and erosional truncation" are discussed further in the Seismic Sequence Stratigraphic Interpretation subsection in the Methods section. Log criteria include large gamma-ray increases associated with sequence boundaries, though these can also be associated with maximum flooding surfaces (MFS) and lithofacies boundaries (Miller et al., 2013). These gamma-ray increases associated with sequence boundaries are due to lag deposits that contain phosphorites and uranium-rich zones (Browning et al., 2008). Furthermore, sequence boundaries can be recognized in cores in several ways. The following criteria are taken from the core observations of Browning et al. (2006) and Miller et al. (2013): (1) irregular contacts; (2) reworking above the contact, including rip-up clasts; (3) heavy bioturbation (e.g., burrows filled with overlying material below the contact); (4) major facies shift at the contact; (5) changes in stacking pattern (e.g. changes from coarsening-upward to fining-upward successions), (6) evidence for age breaks (hiatuses).

The time difference between the surface at the bottom and the top of a sequence gives the amount of time during which that sequence was deposited (Mitchum et al.,

1977). An unconformity may grade basinward into a surface called a “correlative conformity” across which “there is no evidence of erosion or nondeposition and no significant hiatus” (Mitchum et al., 1977).

Exxon Production Research Company researchers introduced sequences as “slug-shaped deposits” (Miller et al., 2013) in a series of publications (e.g., Vail et al., 1977; Mitchum et al., 1977; Vail, 1987; Van Wagoner et al., 1987; Posamentier and Vail, 1988). Sigmoidal (clinoform) unconformities and correlative conformities bound these deposits that consist of thin “topsets” and “bottomsets” and thick “foresets” (Miller et al., 2013). This thesis uses the term “clinothem” for the geometry of Miocene seismic sequences offshore New Jersey. A clinothem is “a package of sediment that progrades seaward and is bounded by sequence boundaries with distinct sigmoidal (clinoform) geometry” (Fig. 3; Miller et al., 2013). Topsets are the deposits with a small gradient in a landward part of a clinothem and their gradient increases gradually in a basinward direction where they grade into the foresets. The place where topsets grade into more steeply dipping foresets is called the “clinothem rollover”. Continuing basinward bottomset deposits develop where the foreset strata decrease in gradient and become very gently basinward dipping strata (Fig. 3).

Sequence stratigraphy focuses on studying three types of surfaces as well as the vertical arrangement of strata within sequences (Fig. 3). These surfaces are: the sequence boundary itself (SB), the transgressive surface (TS), and the maximum flooding surface (MFS). Abrupt upward increases in paleo-water depth (flooding surfaces) are commonly observed second-order surfaces that divide portions of sequences into "parasequences" (Van Wagoner et al., 1987). They are often associated with minor gamma-ray peaks

(Miller et al., 2013) due to an accompanying change in dominant grain size (clay content). The vertical arrangement of parasequences, and groups of parasequences called parasequence "sets", provides important descriptive criteria of sequences termed "stacking patterns" (Vail, 1987; Van Wagoner et al., 1987).

Based on the identification of the three key surfaces, their positions within a sequence, and the stacking patterns of parasequence and parasequence sets, sequence stratigraphic analysis seeks to define "system tracts" for each sequence. These are defined as “the linkage of contemporaneous depositional systems” (Van Wagoner et al., 1987; and references therein). In other words, systems tracts are composed of assemblages of different lithofacies from various environments (Coe, 2003). For example, a systems tract can consist of both deep marine and fluvial deposits. Therefore, the definition of systems tracts clearly explains why sequences are divided on the basis of key surfaces rather than lithofacies. Stacking patterns depend on the ratio of sedimentation rates to rates of change in accommodation and they can be classified as progradational, retrogradational, or aggradational (Van Wagoner et al., 1987). While parasequences within a sequence consist of progradational successions, parasequence sets can have progradational, retrogradational, or aggradational stacking patterns (Fig. 4; Van Wagoner et al., 1987).

Sequences consist of up to four systems tracts that are named lowstand (LST), transgressive (TST), highstand (HST; Vail, 1987; Van Wagoner et al., 1987), and falling stage (FSST) systems tracts (Plint and Nummendal, 2000). This thesis explains systems tracts in siliciclastic systems. Substantial differences exist between siliciclastic and carbonate systems in terms of the way that sediments form and the effect that accommodation change has on the sedimentary record (Emery and Myers, 1996).

The LST is the first siliciclastic systems tract to accumulate in a sequence. It shows a progradational to aggradational stacking pattern (Neal and Abreu, 2009) and generally shoals (coarsens) upward at the top (Fig. 3; Miller et al., 2013). Despite the debates over where to place the LST with respect to the FSST (Coe, 2003), there is consensus that LST deposits lie directly on the sequence boundary (Vail, 1987; Van Wagoner et al., 1987; Coe, 2003; Miller et al., 2013). Exxon researchers divided the LST into three units, a basin-floor fan, a slope fan, and a lowstand wedge (LSW) (Fig. 2B; Van Wagoner et al., 1987; Posamentier and Vail, 1988). Submarine fans deposited on the dipping foresets of the underlying sequence are called basin-floor fans. Fluvial-valley incisions across the topsets leading to submarine canyons deliver material seaward and form the fan. The basin-floor fan is bounded by the sequence boundary at the bottom and a downlap surface at the top, onto which the subsequent slope-fan deposits and progradational wedge usually downlaps. Slope fans result from debris flows and turbidites as a result of margin collapse. The top of the slope-fan is also a downlap surface for this progradational wedge called the LSW. Parasequences within the LST onlap onto the underlying sequence boundary in a landward direction and usually downlap in a basinward direction. The upper boundary of the LST is the TS, which also separates the LST from the TST. This is the first significant flooding surface following the LST (Van Wagoner et al., 1987). The TS marks the most prominent onlap onto the underlying SB landward of the rollover. Also, it is distinct from the relatively minor flooding surfaces in the LST. The TS marks the change from a progradational to a retrogradational stacking pattern (Posamentier and Vail, 1988) and a deepening (fining) upward succession (Fig. 3; Miller et al., 2013). The TS may merge with the sequence

boundary on topsets (Fig. 3). Miller et al. (2013) list two possible reasons for TS-SB merging: (1) there may be no LST deposits within the sequence that generally accumulates on topsets; or (2) the LST deposits may be thin and below seismic resolution, which renders the two surfaces indistinguishable on seismic profiles.

Parasequences within the TST onlap onto the sequence boundary in a landward direction and downlap onto the TS in a basinward direction. The TST is bounded at the top by the maximum flooding surface (MFS) that separates the TST from the HST. The MFS marks the change from a retrogradational to an aggradational stacking pattern (Neal and Abreu, 2009), and consequently parasequences within the HST downlap onto the MFS in a basinward direction.

The MFS is identified in cores by a condensed section of slowly deposited distal sediments (Coe, 2003). Condensed sections commonly consist of abundant foraminifera, concentrations of organic carbon, heavy bioturbation, glauconite, and greater mud versus sand (Miller et al., 2013; and references therein). On geophysical logs, the MFS is associated with high gamma-ray readings (Vail and Vornardt, 1991) due to their high clay and/or glauconite content. The MFS marks a change from transgressive to regressive facies indicated by the change from fining-upward below the MFS (in the TST) to coarsening-upward above the MFS (in the HST).

The surface at the top of the HST is the sequence boundary (Vail, 1987; Van Wagoner et al., 1987, 1988; Posamentier and Vail, 1988). The HST shows an aggradational to progradational stacking pattern (Neal and Abreu, 2009; Fig. 4). The parasequences within the HST onlap onto the sequence boundary in a landward direction and downlap onto the MFS in a basinward direction. Also, due to falling relative sea level

the HST surfaces may be eroded (Poulsen et al., 1998). As a result, toplap terminations are very common in HST deposits.

The fourth systems tract is the FSST (Fig. 5). It lies stratigraphically above and basinward of the HST and below the LST of the overlying sequence. It is generally accepted that the FSST is overlain by the sequence boundary (Plint and Nummendal, 2000), but debate still remains regarding the placement of the sequence boundary (Coe, 2003). The strata within the FSST are characterized by offlap (Plint and Nummendal, 2000) (the term "offlap" is discussed further in the Seismic Sequence Stratigraphic Interpretation subsection in the Methods section).

Several studies have shown that changes in sea-level are the main mechanism controlling the deposition of systems tracts (e.g., Posamentier and Vail, 1988). Consequently, most systems tracts interpretations have been linked to sea-level curves (Nystuen, 1998), though Neal and Abreu (2009) and Miller et al. (2013) argue against linking systems tracts to a global sea-level curve because of subsequent different interpretations. They instead prefer to link them to progradational-aggradational and coarsening-fining upward stacking patterns. Based on the concept that systems tracts are linked to sea-level curves, each systems tract explained above is deposited during a particular time interval on a sea-level curve (Posamantier and Vail, 1988).

2.2 Gamma-Ray Logs

Gamma logs record radiation from naturally occurring radioactive isotopes of elements (predominantly uranium [U], thorium [Th] and potassium [K]) in rocks. In typical continental margin settings, gamma-ray response usually indicates the presence of

either clay minerals or glauconite, and in rare cases (reducing pore water) uranium. In the absence of glauconite, gamma-ray logs are very good indicators of grain size trends.

Because shales contain clay minerals which, in turn, contain concentrations of these radioactive minerals, shales give high gamma-ray response (Rider, 1990; and references therein). Thus, one can qualitatively distinguish shale (high gamma readings) from sand (low gamma readings) using gamma log measurements (Lanci et al., 2002).

Where possible the presence of glauconite should be verified through drill core identification. Then, one can infer whether gamma log responses only mirror the grain size change and not glauconite content (Rider, 1990). In this study, up- or downhole trends of gamma log values show fining or coarsening directions.

2.3 Marine Seismic Acquisition

Refraction and reflection seismology are two main types of seismic techniques used to acquire information about the subsurface. Each has specific methodologies with inherent advantages and disadvantages relative to the other.

In marine environments, refraction seismology involves a passing ship with energy sources (e.g. air guns) sending seismic pulses that travel below the seafloor and return to a receiver either on the seafloor (e.g., Ocean Bottom Seismometer [OBS]) (Jones, 1999) or on the sea surface (e.g., a free floating sonobuoy or a towed seismic streamer).

Similar to refraction surveying, collecting reflection data in marine environments requires a ship using navigational systems to determine and control its position, with sources and receivers (hydrophones) towed in the water behind it. Many reflection profiles have been produced by two-dimensional (2D) multichannel seismic (MCS)

surveying that have a source towed at a fixed depth and offset at a fixed distance behind the vessel, and a single multi-channel streamer connecting the hydrophones towed behind the vessel as well (Fig. 6).

The standard method of 2D MCS surveying is based on the common mid-point (CMP) gather (Kearey, 2002). In CMP profiling, while a ship moves progressively forward along a profile line, the seismic source keeps sending pulses at a prescribed distance along the ship track that is kept as uniform as possible. The main objective of CMP profiling is to record many reflections from a common mid-point (CMP), each reflection derived from a unique source-receiver offset; hence, each trace within a CMP gather is derived from a source-receiver pair that is symmetric about that point (Fig. 7).

In seismic profiling, the first arrival to a receiver is either a wave that travels directly from the source to the receiver, or a refracted wave (Fig. 8). Therefore, in a reflection seismic survey, processing is an important step to differentiate these other arrivals from the reflections of interest. Often unwanted noise can include multiples resulting from the waves reflecting at more than one layer (Figs. 9 and 10), mechanical noise from other ships, marine life, etc. Since “reflected waves are never first arrivals” (Kearey, 2009), processing reflection surveys can be a complicated procedure.

2.4 Seismology

Energy sources used in marine seismic reflection profiling are towed behind a ship and produce compressional waves that propagate downwards through the water column and into the seafloor. Hydrophones enclosed within a seismic streamer towed behind that same ship record the reflections of those waves off the seafloor and structures beneath it. The time recorded by a receiver is expressed as two-way travel time, and that

is the time it takes for a seismic wave to travel through the water column and sediments, to reflect from buried surfaces and return to the receiver. These surfaces are called seismic reflectors (Badley, 1985), and each one represents a boundary between two media having different acoustic properties. These acoustic properties lead to each medium have different acoustic impedance.

Acoustic impedance, Z, is defined by the following equation:

$$Z = V * \rho,$$

where V is the seismic P-wave velocity (speed of sound in the medium) and ρ is the density of that same medium (Badley, 1985). Seismic reflections occur at interfaces where the value of Z changes significantly. Reflection strength for waves striking an interface within a few degrees of perpendicular is proportional to this change in impedance. In other words, the greater the change in impedance across that boundary the stronger the reflected energy, and the easier it is to recognize that interface on seismic profiles (Fig. 10).

Reflections on seismic profiles may correspond to bedding planes, fault planes or any other boundaries marking the changes explained above (Coe, 2003). This means that seismic reflections are more likely to be chronostratigraphic boundaries (time stratigraphic) than they are to be lithostratigraphic boundaries (rock stratigraphic) because impedance is more likely to change abruptly at the former than at the latter (Vail et al., 1977).

However, not every interface with great impedance contrast generates a recognizable reflection. There are several limitations in displaying seismic reflections on the profiles as follows. Seismic resolution, the ability to distinguish meaningfully the

effects of two reflecing surfaces, is one factor determining the limits to what can be detected as a seismic reflection. Vertical resolution is the ability to separate two reflections vertically. One-quarter of the wavelength of the source (λ) gives the smallest vertical distance between reflectors that can be estimated with reliable accuracy (Sheriff and Geldart, 1983; Yilmaz, 1987; Kearey, 2002). Below this separation the reflections can still be discerned but the distance between them is largely unknowable. Also, one-eighth of the wavelength of the source (Widess, 1973) is the minimum vertical resolution possible to only recognize two reflections separately on the profiles, below which the reflections merge and seem as one reflection. For example, suppose that λ is 35 m. The smallest vertical distance between two reflectors that can be estimated is $\lambda/4$=8.75 m. For the same example, the minimum vertical resolution possible to only recognize two reflections separately is $\lambda/8$=4.375 m, below which the two reflections cannot be separated and appear as one reflection.

On the other hand, being able to recognize two horizontally separate features on a seismic section depends on the horizontal resolution of the data. It is essential to know that a reflection is energy bouncing back to the receiver from a region and not from a single point. The Fresnel zone is the area where the reflections are produced (Fig. 11). The width of the Fresnel zone determines the minimum required lateral distance between two reflectors in order to be visually distinguishable on a profile (Yilmaz, 1987; Kearey, 2002). If the distance between two reflectors is smaller than the width of the Fresnel zone, they cannot be separately imaged (Yilmaz, 1987). The width of the Fresnel zone, w, is defined by the following equation:

$$w=(2z\lambda)^{1/2},$$

where z is the depth between the source and the bed, and λ is the wavelength of the source (Yilmaz, 1987). In order to calculate the Fresnel zone, one should know the wavelength and it can be calculated by the following:

$$\lambda=V/f,$$

where V is the p-wave velocity and f is the seismic frequency. For instance, the width of the Fresnel zone on Ew9009 cruise at 750 m can be calculated from the equations above. If V is about 1750 m/s and f is 50 Hz, then λ is 35 m. In this case, the width of the Fresnel zone (the lateral resolution) is about 230 m. This is the minimum horizontal width of a detectable feature and the minimum required lateral distance between two features in order to be visually distinguishable on the profile.

In addition to the effects of seismic resolution on displaying seismic reflections, other constraints may also exist. For example, the amplitude of seismic waves decreases as they radiate away from the source. Two important reasons are spherical spreading and attenuation of the energy. Spherical spreading is the reduction in the amplitude of seismic waves with distance travelled. While a seismic wave generated at the source is spherically spreading out in all directions equally, it loses its energy with increasing distance along this spherical ray path (Kearey, 2002). As a result of this energy loss, there is a depth limit beyond which there is not sufficient energy to generate reflections at interfaces and return to the seismic receiver. On the other hand, attenuation depends on the physical characteristics of the media that seismic waves travel through. In this case,

the change in the media and their physical properties (e.g. attenuation increases with increasing porosity (Barton, 2006) causes the reduction in amplitude of seismic waves.

3 Data

The New Jersey sea-level transect across the mid-Atlantic margin (Fig. 1) comprises a large amount of seismic, corehole and well-log data (Mountain et al., 2010) collected from the coastal plain, continental shelf, slope and rise (Miller and Mountain, 1994). Data used in this study are well-logs and seismic profiles traversing the modern mid- to outer shelf and slope settings. High-resolution 2D multichannel seismic data form the basis of this study (Table 3.1).

3.1 Seismic Profiles

Every seismic profile across the New Jersey margin is listed under the name of the corresponding survey it was collected by (e.g. Ewing 1002 seismic line is collected by R/V *Ewing* survey). Three multichannel seismic (MCS) surveys are discussed: R/V *Ewing* Ew9009, R/V *Oceanus* Oc270, and R/V *Cape Hatteras* CH0698. The following information is taken from Monteverde et al. (2008), Monteverde (2008), and Mountain et al. (2010):

The R/V *Ewing* Ew9009 was the first survey (1990) and achieved the moderately high vertical resolution of 15 m (vs. approximately 25 m resolution in previous industry data; Greenlee et al., 1992). The seismic lines of this survey spanned the modern mid- to outer shelf and slope settings of New Jersey. The *Ew9009* survey focused on imaging Palaeogene and Neogene stratigraphy. The R/V *Oceanus* Oc270 survey was conducted in 1995, and it collected higher resolution data (approximately 5 m vertical resolution)

crossing much of the same region as Ew9009. Finally, R/V *Cape Hatteras* CH0698, also with approximately 5 m vertical resolution, was conducted in 1998 by traversing the inner to middle continental shelf. This study analyzed twenty-nine seismic profiles from the preceding surveys.

3.2 Log Data

Gamma-ray log data at four sites (M29, Shell 632, COST B-2, and Exxon 500-1) are integrated with the available multichannel seismic data in this study. The function converting seismic 2-way travel time to sub-seafloor depth at site M29 (one of the three coreholes in the Expedition 313 and the closest to the area of this study) is used to derive T-D charts of the other wells in this study (see the following section for details). M29 and Shell 632 sites are both located on Oc270 line 629 whereas the COST B-2 well is not located exactly on a seismic line (Table 3.2.1). Since Oc270 line 6 is the closest line to the COST B-2 well (78 m NW of the well), the COST B-2 log data can be easily projected onto this seismic line (Table 3.2.1). The COST B-2 log data provide great insight into interpreting the internal structure of sequences by intersecting Oc270 line 6 with Ew9009 line 1002 (Fig. 33D; see the Results section for details). Then, the COST B-2 well is projected onto the closest point on Ew9009 line 1002 line that is approximately 600 m SW of the well. Therefore, intersection of Oc270 line 6 with Ew9009 line 1002 shows that the COST B-2 projection onto Ew9009 line 1002 is reliable.

4 Methods

4.1 The KINGDOM Software

This study used Seismic Micro Technology (SMT)- The KINGDOM Software Version 8.7.1 (64-bit; http://www.ihs.com/products/oil-gas-information/analysis-software/kingdom-seismic-interpretation/index.aspx?pu=1&rd=smtkingdom). This is a widely used Windows-based geological interpretation module that allows users to visualize and manipulate seismic data on a computer workstation. The module enables interpreters to integrate seismic with well data that consists of lithology, age and log data. This study was carried out by using seismic interpretation tools provided by 2d/3dPAK, and by displaying the project on two computer screens in a workstation setting.

The main data of this study are seismic lines and coreholes located on a base map. All data have been tagged with Global Positioning Satellite (GPS) fixes, providing locations with an accuracy of roughly ± 15 m or better. These coordinates are readily available as latitudes and longitudes in a project where all these data reside. The project is a multi-user setting in which various people can interpret the data.

Working on a computer has many advantages over the alternative method of working on printed copies of seismic profiles and well logs. For example, SMT provides great convenience for visualizing and interpreting seismic data by changing the display magnification by zooming in and out or changing the horizontal and vertical scales independently, displaying profiles in different colors, etc. Each of these adjustments can be made instantly with a mouse click or keystroke to enhance the visibility of features being examined. Also, one can make mistie corrections for any surveys by specifying numbers to “time shift” in milliseconds, “phase rotation” in degrees and “amplitude scale

factor". These changes result in shifting the selected profile up or down, rotating its phase, and changing its amplitude values during display, respectively. Although different surveys or even the same survey have seismic profiles with different characteristics due to differences in processing, one can tie those profiles better by performing mistie corrections to the corresponding profiles. In this study, I applied 0.004 seconds of "time shift" and 180 degrees of "phase rotation" change to all seismic profiles from the CH0698 survey in order to correctly intersect them with seismic profiles from the Ew9009 and Oc270 surveys. In case they were needed, I applied the necessary mistie corrections to the corresponding seismic profiles (e.g., two intersecting seismic profiles each having a different amplitude scale where one of the profiles was invisible or hardly seen, "amplitude scale factor" of the latter was changed).

In addition to these, SMT provides the opportunity to display well-log data on seismic profiles. In order to place any log data, commonly measured in depth, on the seismic profile, measured in seismic reflection time, one has to construct and import a time-depth chart (T-D chart). Equating the well-log data with the seismic line behind it is entirely dependent on the T-D chart imported to SMT. Therefore, the T-D chart plays an important role in accurately placing a log curve on a seismic profile, and subsequently in the seismic interpretation. In this study, I created T-D charts for all three wells (Exxon 500-1, Shell-632 and COST B-2 wells) based on a time-depth function that had been used in Expedition 313. I changed the T-D chart of Expedition 313 by applying the following steps: (1) I found the corresponding two-way travel time of the sea floor on seismic profiles where these three well sites were located; (2) I assumed that the acoustic velocity above sea floor was 1500 m/sec, and recalculated the depths above the sea floor for each

seismic profile; (3) for the depths below sea floor on each profile, the previously calculated depth of the sea floor in step (1) was added to the depths below sea floor in T-D chart of Expedition 313. As a result, I created three different T-D charts and imported them into SMT.

Furthermore, during the interpretation users can create and manage horizons that are key surfaces on seismic profiles, trace them throughout the gridded area and preserve them as color-coded, labeled tracings superimposed on the seismic display. One can trace a horizon on a seismic line and correlate that line with intersecting lines. By examining intersecting lines, users are able to trace horizons across the entire study area and verify the consistency of their interpretations.

4.2 Seismic Sequence Stratigraphic Interpretation

Sequence stratigraphic interpretation on a seismic profile is based on the observation of seismic reflections. Seismic reflections are governed by the acoustic impedance contrast between two adjacent rocks across the interface (see the Seismology section for details).

A sequence was originally defined as "a succession of genetically related strata bounded at its top and base by unconformities or their correlative conformities" (Mitchum et al., 1977); likewise a sequence on a seismic profile is "a succession of reflections, bounded by surfaces marked by reflection terminations" (Vail et al., 1977).

The methods used in this study can be summarized in the following order: (1) identify stratal geometries of the clinothems (prograding sigmoidal sequences); (2) identify stratal terminations within the clinothems; (3) identify stacking patterns; (4) integrate gamma-ray log to the seismic interpretation.

The observation of seismic reflections starts with the recognition of stratal terminations, stacking patterns, and stratal geometries. They are the fundamentals of identifying sequence stratigraphic surfaces, systems tracts, and sequences, respectively.

In this study, first stratal geometries were observed by identifying clinothem rollovers that were visually detectable on seismic lines around the study area (Fig. 3). Mitchum et al. (1977) presented three different geometries of clinothems: sigmoidal, oblique or complex sigmoid-oblique. Each can provide information about accommodation history of prograding shelf-slope systems (Catuneanu et al., 2009). While sigmoidal prograding systems have parallel stratal units (topsets) at their proximal portions, oblique prograding systems lack topsets and have terminations at the distal parts (Fig. 12). The complex sigmoid-oblique geometry has both sigmoidal and oblique shapes. A sigmoidal geometry implies positive accommodation space on the shelf, whereas an oblique geometry indicates little or no accommodation space on the shelf during progradation (Catuneanu et al., 2009).

After observing stratal geometries, reflection terminations on the seismic profiles were identified based on the definition of Mitchum et al. (1977). Erosional truncation, toplap, onlap, downlap and offlap are the basic types of reflection terminations used in determining key surfaces on seismic data (Fig. 13) and described as follows:

Erosional Truncation: Reflections terminated by an overlying irregular surface on a seismic section imply truncation. Truncation is a result of erosion of the underlying strata by the overlying erosional surface. It is an important criterion for specifying a sequence boundary (Catuneanu, 2002).

Toplap: Termination of seismic reflections of inclined strata by an overlying surface of lower dip represents toplap. It is difficult to distinguish toplap from erosional truncation in most seismic reflection data. While erosional truncation is typically associated with an irregular surface, toplap has a smooth surface. This does not mean that no erosion occurs along smooth surfaces. Toplap is below the sequence boundary and it forms as a result of sediment bypassing with or without minor erosion (Mitchum et al., 1977). It is an important feature for identifying sequence boundaries and the Highstand Systems Tracts.

Onlap: Reflections of strata that terminate against a steeper seismic surface represent onlap. The Lowstand, Transgressive and Highstand Systems Tracts have onlap reflection terminations against a sequence boundary.

Downlap: Downlap is represented by the termination of reflections of inclined strata against an underlying surface with shallower dip. Downlap can be an important type of reflection termination used to specify a Maximum Flooding Surface. However, not every downlap surface is a Maximum Flooding Surface.

Offlap: Inclined sets of reflections of conformable strata progressively shifting basinward represent offlap. For this type of termination, the younger package of conformable strata does not overlie the top of the older unit thoroughly but leaves some portion exposed (Plint and Nummedal, 2000; and references therein). Basinward downward stepping strata are associated with offlap terminations.

After the preceding types of reflection terminations were identified on profiles, stacking patterns were identified based on the definition of Neal and Abreu (2009).

Stacking patterns give information about depositional units within successions and are used to identify systems tracts (Fig.14) as follows:

Lowstand Systems Tract: Progradational to aggradational,

Transgressive Systems Tract: Retrogradational,

Highstand Systems Tract: Aggradational to progradational,

Falling Stage Systems Tract: Progradational stacking pattern.

Finally, gamma-ray log data was correlated to the seismic data by recognizing high (representing clay-rich) and low (representing sand-rich) gamma-ray values to identify parasequence sets (Vail and Vornardt, 1991; Catuneanu, 2006; Miller et al., 2013) (see the Gamma Logs section for details).

5 Results

I have analyzed twenty-nine seismic reflection profiles in a seismic grid obtained on Ew9009, Oc270 and CH0698 cruises offshore central to northern New Jersey (Fig. 1). Pliocene strata are poorly preserved in the slope coreholes (Miller et al., 1996) and based on available seismic data apparently absent on the shelf area that was examined. In this study, the Miocene record is bounded at the base by reflector m6 (23.8 ± 0.2 Ma; Miller et al., 1996), and by reflector P4 at the top (the base of the Pleistocene, Mountain et al., 2007). I used the tracing of P4 from these latter workers on Oc270 lines 8, and extended it to Ew9009 line 1002, and then loop-correlated it throughout the seismic grid.

This thesis examines Miocene sequences above sequence m4.3 in detail. Monteverde et al. (2008), Monteverde (2008), Mountain et al. (2010), and Miller et al. (2013) previously identified seismic sequence boundaries from m6 through m4.3 on the

inner to middle New Jersey continental shelf (Fig. 15). Sequences identified in the Expedition 313 study area were referred to by the name of the underlying sequence boundary, such that reflector m6 is the base of sequence m6 (Monteverde, 2008). Fig. 16 illustrates the locations of all profiles displayed in Figures 17-33 on a base map.

After loop correlating mappable surfaces throughout the seismic grid, fourteen seismic sequence boundaries were identified above m4.3 on Ew9009 line 1002 (Fig. 17). In this study, reflectors above m4.3 were designated with letters in alphabetical order (A is oldest, N is youngest). Additional surfaces identified between sequence boundaries were named as the following: surfaces between D and E were named D1, D2, D3, with D1 being the oldest and D3 the youngest.

5.1 Sequences from m6 to m4.3

I traced sequence boundaries m6 through m4.3 across the Expedition 313 coreholes on Oc270 line 629, and tied each surface onto Ew9009 line 1002 (Fig. 1). These sequences are also identifiable on CH0698 line 21 approximately 12.5 km NE and parallel to Oc270 line 629. Since most of these sequences have sigmoidal clinothem shapes, and become thinner in the basinward direction and either become truncated by overlying sequence boundaries or appear to merge below seismic resolution. NE of Oc270 line 629, Ew9009 line 1002 starts on the bottomsets of these sequences and continues seaward (Fig. 1). As a result, only 8 of the 14 sequences in this study can be tracked basinward and tied to Ew9009 line 1002 by intersecting Oc270 line 629, Ew9009 lines 1023 and 1002 (Fig. 18). Since these eight sequence boundaries (m5.8, m5.7, m5.47, m5.33, m5.2, m5, m4.5, m4.3) are parallel and close to each other (a few tens of

milliseconds apart) on Ew9009 line 1002, internal reflections between them cannot be seen.

5.2 Sequence A

Reflector A is determined as the lower sequence boundary of sequence A on CH0698 line 21, using criteria of onlap, downlap and erosional truncation (Fig. 19B). This reflector has a strong sigmoidal shape, which is seen on both Oc270 line 629 and CH0698 line 21, but more visible on the latter because there the sequence A is thicker and is more clearly expressed. Although reflector A is difficult to trace on Oc270 line 629, the small decrease in gamma log values at 463 msec at Site M29 supports that this reflector is a sequence boundary (Fig. 20).

Sequence A has two possible seismic interpretations on CH0698 line 21. The first interpretation is consistent with the Exxon model that consists of three systems tracts from bottom to top, the LST, TST, and HST. According to this model the LST is divided into three units, a basin-floor fan, a slope fan, and a lowstand wedge (LSW) (Fig. 2B). In this interpretation the horizontal reflectors are considered as multiples; in other words, they do not indicate actual surfaces (see Fig. 9). Figure 19B shows internal terminations of sequence A clearly. Reflectors A1 and A2 are two downlap surfaces basinward of the clinothem rollover. A1 onlaps and downlaps the underlying A sequence boundary in the basinward portion. Overlying reflectors downlap onto A1 on the base of the clinothem slope. These features suggest that the area between the sequence boundary A and the reflector A1 are basin-floor fan deposits. Any possible reflectors beneath A1 are below seismic resolution and therefore undetectable. Reflectors above A1 onlap onto the sequence boundary A on the lower portions of the slope and are overlain by reflector A2.

A2 is a downlap surface for the prograding lowstand wedge deposits (LSW). Reflectors within the LSW onlap against the sequence boundary A on the upper portions of the slope and below the clinothem rollover. Reflector A3 has the most prominent onlap against the sequence boundary A seaward of the rollover, thereby suggesting a transgressive surface (TS). The sediments restricted by the sequence boundary at the bottom and by the reflector A3 at the top are the LST of sequence A. The reflector A4 is interpreted as a maximum flooding surface (MFS) as it onlaps landward of the rollover and has highstand systems tract (HST) deposits downlap onto it. This suggests that TST deposits are thin or below seismic resolution. Therefore, the interval between A3 and A4 is interpreted as the transgressive systems tract (TST). According to the Exxon model, the sequence A has a very thick LST (~ 140 ms), a thin TST, and a prograding HST, and the LST consists of three units; a thin basin-floor fan, slope-fan, and a thick LSW.

The second interpretation of sequence A on CH0698 line 21 is consistent with the results of Miller et al. (2013). Reflector A5 is tentatively interpreted as a TS associated with onlap and downlap onto the underlying sequence boundary A (Fig. 19C). Miller et al. (2013) proposes, “In sequences where there is more than one downlap surface, the stratigraphically lowest is taken as the seismic MFS”. Therefore, the reflector A6, the major downlap surface within the sequence A is interpreted as the MFS (Fig. 19C). In this interpretation, the sequence A has a thin LST, TST, and a very thick HST (~ 160 ms) associated with many flooding surfaces. The most prominent flooding surfaces are identified as A7 and A8. There may be more flooding surfaces between the MFS and the reflector A7. Since gamma ray log of Exxon 500-1 site measures only the bottomset of

sequence A, it is difficult to determine possible flooding surfaces within the sequence based on gamma-ray log character (Fig. 19C).

5.3 Sequence B

Reflector B corresponds to a sharp decrease from higher to lower gamma ray values at 435 msec at Site M29 on Oc270 line 629 (Fig. 20). Also, there is a sharp decrease in gamma values where Reflector B is traced along CH0698 line 21 to the Exxon 500-1 site (Fig. 19C).

This reflector is a clear seismic sequence boundary that truncates a portion of topset and foreset reflections of sequence A. These toplap terminations are between common depth points (cdp) 5000-8000 on CH0698 line 21 (Fig. 21), where this sequence is the thickest. Although sequence B appears thickest on this line and sequence boundary B has a strong clinothem shape, it is difficult to see the internal reflections within the sequence because of the low resolution of available seismic data. However, it is clear that reflectors onlap and downlap onto the sequence boundary B on this line (Fig. 21).

5.4 Sequence C

Sequence C has a well-formed clinothem shape on CH0698 line 21 (Figs. 21 and 22). Its basal reflector truncates the topset strata of underlying sequence B. Seismic reflectors onlap and downlap onto sequence boundary C seaward of the clinothem rollover (Fig. 22). Going upward, this sequence boundary marks a shift from higher to lower gamma-ray values at 685 msec on CH0698 line 21 at site Exxon 500-1 (Fig. 22) and the highest values in gamma corresponds to the MFS (reflector C2) of Sequence C at Site M29 on Oc270 line 629 at 415 msec (Figs. 20 and 23B). It is difficult to interpret the

important surfaces within this sequence due to the seismic data resolution. Therefore, the internal reflections of sequence C can best be interpreted based on gamma-ray measurements at the Exxon 500-1 site on CH0698 line 21. This log shows an upward increase in gamma ray values at reflector C1 (607 msec; Fig. 22), interpreted as the TS. The highest gamma reading corresponds to 580 msec, suggesting that reflector C2 is the MFS. Gamma values gradually decrease up section, indicating coarsening above the MFS. This inferred coarsening continues up to the overlying sequence boundary D and records prograding deposits forming the HST of this sequence.

The HST of sequence C contains a progradational set of parasequences suggesting that the rate of sedimentation while sequence C was accumulating exceeded the rate of change in accommodation. Flooding surfaces bracket these parasequences. Reflectors C6 and C7 represent the first two flooding surfaces in the HST and they are recognized by local peaks of gamma values representing mud at Site M29 on Oc270 line 629 (Fig. 23C). Other flooding surfaces (reflectors C8-C9) are recognized by only using seismic data and are loop correlated in the seismic grid (Fig. 24). Intersection of Oc270 line 629, Ew9009 line 1023, and CH0698 line 21 reveals that these highstand deposits are deposited by two different sediment supplies, the older one coming from the North and the younger one coming from the West (Figs. 24 and 25**)**. These two different directions of sediment supply (the older deposits are C3-C5 while the younger deposits are C6-C12) are more visible on Ew9009 1023 line (Fig. 26).

Sequence C has three systems tracts: the LST bounded by the sequence boundary C and the TS (reflector C1), the TST bounded by the TS and the MFS (reflector C2), and the HST bounded by the MFS and the sequence boundary D at the top (Fig. 22).

5.5 Sequence D

The basal reflector of sequence D truncates the top of the prograding HST of the underlying sequence C (Fig. 27). This sequence boundary appears highly erosional with many small channels landward of the rollover (Fig. 27). Horizontal reflections under the sequence boundary D are interpreted as multiples on Oc270 line 629. For example, at each cdp on Oc270 line 629, two-way travel time difference between sequence boundary E and its multiple is equal to the time difference between the sea surface and sea-floor (Fig. 28). Similarly, reflectors above sequence boundary E have their multiples below the sequence boundary that are even stronger than the reflectors of prograding deposits of underlying sequence C. Thus, multiples in this area prohibit detailed examination of the internal reflections within this sequence. However, key surfaces can be determined by examining gamma-ray log data of the Shell-632 well.

Above the sequence boundary D, gamma ray values at Site Shell-632 decrease upwards until 633 msec where the trend stops and values begin to increase gradually (Fig. 29). This point marks the change from a progradational to a retrogradational stacking pattern. Thus, reflector D1 corresponds to the TS of this sequence. Gamma values reach a maximum at approximately 590 msec, where reflector D2 represents the MFS of sequence D. The gamma curve shows a decreasing upward trend above the MFS representing highly prograding deposits. D4 has a sigmoidal shape and reflectors above it prograde seaward that are tentatively interpreted as the FSST. After determining these surfaces, they are tied to the adjacent Oc270 line 44. These prograding units are clearly seen on this line. Two incised valleys at cdps 300-1400 and many small channels exist at cdps 3250-4000 associated with these units (Fig. 30).

5.6 Sequence E

The Shell-632 gamma curve has a large increase in values where it projects onto Oc270 line 629 at 496 msec (Fig. 29). Reflector E has a strong sigmoidal shape and reflectors onlap onto it, and it truncates the possible FSST of the underlying sequence D. Multiples mask the internal structures of this sequence along line 629. Reflector E is associated with a large incised valley at cdps 3650-4000 (Fig. 30). This incised valley suggests that reflector E is a sequence boundary formed as a result of subaerial exposure. Intersection of lines Oc270 629, 42 and 145 shows a few strong reflectors that can be traced throughout much of the seismic grid (Fig. 31). Reflectors E1 and E2 can be seen more clearly on Oc270 line 145. The reflector E2 is the boundary at the bottom of prograding deposits that have toplap terminations against the sequence boundary F at cdp 10300-10650 (Fig. 32).

After determining the reflectors E1, E2 and the sequence boundary F on Oc270 line 145, they are carried to Oc270 line 629 (Fig. 32). Gamma log data at Shell-632 site on line 629 is consistent with the seismic interpretation explained above. The highest value on gamma log at 492 msec corresponds to the MFS (reflector E2). Above the MFS, the gamma slope decreases up to 485 msec where the overlying sequence boundary F is present. This sequence boundary is a very high amplitude reflection with a sigmoidal shape. The interval between the MFS and the sequence boundary F corresponds to the HST of this sequence.

5.7 Sequence F

The basal surface of sequence F is associated with a submarine canyon basinward of the bottomset of this sequence. This submarine canyon is seen at cdp 2800-3100 on

Ew9009 line 1002 (Fig. 17C). Sequence boundary F truncates the HST deposits of the underlying sequence E on Oc270 line 42 (Fig. 31). On Oc270 line 629, only onlap terminations against this boundary can be recognized. In contrast, Oc270 line 145 shows the sequence boundary F more clearly (Fig. 32). Reflector F1 overlies the submarine levees basinward of the clinothem rollover where it onlaps onto the sequence boundary F (Fig. 32). Five prograding packages downlap onto the reflector F1 (Fig. 32), suggesting that this reflector is the MFS. These packages progressively step down into the basin having the possible offlap terminations; therefore, these packages are interpreted as the FSST of this sequence. Seismic resolution is not enough to see whether they aggrade or bypass the underlying topsets.

5.8 Sequence G

Only reflection terminations associated with reflector G are onlaps against the reflector that makes it difficult to interpret this reflector as a sequence boundary (Fig. 31). However, at 435 msec on Oc270 line 629, equivalent to the total depth below sea level at the Shell-632 well reflector G corresponds to an abrupt upsection shift to low gamma values, suggesting that this reflector is a sequence boundary (Fig. 31). Above reflector G, gamma ray values increase steadily upsection to the next overlying sequence. This sequence is more visible on Oc270 line 145 than on line 629 because it thickens towards the NE and an apparent depocenter. Reflections onlap at the clinothem rollover and downlap onto the sequence boundary G on the bottomset of this sequence (Fig. 32). However, other reflection terminations are difficult to see because of the strong horizontal multiples.

5.9 Sequence H

On Oc270 line 145, reflector H is an erosional surface with small channels on the landward side of the clinothem rollover at cdp 10700-11200 (Fig. 32) that indicate a relative sea level fall that subaerially exposed the shelf. All of these suggest that reflector H is a sequence boundary.

On three parallel seismic lines, Oc270 line 145, Ew9009 line 1002 and 1024, the internal reflections within this sequence can not be clearly seen because of the multiples and absence of seismic lines crossing these parallel seismic lines.

5.10 Sequence I

Reflector I overlies sequence H, and is associated with small channels on the landward part of the clinothem rollover on Oc270 line 145 (Fig. 32-B). The same reflector marks a shift to lower gamma values at 893 msec at COST B-2 well on Ew9009 line 1002, suggesting a sequence boundary (Fig. 33). Because of low resolution of the seismic data, this gamma log is used to analyze the seismic section between the I sequence boundary and the base of Pleistocene. At 890 msec, a small kick in gamma ray values changing from gradual decrease in slope to lower values represents the I sequence boundary. Immediately above this kick, the slope in gamma ray values increases and maximum values are reached at 833 msec, representing a MFS. This point corresponds to reflector I1 that reaches to the clinothem rollover on Ew9009 line 1002 (Fig. 33B). Above the MFS, the gamma log progressively decreases until the next sequence boundary. On seismic data, possible downlap terminations onto this MFS are difficult to identify due to strong horizontal multiples on the profile. It is difficult to interpret the reflectors below the MFS (reflector I1) as the TST and/or LST.

5.11 Sequence J

Reflector J marks a change from a decreasing trend in gamma ray values to a gradual increasing trend at 798 msec on the COST B-2 gamma log, suggesting a sequence boundary overlying the HST of sequence I (Fig. 33). Gamma ray values reach a maximum at 789 immediately above the sequence boundary J. Above the MFS, gamma ray logs show a characteristic blocky pattern of the HST suggesting a sand rich section. It is hard to recognize internal terminations of this sequence on seismic data due to low resolution and dominant horizontal multiples.

5.12 Sequence K

Reflector K marks the top of the blocky pattern on the gamma ray log at 665 msec on Ew9009 line 1002 at COST B-2 site, suggesting a sequence boundary. Gamma values reach their maximum associated with a MFS at 661 msec, marked by reflector K1 (Fig. 33). In addition, prograding deposits above the reflector K1 correspond to lower values on gamma-ray log and downlap onto the MFS on Ew9009 line 1002.

5.13 Sequence L

On top of the prograding HST deposits of the sequence K, sequence L is bounded by sequence boundary L at the bottom and M at the top (Fig. 33). Although this sequence is more clearly seen on Oc270 line 43 and dominated by prograding deposits, it is hard to see internal reflections rather than the oblique lines representing these prograding units.

5.14 Sequence M

At 393 msec, the prograding units of the underlying sequence L is truncated by sequence boundary M where this boundary marks a change from higher to lower gamma

ray values (Fig. 34). Based on downlap terminations on reflector M1, this reflector is identified as the MFS of this sequence (Fig. 34). In addition, this reflector corresponds to 370 msec where there is a small kick towards higher values on COST B-2 gamma-ray log on Ew9009 line 1002 (Fig. 33). Reflectors between the sequence boundary M and the MFS are hard to identify but this area can be tentatively interpreted as the LST and TST of this sequence.

5.15 Sequence N

This is the youngest sequence in the study area bounded below by sequence boundary N and by the base of the Pleistocene above (Fig. 33). The base of the Pleistocene is carried to Ew9009 line 1002 from Oc270 line 8 where it was previously identified by Mountain et al. (2007).

Neither the gamma ray log at the COST B-2 site or seismic profiles in the seismic grid make it possible to interpret the internal reflections due to having a stable slope on gamma log and having strong horizontal multiples on seismic sections. Only prograding reflections and the clinothem shape of the sequence boundary N can be observed on Ew9009 line 1002. Very thick prograding deposits of this sequence are eroded by the base of the Pleistocene boundary and clearly show erosional truncation terminations on the same line (Fig. 33).

6 Discussion

6.1 Sequence stratigraphic interpretations

Previous sequence stratigraphic interpretations (Poulsen et al. (1998) also identified sequence boundaries on Ew9009 line 1002, focusing on three dimensional

changes in sequence and systems tracts thickness. They identified eight seismic sequence boundaries on Ew9009 line 1002, tied them throughout the seismic grid, and made a sequence stratigraphic interpretation of each individual sequence in detail. In contrast, I have identified fourteen sequences. The differences in sequence stratigraphic interpretations are most likely due the spatial density and vertical resolution of the Oc270 and CH0698 data used in this study that was not available to Poulsen et al. (1998).

Other differences between this study and Poulsen et al. (1998) may be due to the differences in interpretations of gamma log data. Poulsen et al. (1998) used log data from 684-1, COST B-2, 590-1, 544-2, and 500-1. Gamma logs measured in depth were incorporated into seismic data measured in time by using time-depth charts. In this study, T-D charts were created for all three wells (Exxon 500-1, Shell-632 and COST B-2 wells) based on a time-depth function that had been used in Expedition 313. Therefore, there may be differences in the T-D charts leading to different interpretations.

Interpretations based on only seismic data can be very limited. There are places where seismic profiles are dominated by multiples, or seismic resolution is not high enough to image reflections clearly. In these cases, gamma-ray logs play a critical role in identifying sequence boundaries, dividing sequences into systems tracts, and interpreting the internal reflections of sequences on even high-resolution seismic profiles. In general, there is progressively deeper erosion and/or increased progradation moving up in the Miocene stratigraphic succession in the study area. However, COST B-2 gamma-ray log enhanced interpretations of the sequences above sequence I on Ew9009 line 1002.

6.2 Testing sequence stratigraphic models

Reflectors onlapping onto an underlying sequence boundary below clinothem rollovers usually downlap onto the sequence boundary at the distal toe of the sequence. The body of strata defined by this reflector geometry generally was considered to be the LST. Only sequence A has possible basin-floor fan and slope-fan deposits in the LST (Fig. 19B). Also, deposits below the transgressive surfaces identified on gamma logs were interpreted as the LST deposits when seismic reflection terminations were unidentifiable (in sequences C and D; respectively, Figs. 22 and 27).

It was difficult to place the most prominent onlap onto the underlying sequence boundary landward of the rollover, and subsequently to identify transgressive systems tracts by only looking at seismic reflection terminations on seismic profiles. The difficulty was either due to low resolution of seismic data, or thin to absent TST in sequences. Three thin TST were identified (in sequences A, C, and D) in clinothems. Since gamma log data at the Exxon 500-1 site only penetrates the bottomset of sequence A, the transgressive surface in this sequence was interpreted based on seismic reflections alone. This resulted in two different interpretations of placing the transgressive surface in sequence A (See the Results section for details; Figs. 19B and 19C). In cases where seismic reflections and terminations within the sequences were difficult to see, key surfaces were determined by correlations to available gamma log curves. As a result, two more transgressive systems tracts were identified in sequences C (Fig. 22) and D (Fig. 27).

Similarly, most of the maximum flooding surfaces in sequences were identified by local maxima in gamma-ray log values (reflectors I1, J1, K1, M1; Fig. 33).

Downlapping reflectors onto the MFS were generally difficult to resolve. In these cases, deposits bounded by the MFS and the overlying sequence boundary were assumed to be the HST. In places where there were no gamma logs available to identify the MFS, reflectors below the prograding deposits were selected as the MFS (reflectors D2 and F1) and two possible FSST were identified in sequence D (Fig. 27) and sequence F (Fig. 32), where reflectors stepped basinward.

Sequence boundaries D (Fig. 27), H and I (Fig. 32) have channels on topsets and sequence boundary E (Fig. 30) is associated with a large incised valley. These small channels and the incised valley are likely formed as a result of subaerial exposure.

Table 6.2.1 shows 14 sequence boundaries found in this study with seismic profiles on which they are identified, and the criteria used to identify these sequence boundaries.

6.3 Depositional History

Sequences in this study have characteristic clinothem shape and consist of prograding deposits. These deposits have thin, low-gradient topsets on the shelf. These topsets grade into more steeply dipping foresets seaward of the rollover, thicken rapidly, and at the distal toe thin into low-gradient bottomsets that pinch onto the underlying sequence boundary, or are truncated by the overlying sequence boundary (Fig. 3). Clinothems identified in this study have variable foreset thicknesses, with the general pattern that those closest to the sediment sources are the thickest. Older sequences A, B, C, and D in the present study appear thickest in the central area of the seismic grid (CH0698 line 21) (Fig. 1), and thin in the northern and southern areas. Sequences above sequence D and below sequence L reach their maximum thicknesses in the NE part of the

grid (Ew9009 lines 1002 and 1024). Younger sequences (L, M, and N) are the thickest examined in this thesis (Fig. 17C). Hence, sequences have thicker topsets in the outer continental shelf suggesting higher aggradation in these areas.

In addition to change in sequence thicknesses, the locations of clinothem rollovers also change with time. Change in the rollover position of a sequence boundary on different seismic profiles gives insight into how much that sequence has prograded. Figure 34 shows the clinothem rollover positions on each sequence. This figure reveals that all Miocene sequences in the study area advance basinward (SE) through time. Sequences D and E have the maximum progradation observed in the seismic grid. For these two sequences, the largest progradations are observed in the southwestern (Ew9009 line 1028) and the northeastern parts (Ew9009 lines 1002 and 1024) of the seismic grid (Figure 34). Clinothem rollovers of sequences above E could only be mapped in the northeastern part of the grid (Ew9009 lines 1002 and 1024) where the rollovers are closely spaced.

6.4 Ages of the sequence boundaries

Several previous studies (Greenlee et al., 1992; Mountain et al., 1996, 2010; Miller et al., 1996; 2013) have named and mapped (within a limited region) several of the 14 sequences discussed in this thesis (Table 6.3.1). Karakaya et al. (in review) report 10 sequences, two of which were not confirmed by this study. However, none of these prior studies has traced each sequence across the region examined here to establish correlations between the Expedition 313 drill sites and the COST B2 well on the outer shelf, 60 km to ESE.

Age estimates of the 14 sequences A-N reported here are assigned on the basis of correlations to Expedition 313 studies (Miller et al., 2013; Browning et al., 2013) (Table 6.3.1; Fig. 35). Age estimates for sequences m4.2, m4.1, m4, m3, m2, and m1 (Browning et al., 2013) allow correlation to sequences A, B, D, H, K, and L, respectively with an age resolution as good as ±0.25 Myr (see Browning et al., 2013). Age estimates of sequence boundaries in Karakaya et al. (in review) are assumed by correlation to the $\delta^{18}O$ record (Figs. 36 and 37). Estimated ages of the sequence boundary A (13.1-12.9) and show that development of the sequence A coincides with a major shift in $\delta^{18}O$ towards higher values (Mi4 in Fig. 37; Miller et al., 1991) and about the time of the permanent Antarctic ice sheet development.

Although the age estimates of sequences M and N are not known, these sequences are only constrained to younger than sequence m1 (~ 11.4 Ma; Browning et al., 2013) and older than the Pleistocene (reflector P4, the top of sequence N; Mountain et al., 2007).

6.5 Correlation with the $\delta^{18}O$ record

High-resolution benthic oxygen isotope record from ODP Site 1085 at the Southwestern African continental margin (Westerhold et al., 2005) were used to evaluate the correlation of sequence boundaries found in this study with $\delta^{18}O$ increases spanning the late-middle Miocene (13.1-11.9 Ma).

Million year scale oscillations of the Miocene $\delta^{18}O$ record (Mi-Events) have been attributed to waxing and waning of the Antarctic Ice Sheet (EAIS) (Miller et al., 1991). It is likely that such large changes in polar ice volume caused glacioeustatic changes, with

the major glacioeustatic lowerings generating hiatuses and sequence boundaries in shallow-water Miocene strata such as those examined in this study.

In Figure 37, timing of sequences in the present paper is compared with $\delta^{18}O$ increases in the record from Site 1085A. Bold magenta lines on the oxygen isotope record indicate Mi-Events (Mi4 and Mi5) between 13.2-11 Ma. Browning et al. (2013) place Mi-Events in the oxygen isotope record at the inflections of the $\delta^{18}O$ increases. Based on the age estimates of Browning et al. (2013), Mi4 and Mi5 events are at 13.0 and 12.0 Ma, respectively.

The $\delta^{18}O$ also allows identification of 100 kyr scale variations, and previous studies have reported a similar number of sequences (Fig. 37; Karakaya et al., in review). Age estimates of the 9 out of 14 sequence boundaries show that the time between the oldest and the youngest boundaries is 1.2 Myr, suggesting an average interval between each of 130 kyr.

7 Conclusion

The Miocene stratigraphy of the middle to outer continental shelf off New Jersey is characterized by a series of prograding clinothems. The sequence stratigraphic approach was applied in this study area by integrating high-resolution multichannel seismic profiles with gamma ray logs to test sequence stratigraphic models. Analysis of twenty-nine seismic profiles from R/V *Ewing* Ew9009, R/V *Oceanus* Oc270 and R/V *Cape Hatteras* CH0698 cruises outlined 14 late middle to late Miocene sequences above sequence m4.3. Seismic sequence boundaries were determined based on stratal termination definitions of Mitchum et al. (1977). When reflections were difficult to see,

gamma logs were used to place sequence boundaries and key surfaces within sequences on the profiles.

Most of these sequences were then divided into systems tracts by tying nearby gamma-ray logs to the seismic profiles. Stacking patterns on the logs were examined to identify key surfaces within the sequences that are the TS and the MFS. As a result, most of the TST and HST of sequences were distinguished on gamma-ray logs. Where there were no gamma-logs available to identify these surfaces, downlap surfaces below the prograding deposits were interpreted as the MFS on seismic profiles.

Sequences m4.2, m4.1, m4, m3, m2 and m1 that are identified in the Expedition 313 studies (Mountain et al., 2010; Miller et al., 2013) are correlated with sequences in this study A, B, D, H, K, L, respectively (Figure 35). Age estimates from Browning et al. (2013) were then used to estimate ages of all sequences in this thesis. The older sequence A is 13.1-13.0 Ma, the younger sequences M and N are only constrained to younger than 11.4 Ma and older than 1.8 Ma (the base of Pleistocene).

Sequences that have thicker topset and foreset deposits in the middle to outer continental shelf than in the inner continental shelf of New Jersey show that aggradation and progradation is higher in these areas. Poulsen et al. (1998) suggest that high progradational deposits of middle to late Miocene sequences in New Jersey middle to outer continental shelf may have been the result of deltaic progradation and migration. In addition to deltaic effect on the development of sequences in this area, compaction and sediment loading may have created the accommodation for these thick, shallow-marine deposits.

This study evaluates sequence stratigraphic models by taking advantage of high sedimentation rate strata in addition to the available gamma-ray logs and seismic profiles in the middle to outer continental shelf off New Jersey. Sequence A is a good example to compare and contrast the classic Exxon model with the model derived from Expedition 313 studies. The latter concluded the maximum flooding surface is the first major downlap surface within a sequence, implying that sequence A is dominated by thick highstand deposits. By contrast, the widely cited Exxon model sees the reverse, i.e. sequences have thick lowstand units separated by several flooding surfaces, and generally have thinner highstand deposits. But this study showed that not all sequences are alike. Shell-632 gamma-ray log shows that sequence D has thick lowstand and transgressive, and thin highstand systems tracts consistent with the Exxon model. In contrast, the other sequences agree with the model in Expedition 313 that has thinner lowstand and transgressive systems tracts that are either below seismic resolution, or very thin, and overlain by thick highstand systems tracts.

This thesis shows that when used alone, seismic data are limited in testing sequence stratigraphic models with certainty. Although integrating high-resolution seismic with log data provides great insight into testing different sequence stratigraphic models on the Miocene sequences offshore New Jersey, future studies integrating core data to the available seismic and well-log data will evaluate sequence stratigraphic history of this area with more certainty.

8 Figures

1A

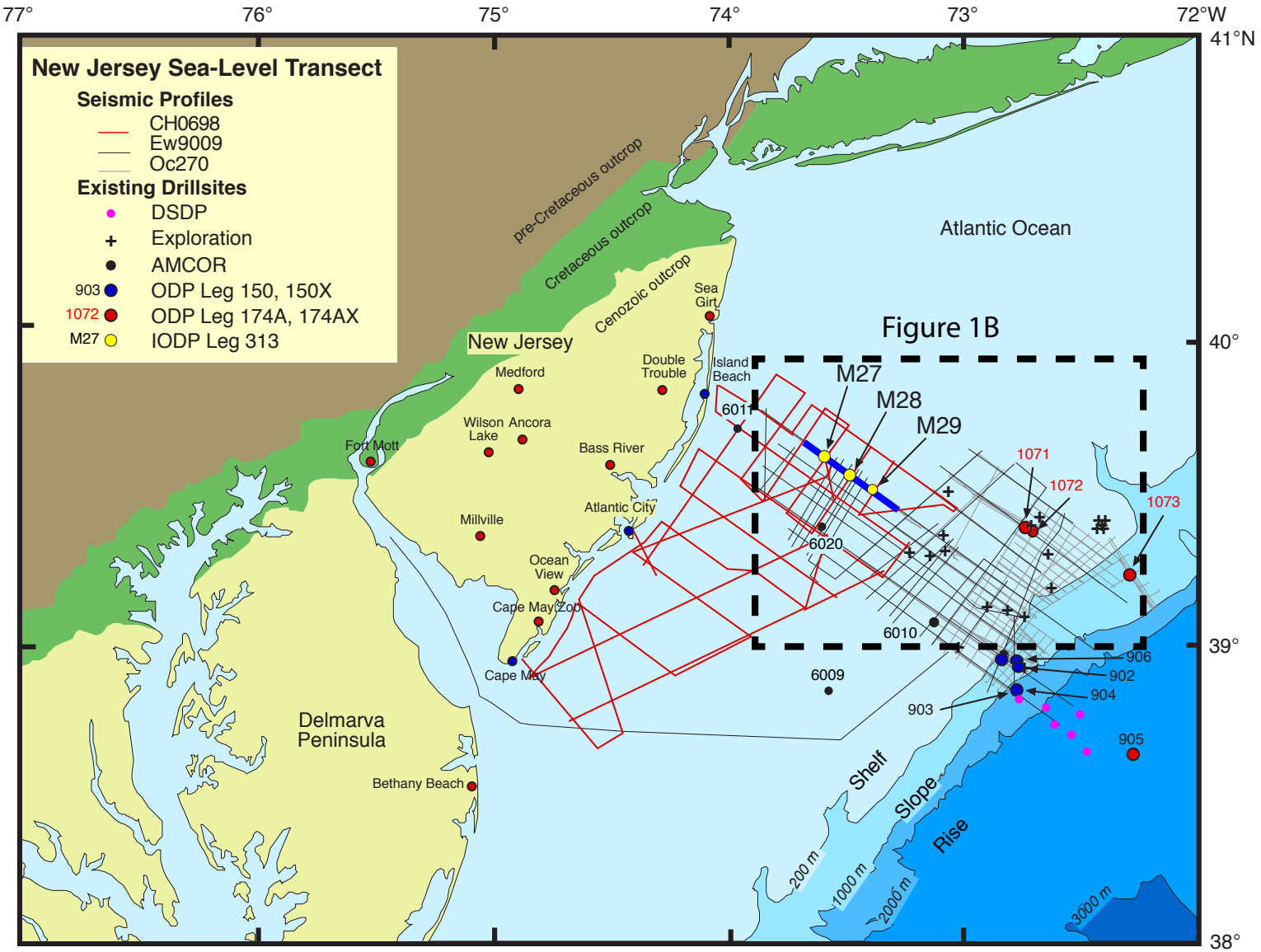
77°
76°
75°
74°
73°
72°W
41°N
40°
39°
38°
New Jersey Sea-Level Transect
Seismic Profiles
CH0698
Ew9009
Oc270
Existing Drillsites
DSDP
Exploration
AMCOR
903 ODP Leg 150, 150X
1072 ODP Leg 174A, 174AX
M27 IODP Leg 313
pre-Cretaceous outcrop
Cretaceous outcrop
Cenozoic outcrop
Atlantic Ocean
New Jersey
Figure 1B
Sea Girt
Double Trouble
Island Beach
Medford
Wilson Lake
Ancora
Fort Mott
Bass River
Atlantic City
Millville
Ocean View
Cape May Zoo
Cape May
Delmarva Peninsula
Bethany Beach
M27
M28
M29
6011
6020
6010
6009
1071
1072
1073
906
902
904
903
905
Shelf
Slope
Rise
200 m
1000 m
2000 m
3000 m

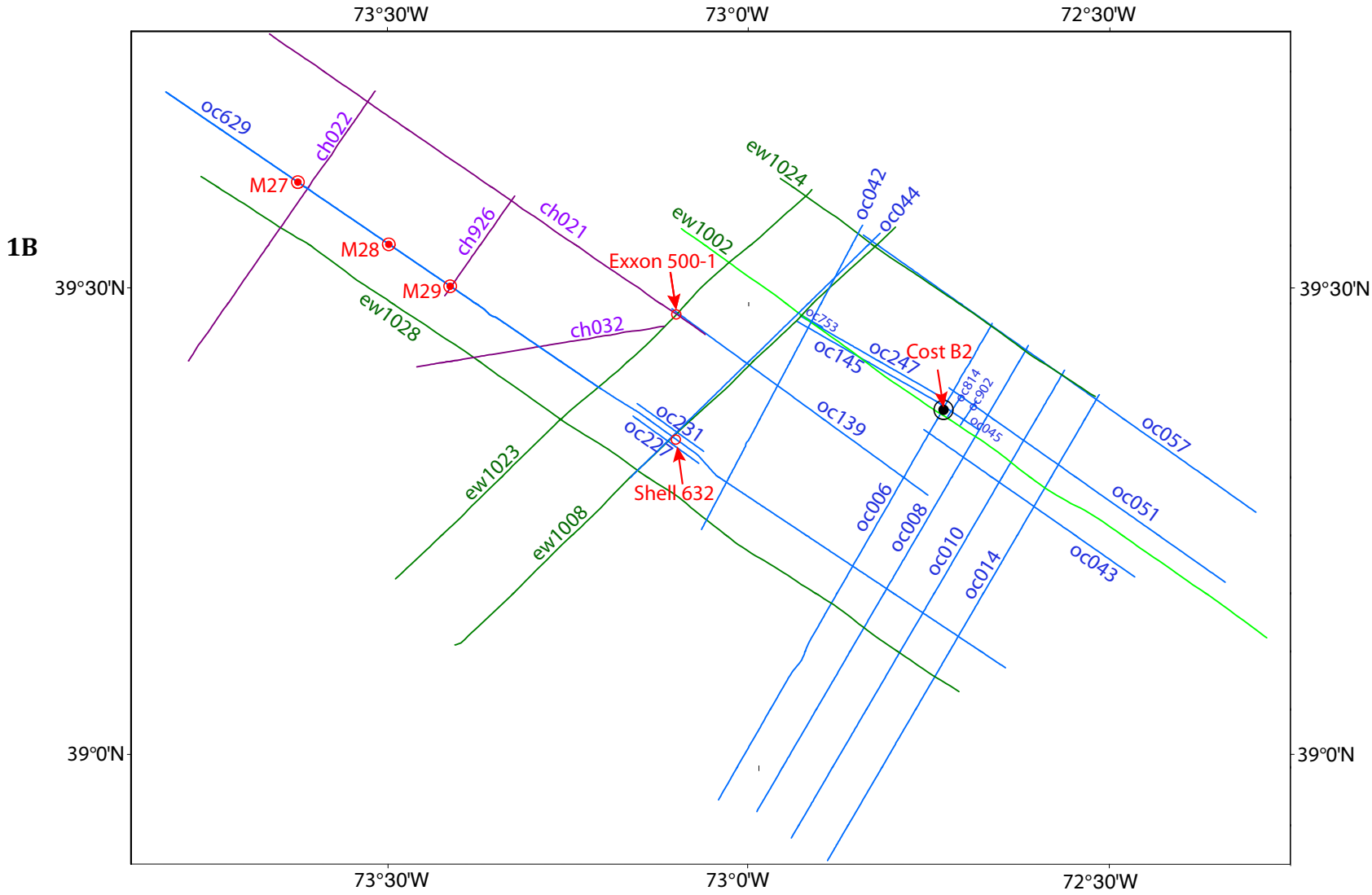

Figure 1. (A) The New Jersey sea-level transect across the mid-Atlantic margin showing multichannel seismic data from the three cruises that provided data analyzed in this study (R/V *Ewing* Ew9009, R/V *Oceanus* Oc270, R/V *Cape Hatteras* CH0698). Onshore and offshore drillsites were assembled from several sources (modified from Miller et al., 2013); (B) Enlarged view of the area examined in this study showing the location of profiles that were interpreted and the location of wells (red font) providing litho- and chronostratigraphic correlations with wireline logs and/or core samples.

2A

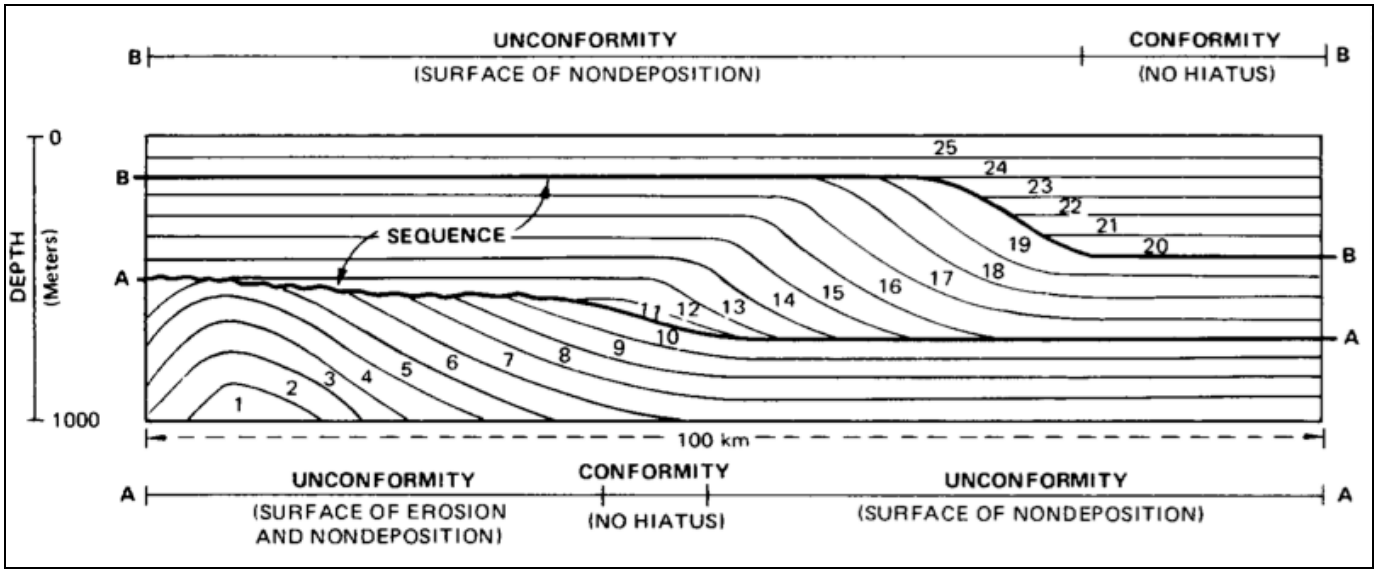
B
UNCONFORMITY
(SURFACE OF NONDEPOSITION)
CONFORMITY
(NO HIATUS)
B
0
DEPTH
(Meters)
1000
B
A
SEQUENCE
1
2
3
4
5
6
7
8
9
10
11
12
13
14
15
16
17
18
19
20
21
22
23
24
25
B
A
100 km
A
UNCONFORMITY
(SURFACE OF EROSION
AND NONDEPOSITION)
CONFORMITY
(NO HIATUS)
UNCONFORMITY
(SURFACE OF NONDEPOSITION)
A

2B

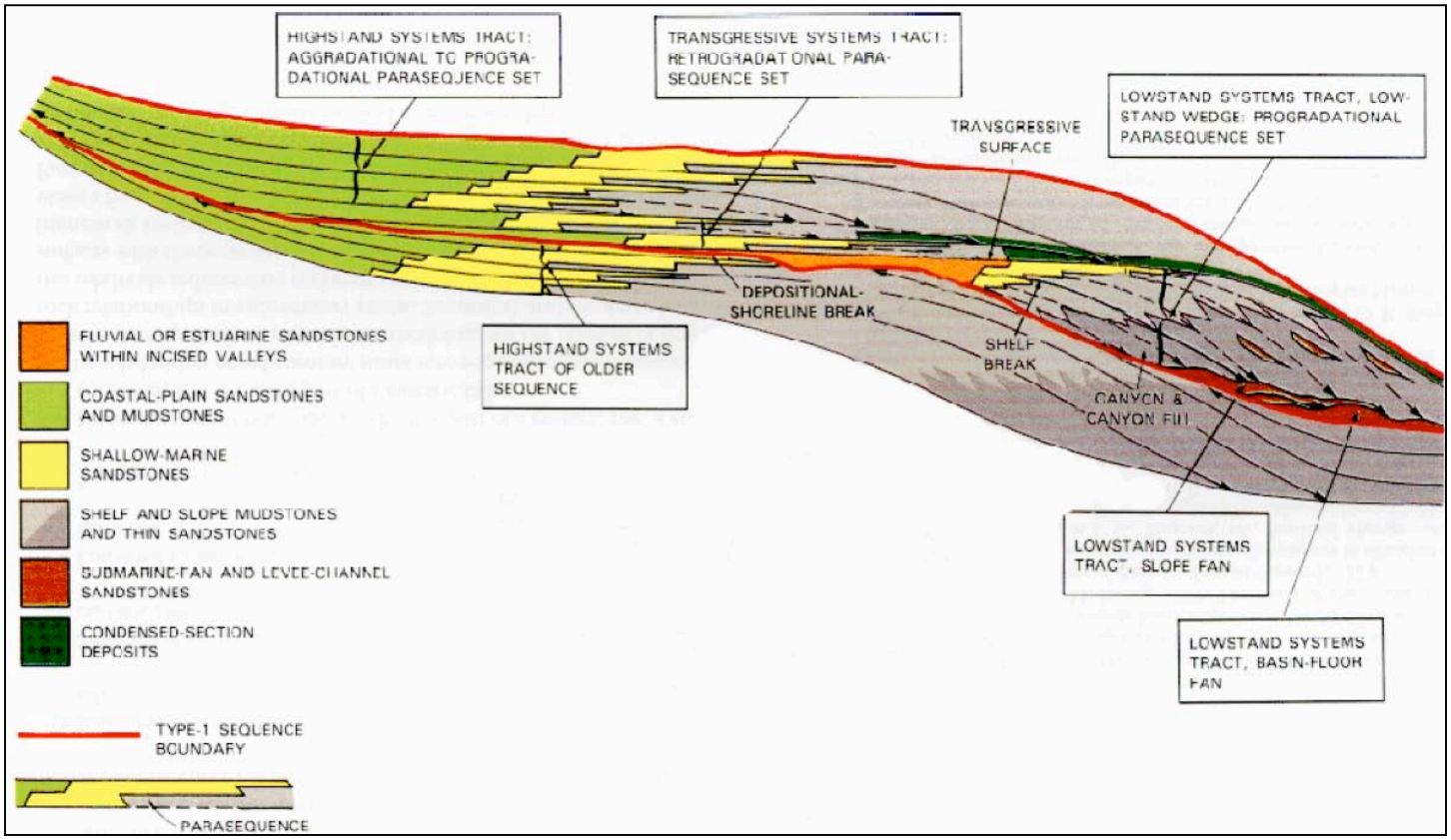

Figure 2. (A) Stratigraphic section showing basic concepts of a sequence (from Mitchum et al., 1977). Sequence boundaries A and B divide the succession of strata (1 through 25) and represent hiatuses where strata are missing. Erosion and/or nondeposition is usually associated with the sequence boundaries. Where strata are conformable, sequence boundaries are assumed to represent no hiatus; (B) The Exxon model showing the "slug-shaped" sequence consisting of three systems tracts from bottom to top; the lowstand systems tract (LST), transgressive systems tract (TST), and highstand systems tract (HST). According to this model the LST is divided into three units, a basin-floor fan, a slope fan, and a lowstand wedge (LSW) (from Van Wagoner et al., 1987).

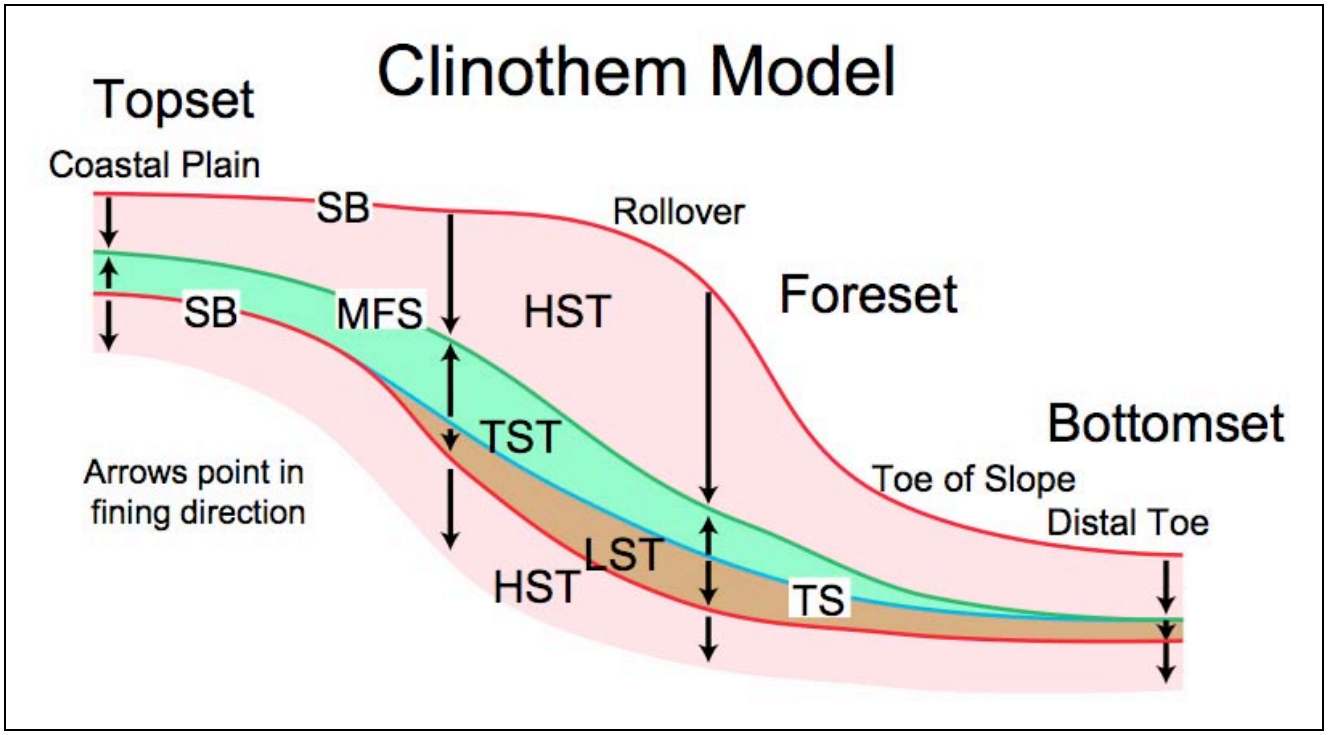

Figure 3. Clinothem model showing the 3 major types of surfaces that characterize depositional sequences: SB—sequence boundary (red lines); TS—transgressive surface (blue lines); MFS—maximum flooding surface (green lines). These surfaces divide a sequence into component systems tracts: LST—lowstand systems tract (brown); TST—transgressive systems tracts (green); and HST—highstand systems tract (light pink). Arrows indicate fining (deepening) direction (from Miller et al., 2013).

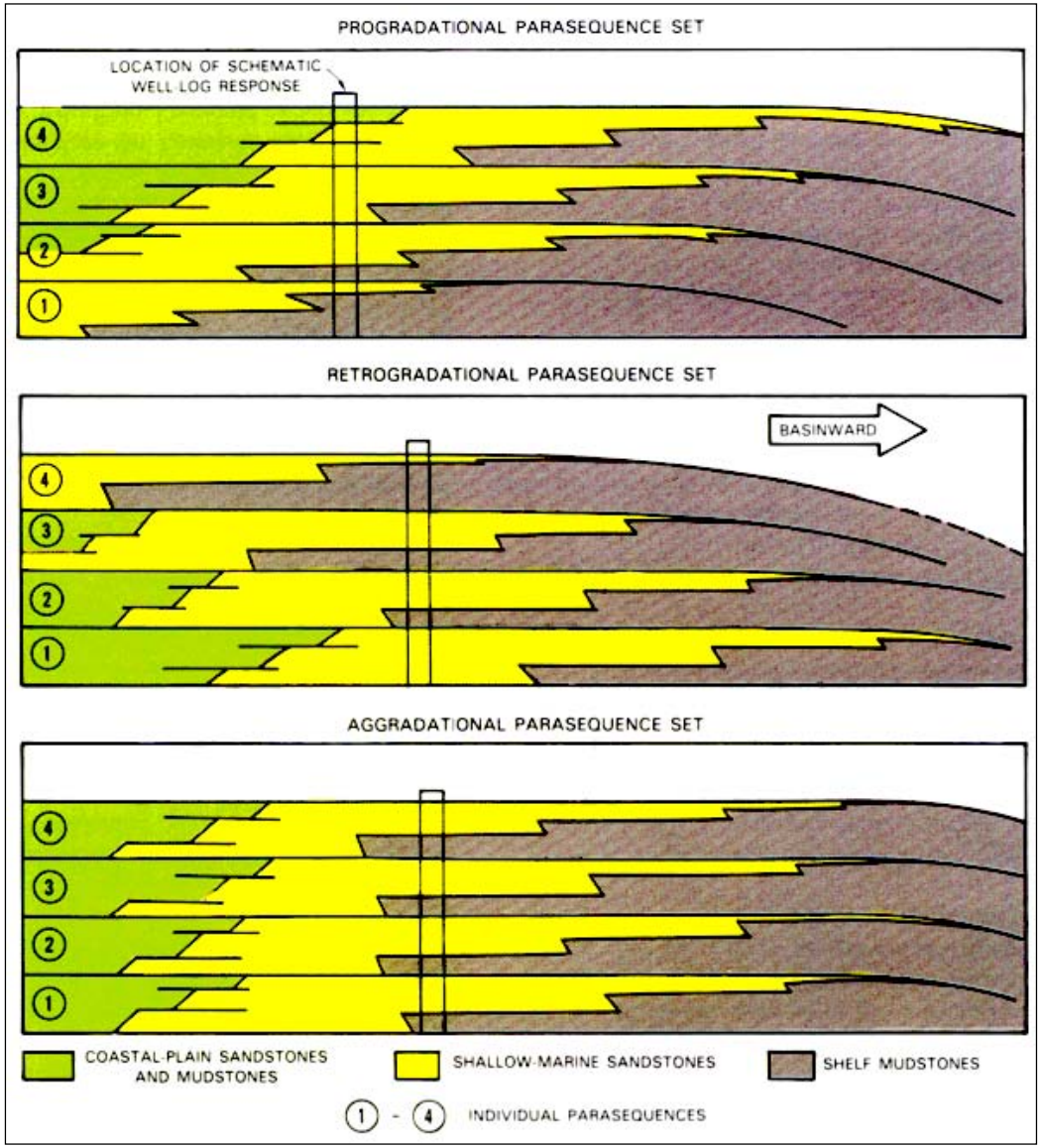

Figure 4. Parasequences are a second-order division of sequences and typically are arranged in a vertial succession of parasequence "sets" that show any of three types of stacking patterns as diagrammed here: progradational, retrogradational, and aggradational (from Van Wagoner et al., 1987).

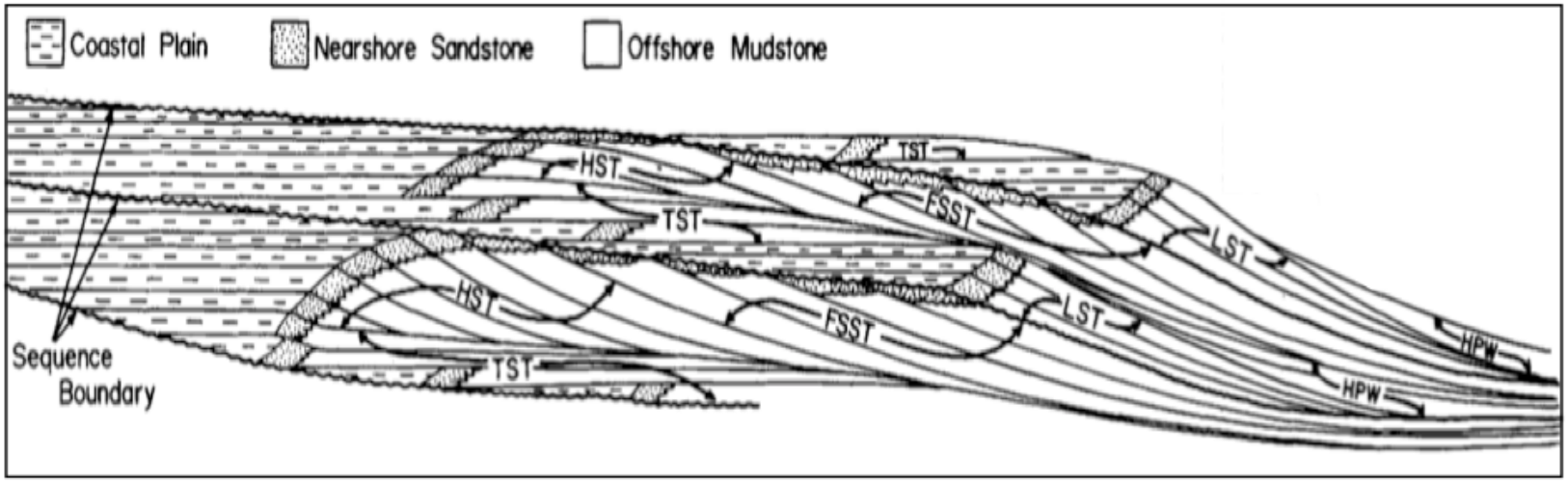

Figure 5. The falling stage systems tract (FSST) lies stratigraphically above and basinward of the HST, and below the LST of the overlying sequence. The strata within the FSST are characterized by offlaps that are inclined sets of conformable strata progressively shifting basinward (from Plint and Nummendal, 2000).

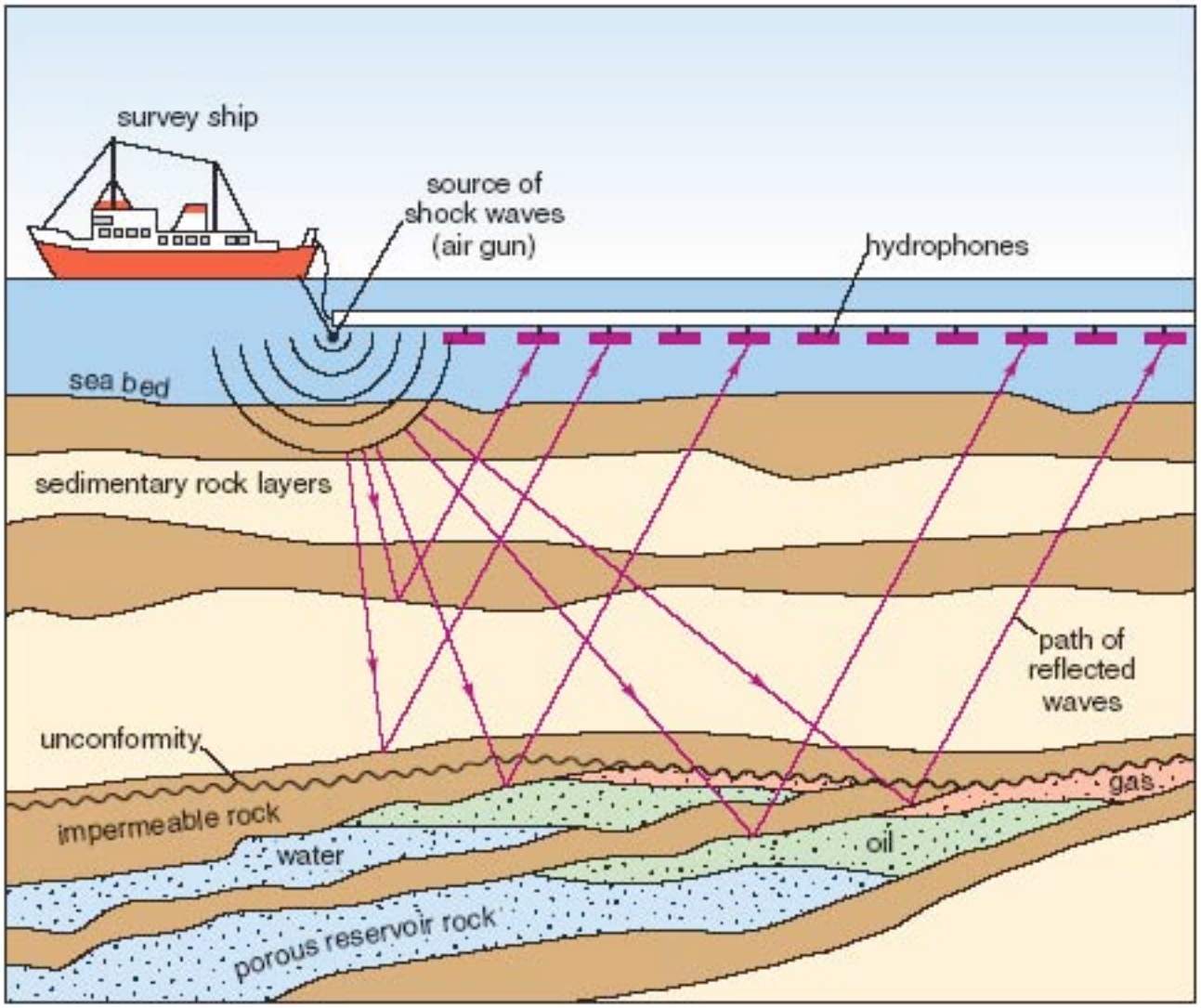

Figure 6. Marine seismic data acquisition. Two-dimensional (2D) multichannel seismic (MCS) surveying requires a ship that has a source towed at a fixed depth and offset behind the vessel. The source sends seismic pulses that travel below the seafloor and return as reflections to the hydrophones connected on a single multi-channel streamer towed behind the vessel (from http://openlearn.open.ac.uk/mod/resource/ view.php?id=172129).

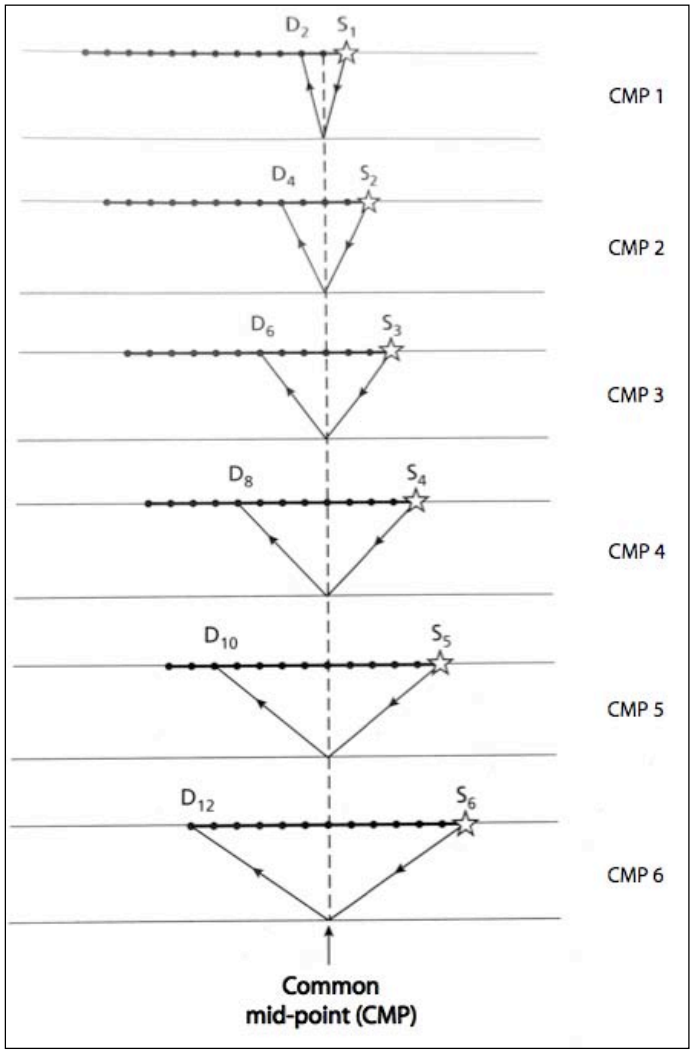

Figure 7. Procedure for common mid-point (CMP) profiling that is the standard method of 2-dimensional multichannel seismic surveying (from Kearey, 2002). The source and receiver have to be symmetric at the same point (common mid-point) while the ship is advancing forward at each shot. Then, the collected reflection data are stacked in order to improve the signal/noise ratio, and to minimize the multiple reflections.

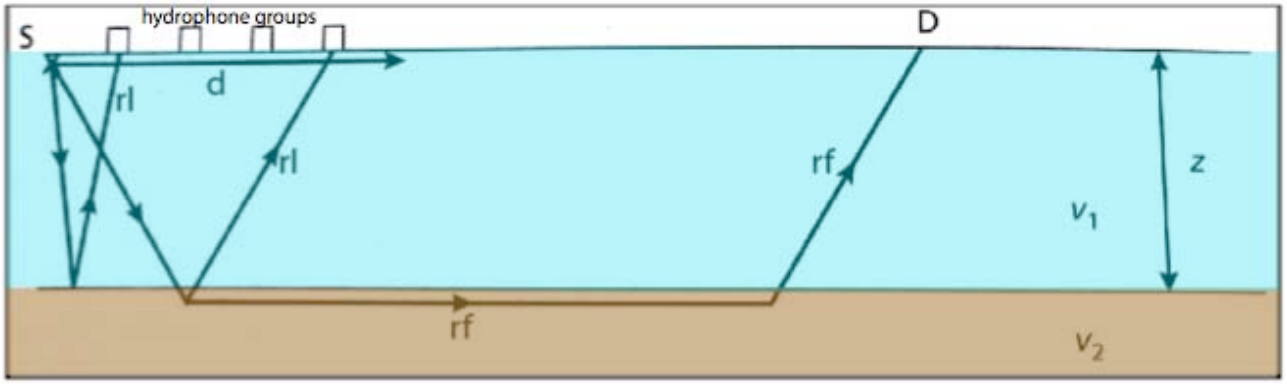

Figure 8. Three types of ray-paths: d—direct, rl—reflected; rf—refracted ray-paths; S— source; D—detector; z—water depth; V_1—speed of sound in the first layer, V_2—speed of sound in the second layer (modified from Kearey, 2002). The first arrival to a receiver is either a direct wave (d) that travels directly from the source to the receiver, or a refracted wave (rf) that travels within the sediment. A reflection seismic survey is interested in collecting reflected waves (rl) rather than the other arrivals.

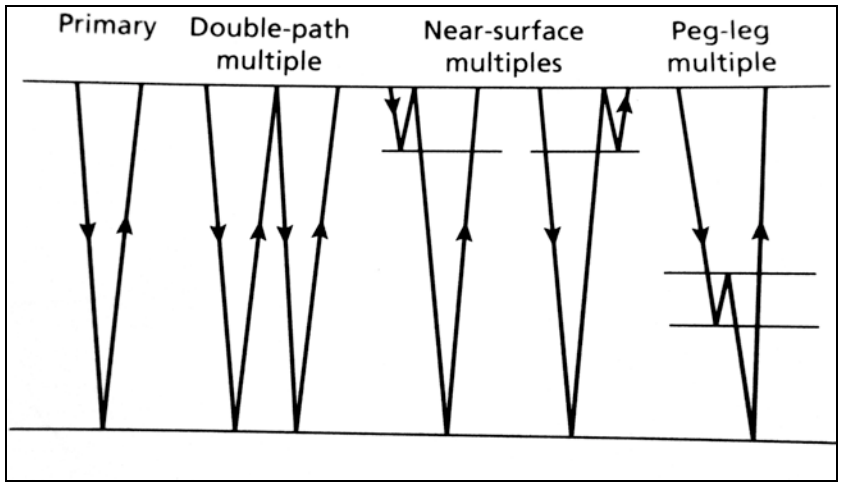

Figure 9. Four types of seismic multiples resulting from the waves reflecting at more than one layer (from Kearey, 2002).

10A

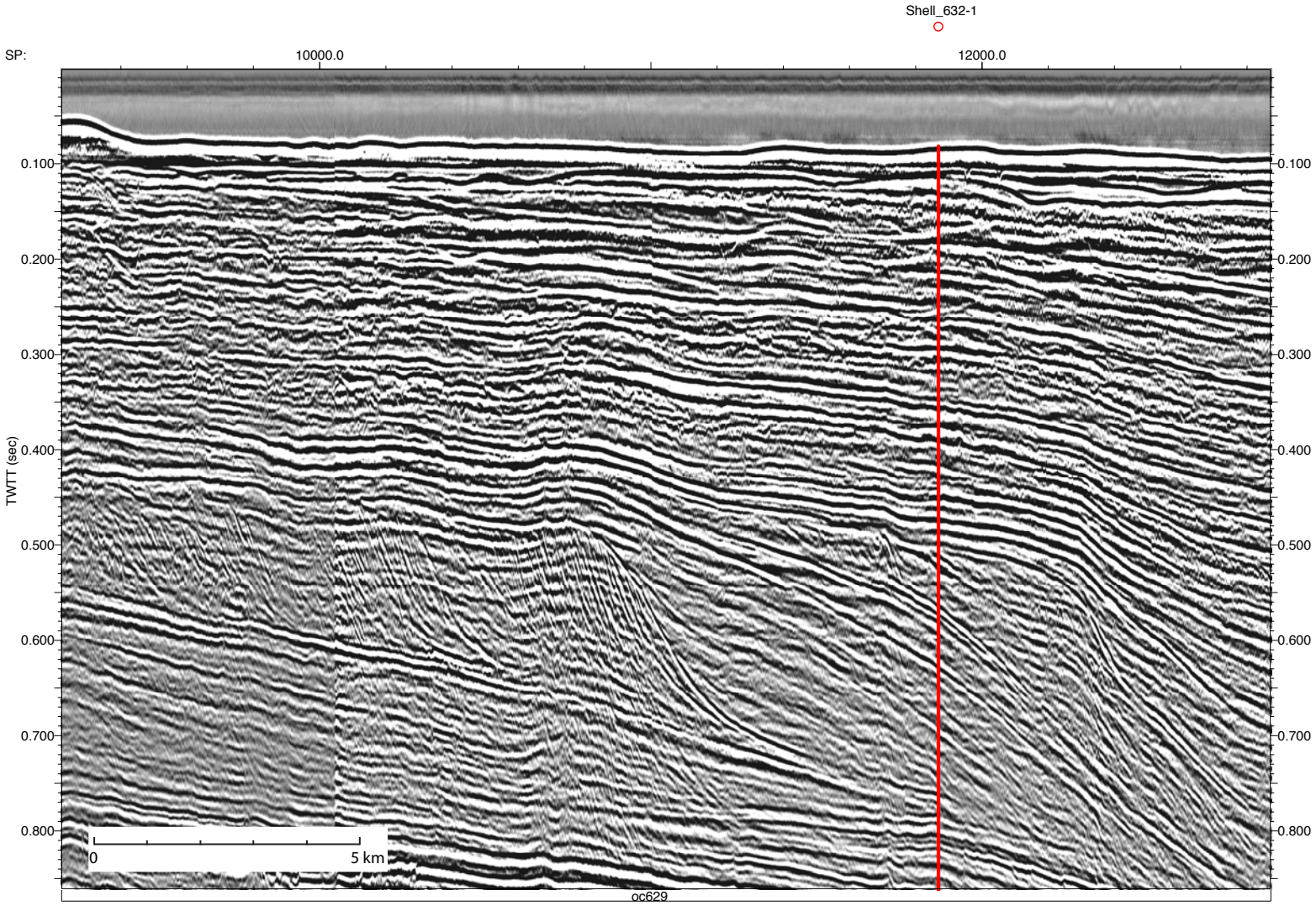
Shell_632-1
SP:
10000.0
12000.0
0.100
0.200
0.300
0.400
0.500
0.600
0.700
0.800
TWTT (sec)
0
5 km
oc629

10B

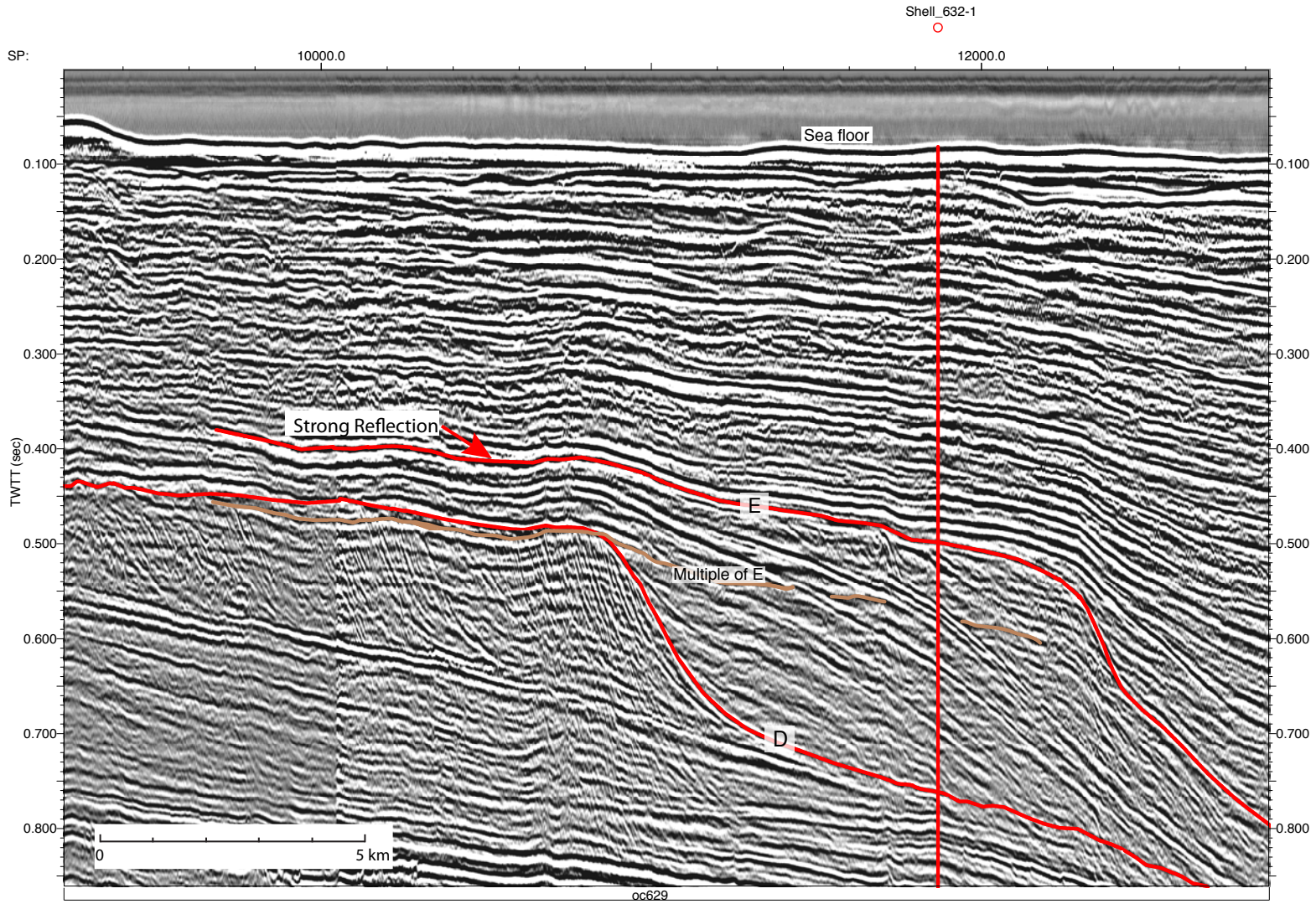

Figure 10. (A) Uninterpreted version of (B); (B) A strong reflection with high impedance contrast. The greater the change in impedance across a boundary, the stronger the reflected energy is. Multiple of E is an example of near-surface multiple where seismic energy bouncing off the sea floor subsequently makes an extra travel path in the water column (Fig. 9). Therefore, the separation between the reflector E and its multiple is equal to the travel time of the water column.

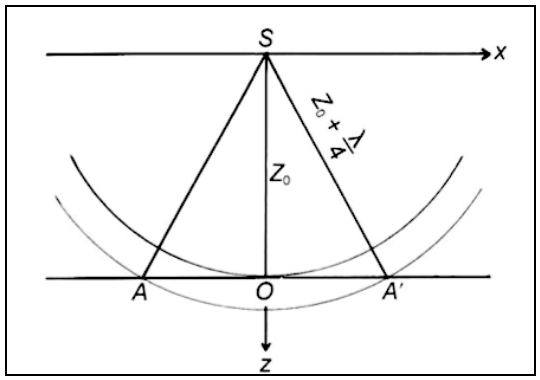

Figure 11. The width of the Fresnel zone AA`. S—source; Z—depth between the source and the reflector; λ— wavelength of the source. The width of the Fresnel zone, *w*, is defined by the following equation: $w=(2z\lambda)^{1/2}$. For Ew9009 data, assume that λ=35 m and z=750 m, w is approximately 230 m. This is the minimum horizontal width of a detectable feature and the minimum required lateral distance between two features in order to be visually distinguishable on the profile (from Yilmaz, 1980).

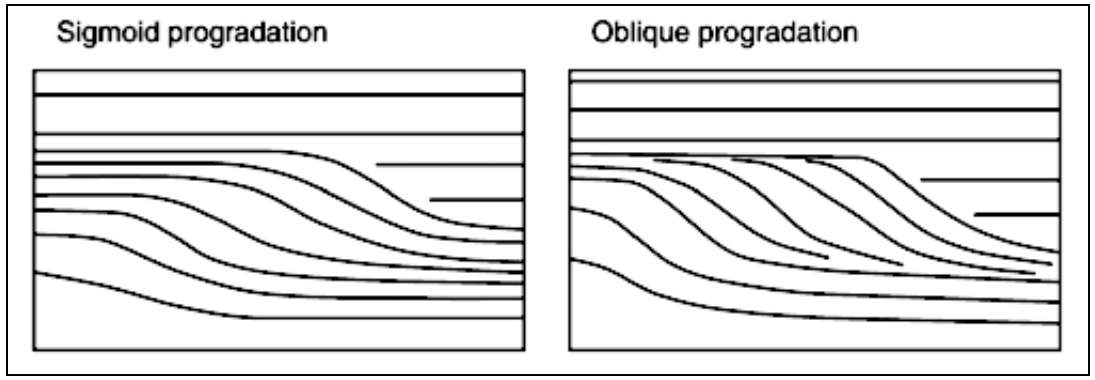

Figure 12. Two different geometries of prograding systems: sigmoidal and oblique. A sigmoidal geometry implies positive accommodation space on the shelf, whereas an oblique geometry indicates little or no accommodation during progradation (from Catuneanu et al., 2009).

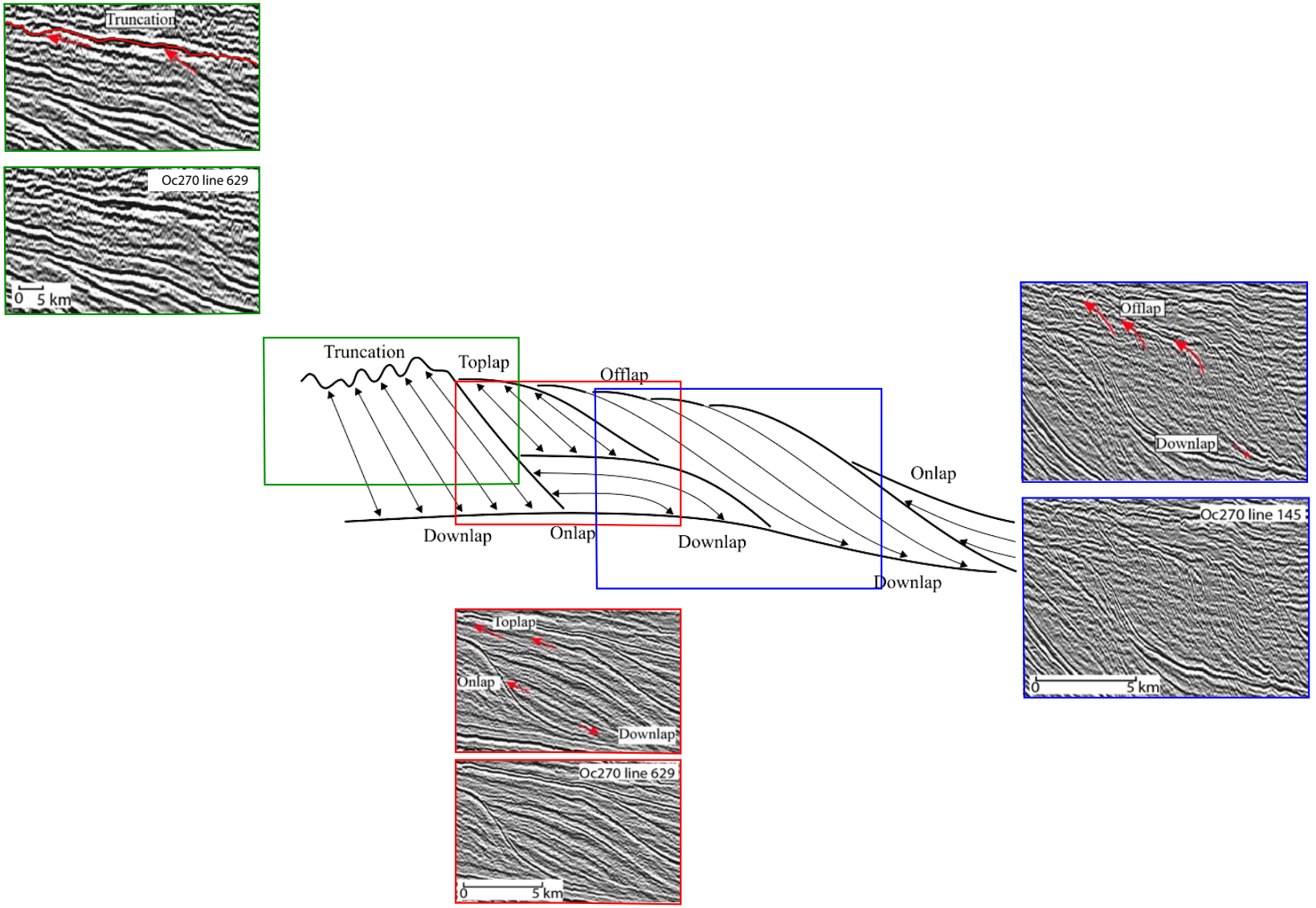

Figure 13. Examples of basic types of reflection terminations (erosional truncation, onlap, downlap, and toplap) highlighted with red arrows on Oc270 lines 145 and 629. Each seismic profile is outlined with its corresponding outline box (green, red, blue) in the diagram. Uninterpreted versions are shown below each profile (modified from Catuneanu et al., 2009).

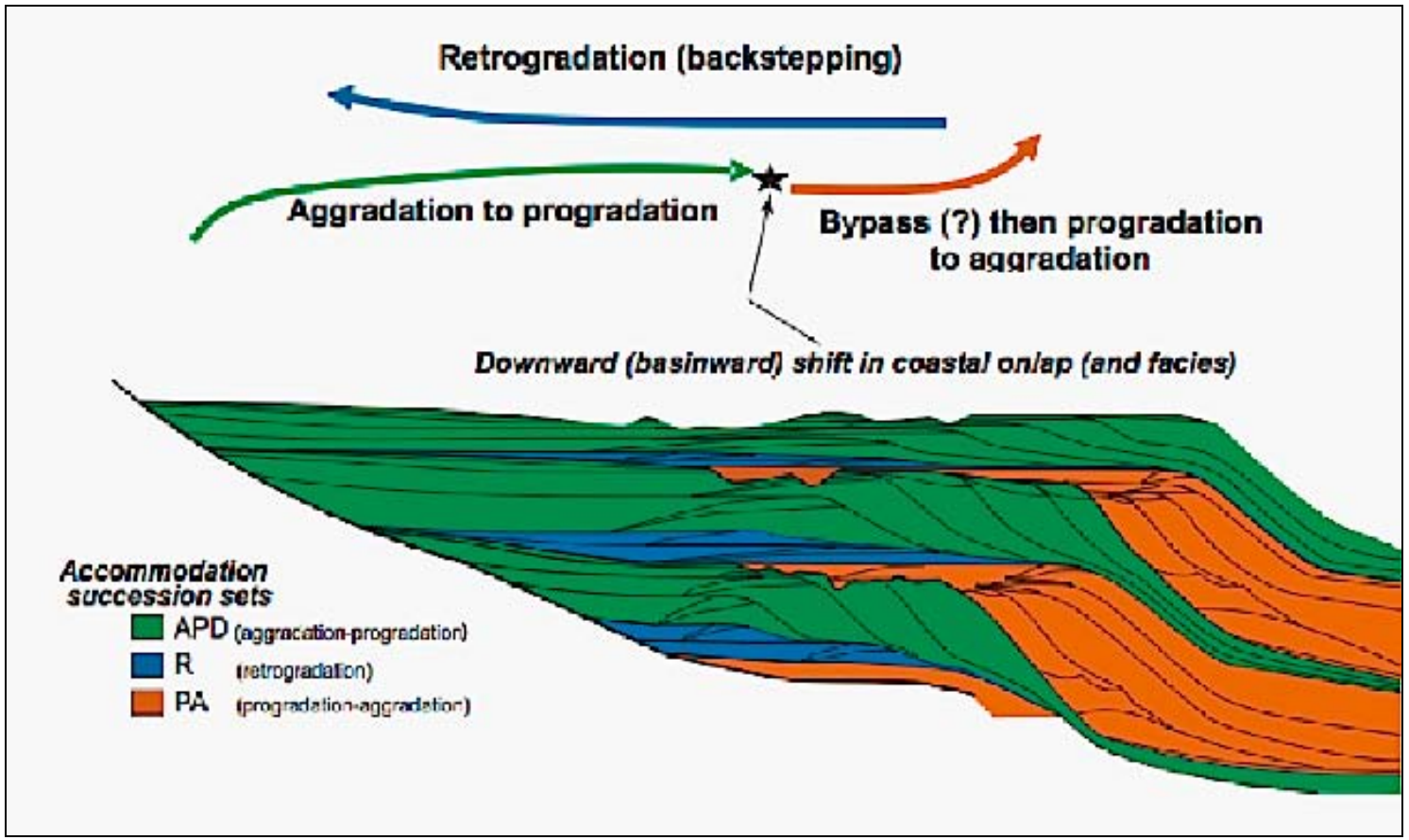

Figure 14. Stacking patterns of three systems tracts. Lowstand systems tract (PA—progradation-aggradation); transgressive systems tract (R—retrogradation); highstand systems tract (APD—aggradation-progradation) (modified from Neal and Abreu, 2009).

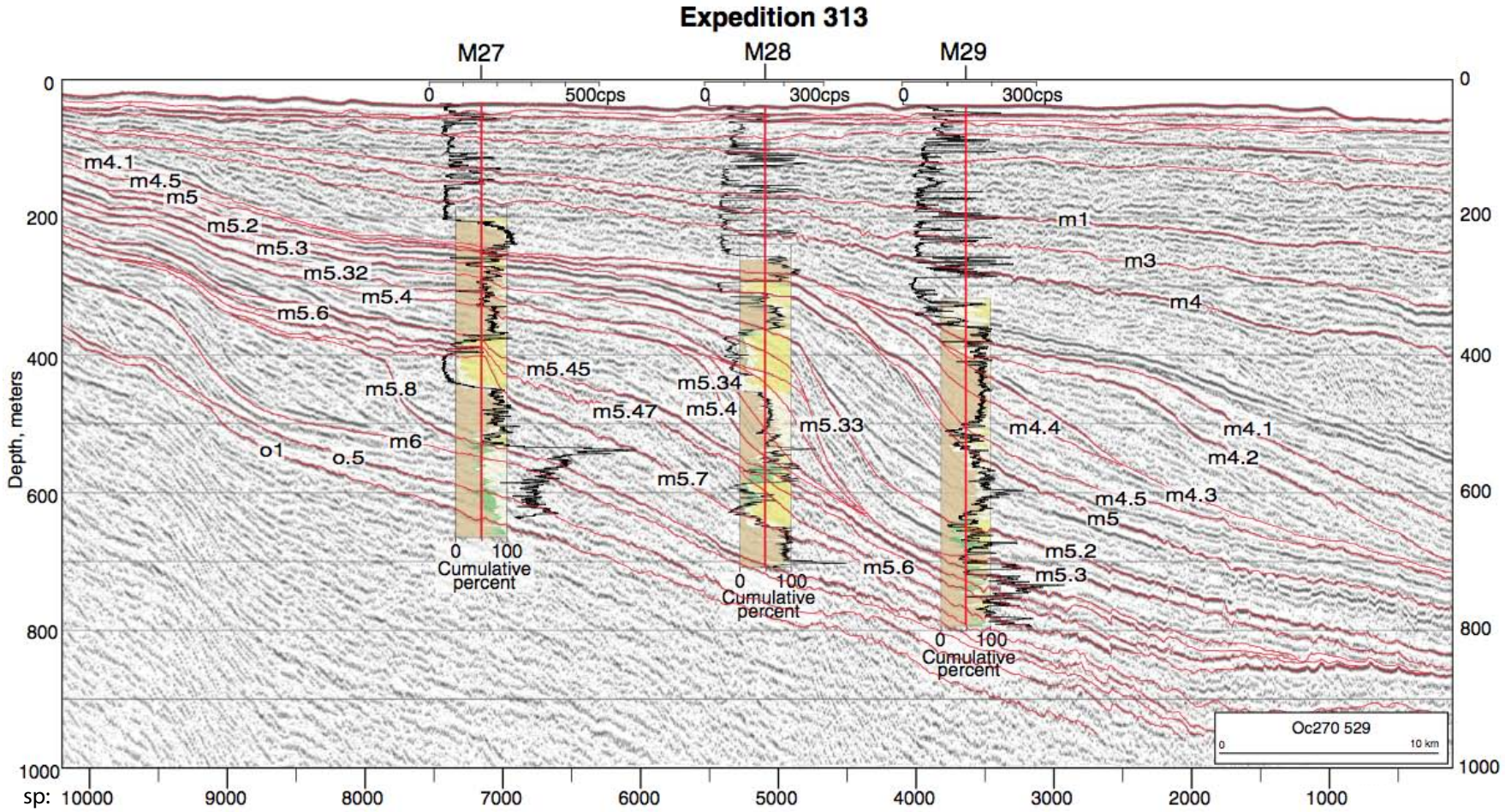

Figure 15. Multichannel seismic profile Oc270 629 with sites M27-M29 in region of Integrated Ocean Drilling Program Expedition 313 (see Figure 1 for location). Vertical red lines show locations of sites. Axes are two-way travel time (TWTT) in seconds versus cmp (labeled incorrectly as "sp"). Scale is given on lower right in km. Seismic sequence boundaries are shown in red. The coarse fraction cumulative percent lithology and gamma logs (in counts per second, cps) are superimposed at each site (modified from Miller et al., 2013).

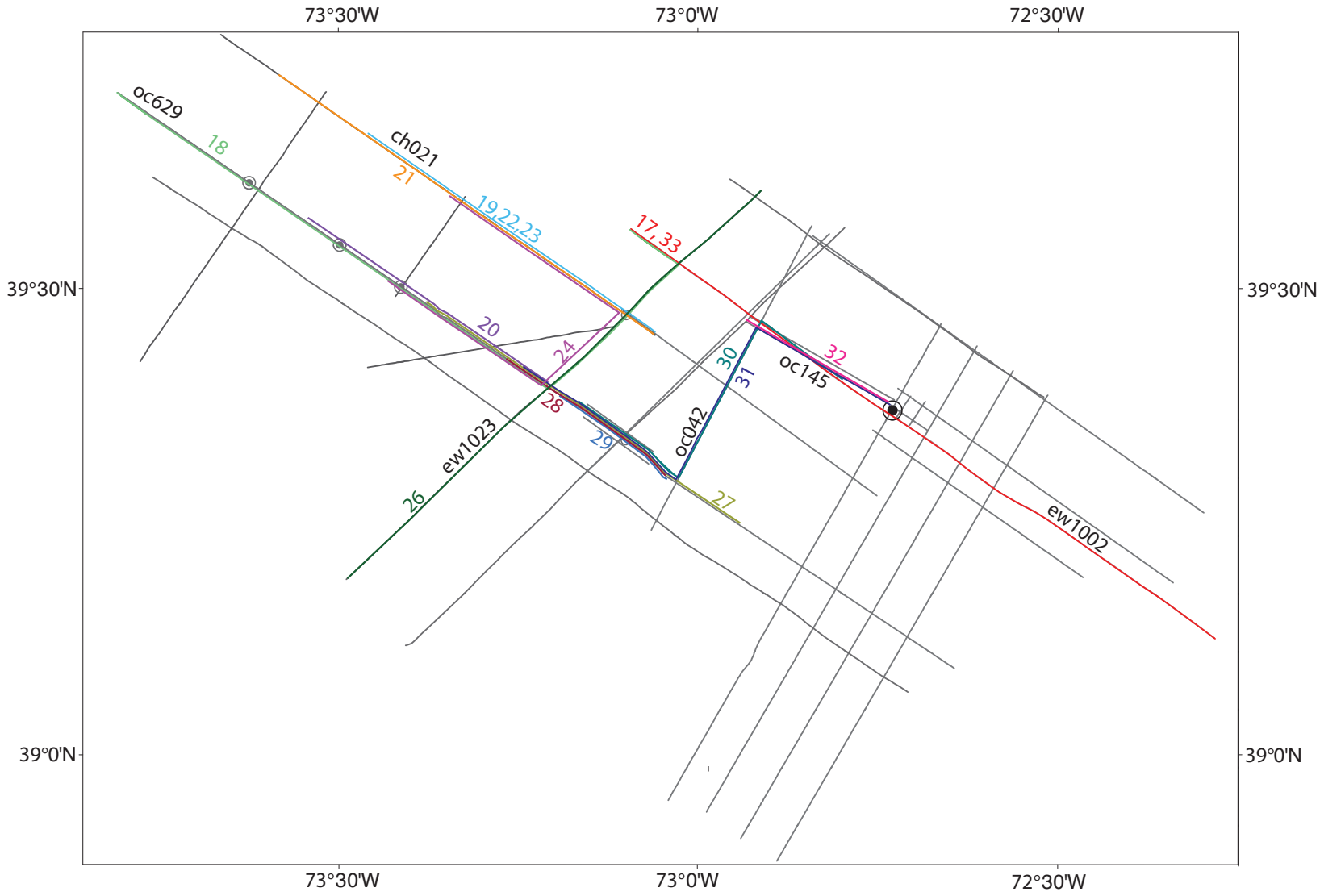

Figure 16. Map showing the locations of seismic profiles illustrated in Figures 17-33. Numbers adjacent to lines indicate figure numbers. Each figure is highlighted in a different color. Black fonts show the seismic profile names.

17A

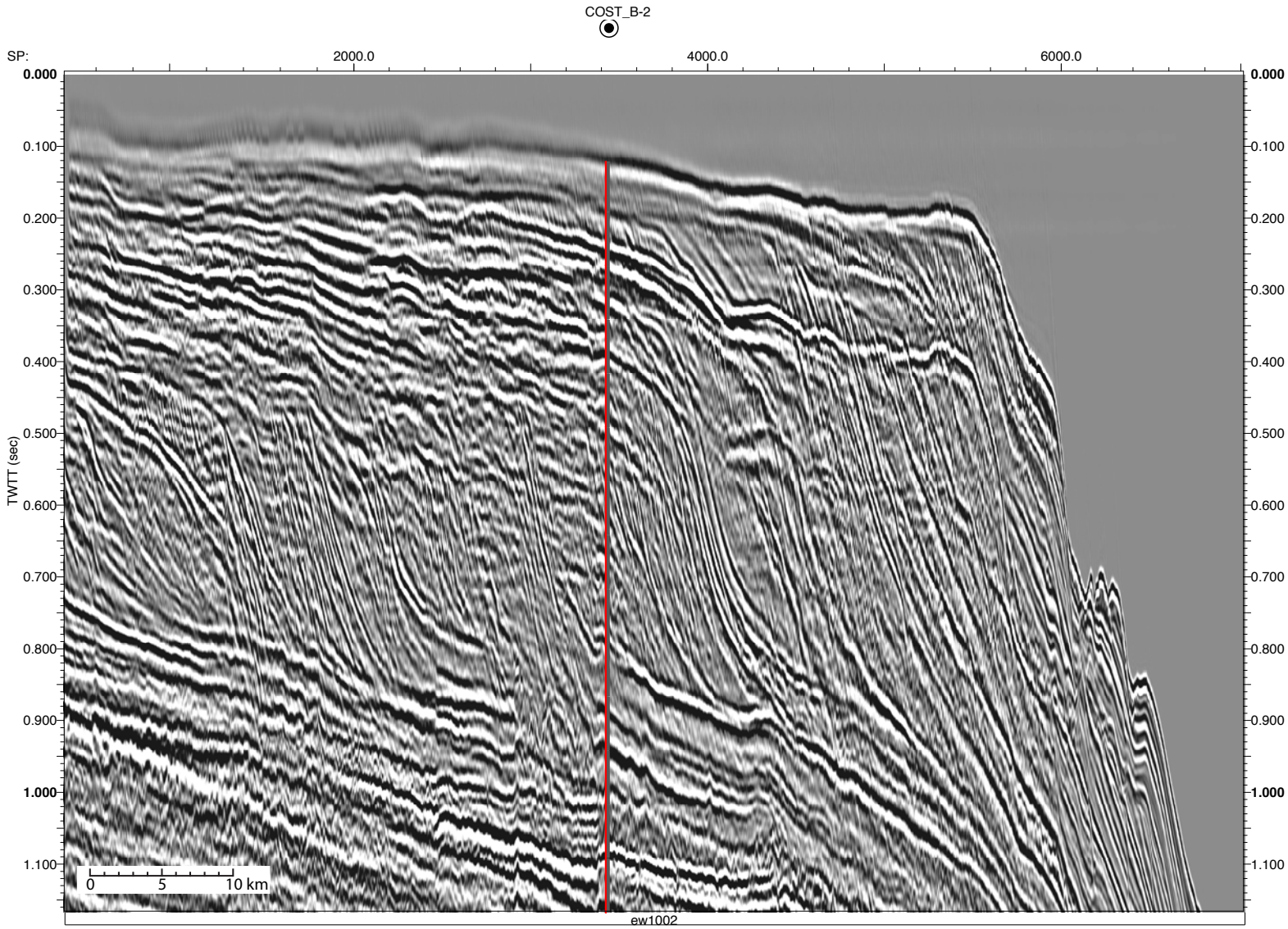
COST_B-2
SP:
2000.0
4000.0
6000.0
0.000
0.100
0.200
0.300
0.400
0.500
0.600
0.700
0.800
0.900
1.000
1.100
TWTT (sec)
0
5
10 km
ew1002

17B

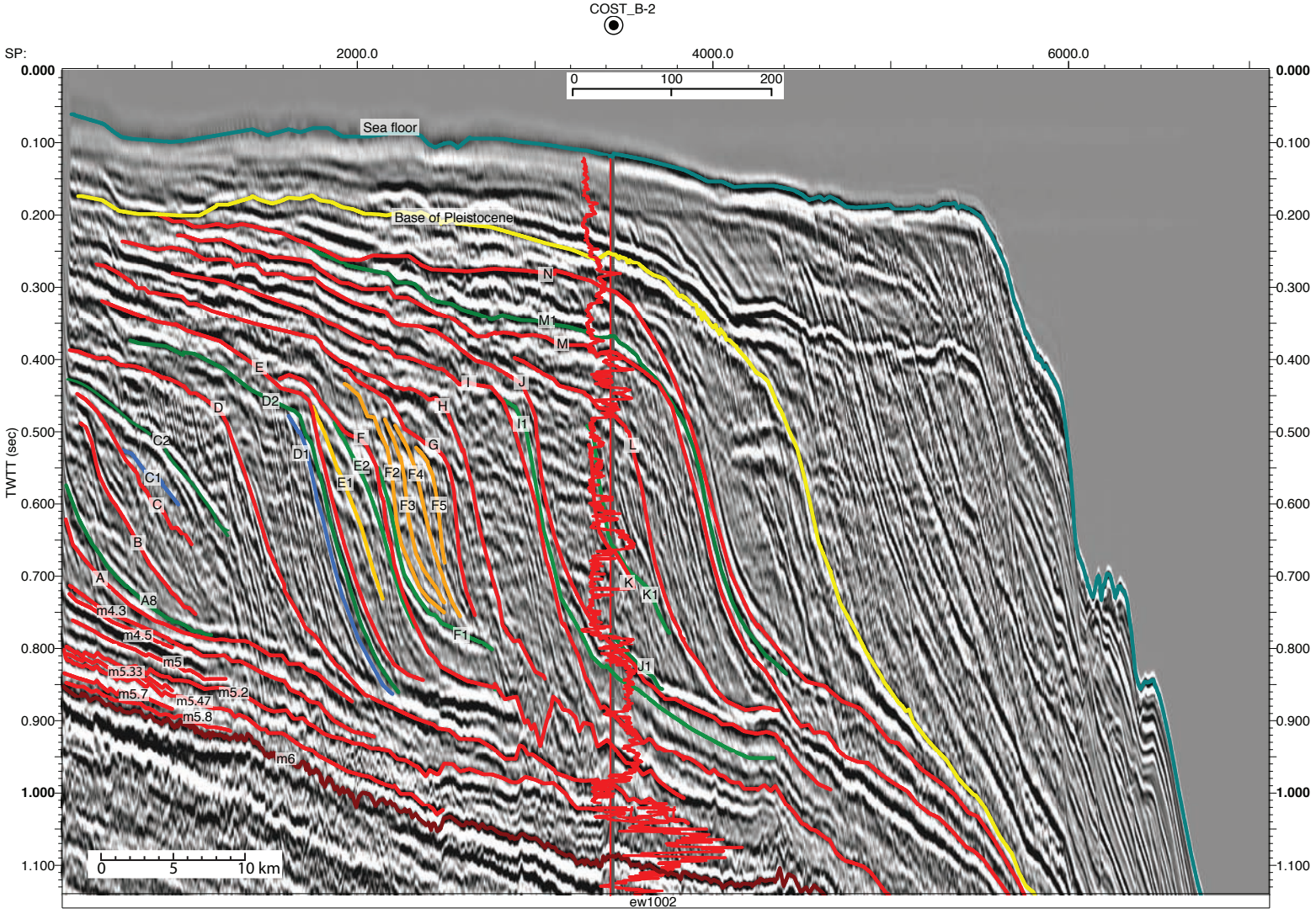
COST_B-2
SP:
2000.0
4000.0
6000.0
0
100
200
Sea floor
Base of Pleistocene
N
M1
M
E
D
D2
C2
C1
C
B
A
A8
m4.3
m4.5
m5
m5.33
m5.7
m5.47
m5.2
m5.8
m6
I
J
H
I1
F
G
D1
E2
E1
F2
F4
F3
F5
F1
L
K
K1
J1
0
5
10 km
ew1002
TWTT (sec)
0.000
0.100
0.200
0.300
0.400
0.500
0.600
0.700
0.800
0.900
1.000
1.100

17C

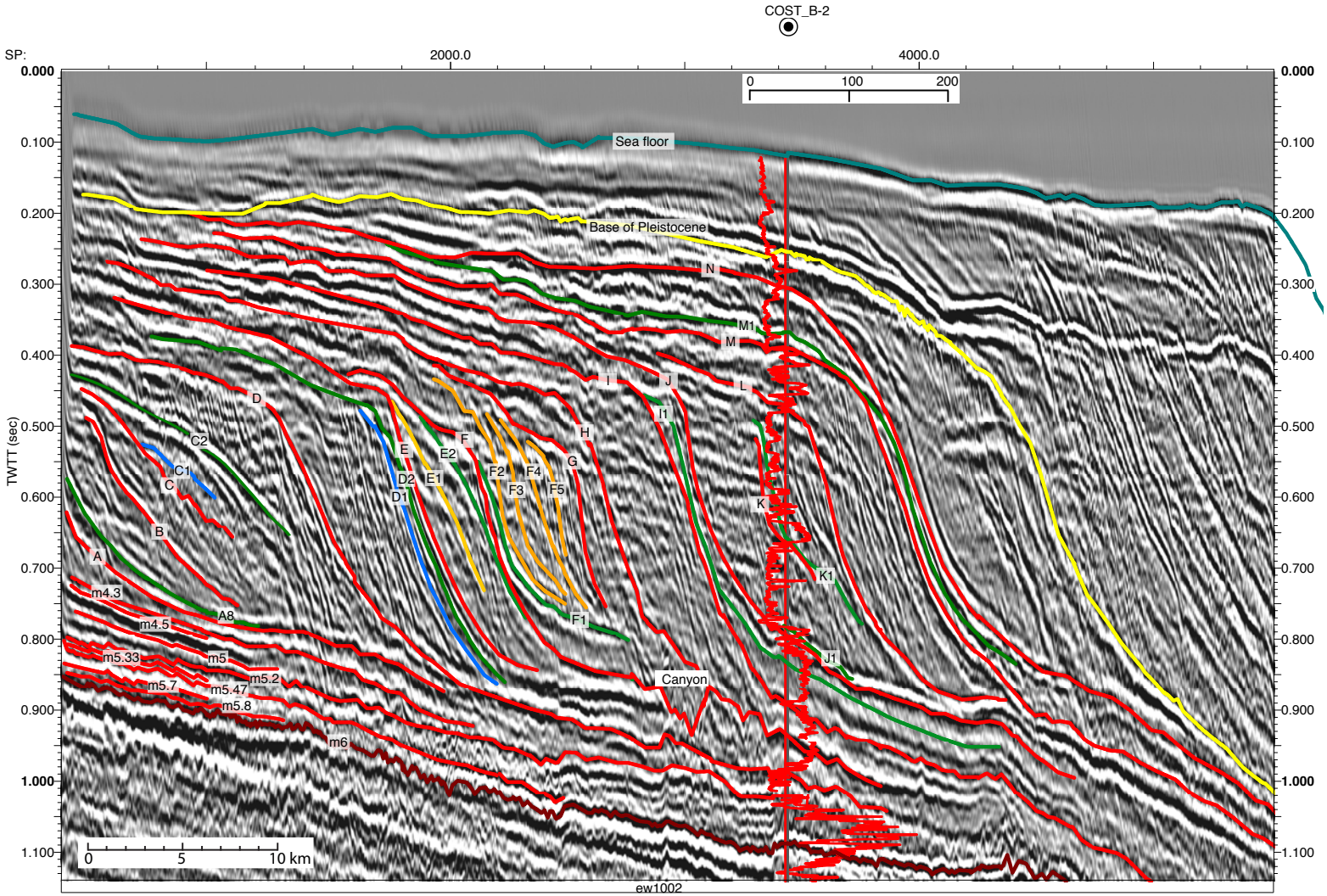

Figure 17. (A) Uninterpreted seismic profile of Ew9009 1002; (B) Interpreted seismic profile of Ew9009 1002 with Cost B2 site (see Figure 16 for location). Vertical red line shows location of the site. Gamma-ray log is superimposed on the site. Axes are two-way travel time (TWTT) in seconds versus common-mid point (cmp; labeled incorrectly as "sp" on the axis). Scale is given on lower left in km. Seismic line names are at the bottom of the profile. Reflectors in red indicate sequence boundaries; reflectors in blue indicate the transgressive surfaces (TS); and reflectors in green indicate the maximum flooding surfaces (MFS). Other internal reflections are indicated in shades of yellow. Base of Miocene (m6) and base of Pleistocene reflections are colored in burgundy and yellow, respectively; (C) Interpreted seismic profile of Ew9009 1002 with a different aspect ratio than (A). A submarine canyon (labeled) is associated with sequence boundary F at the toe of the sequence. Caption as in (B).

18A

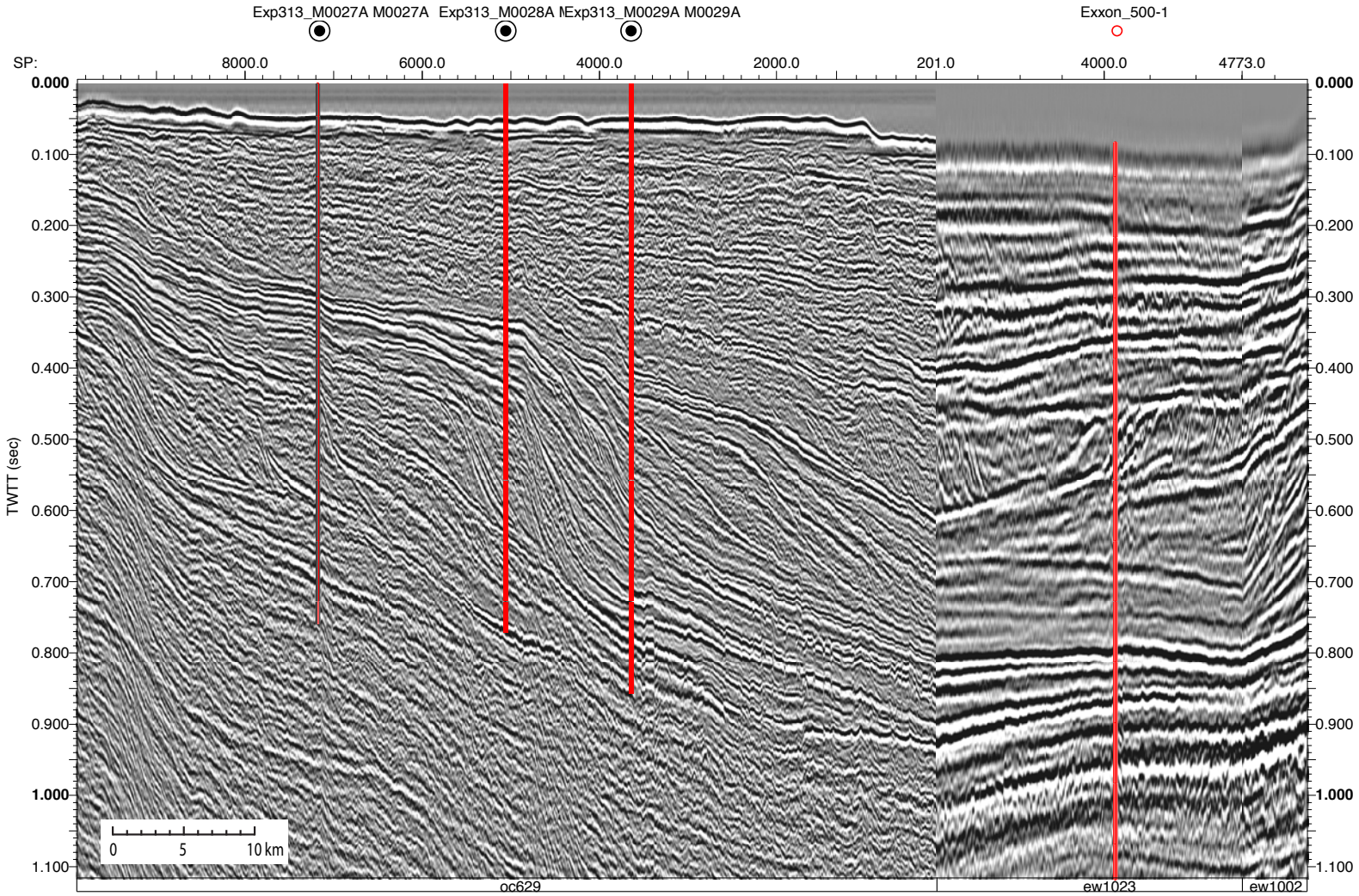
Exp313_M0027A M0027A
Exp313_M0028A M0028A
Exp313_M0029A M0029A
Exxon_500-1
SP:
8000.0
6000.0
4000.0
2000.0
201.0
4000.0
4773.0
TWTT (sec)
0.000
0.100
0.200
0.300
0.400
0.500
0.600
0.700
0.800
0.900
1.000
1.100
0
5
10 km
oc629
ew1023
ew1002

18B

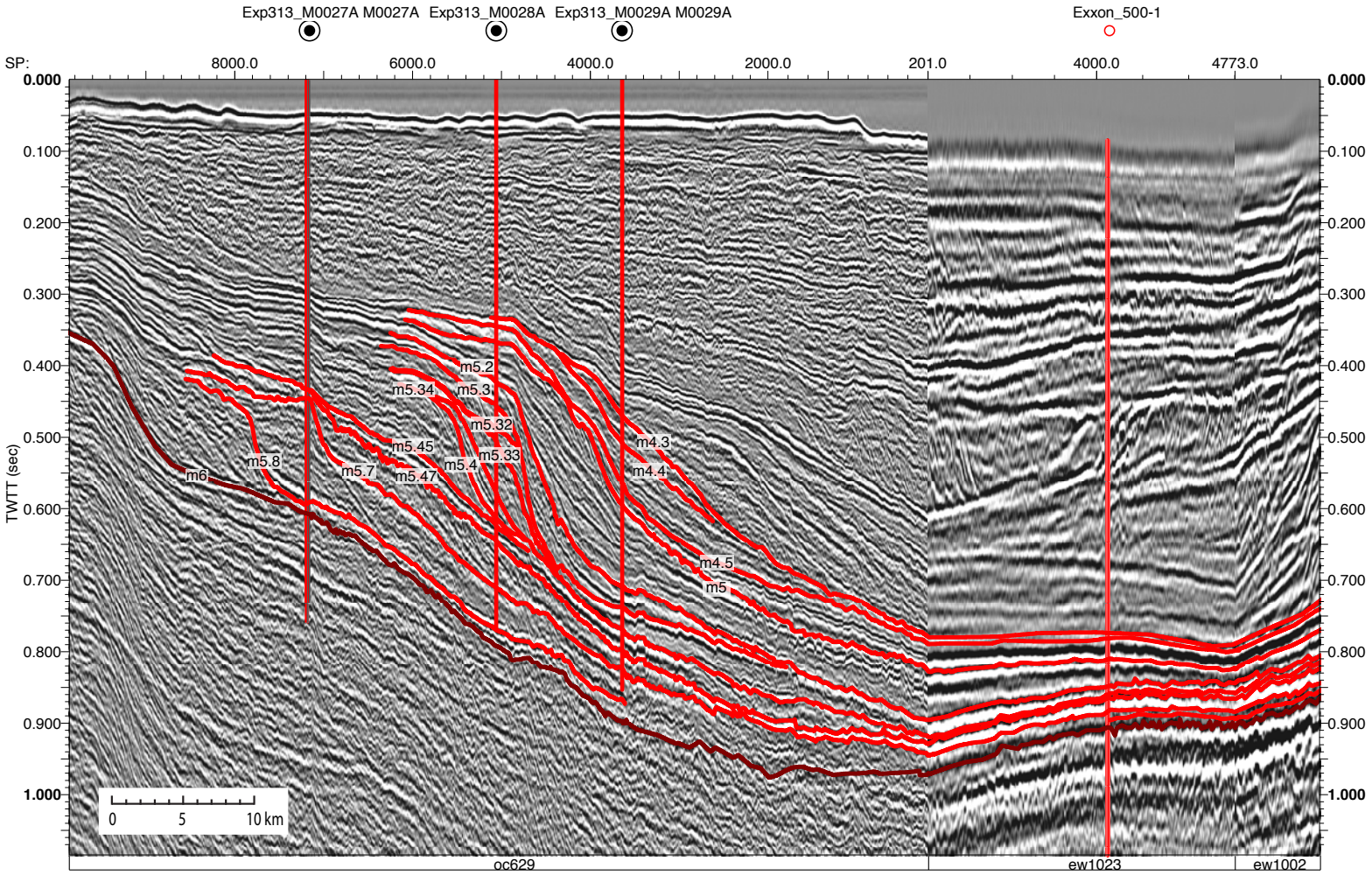

Figure 18. (A) Uninterpreted version of intersection of seismic lines Oc270 629, Ew9009 1023 and 1002; (B) Interpreted version of intersection of seismic lines Oc270 629, Ew9009 1023 and 1002 showing sequence boundaries between m6 and m4.3 (see Figure 16 for location). Sites M27–M29 and Exxon 500-1 are located on this profile. Vertical red lines show locations of sites. Axes are two-way travel time (TWTT) in seconds versus common-mid point (cmp; labeled incorrectly as "sp" on the axis). Scale is given on lower left in km. Seismic line names are at the bottom of the profile. Reflectors in red indicate sequence boundaries.

19A

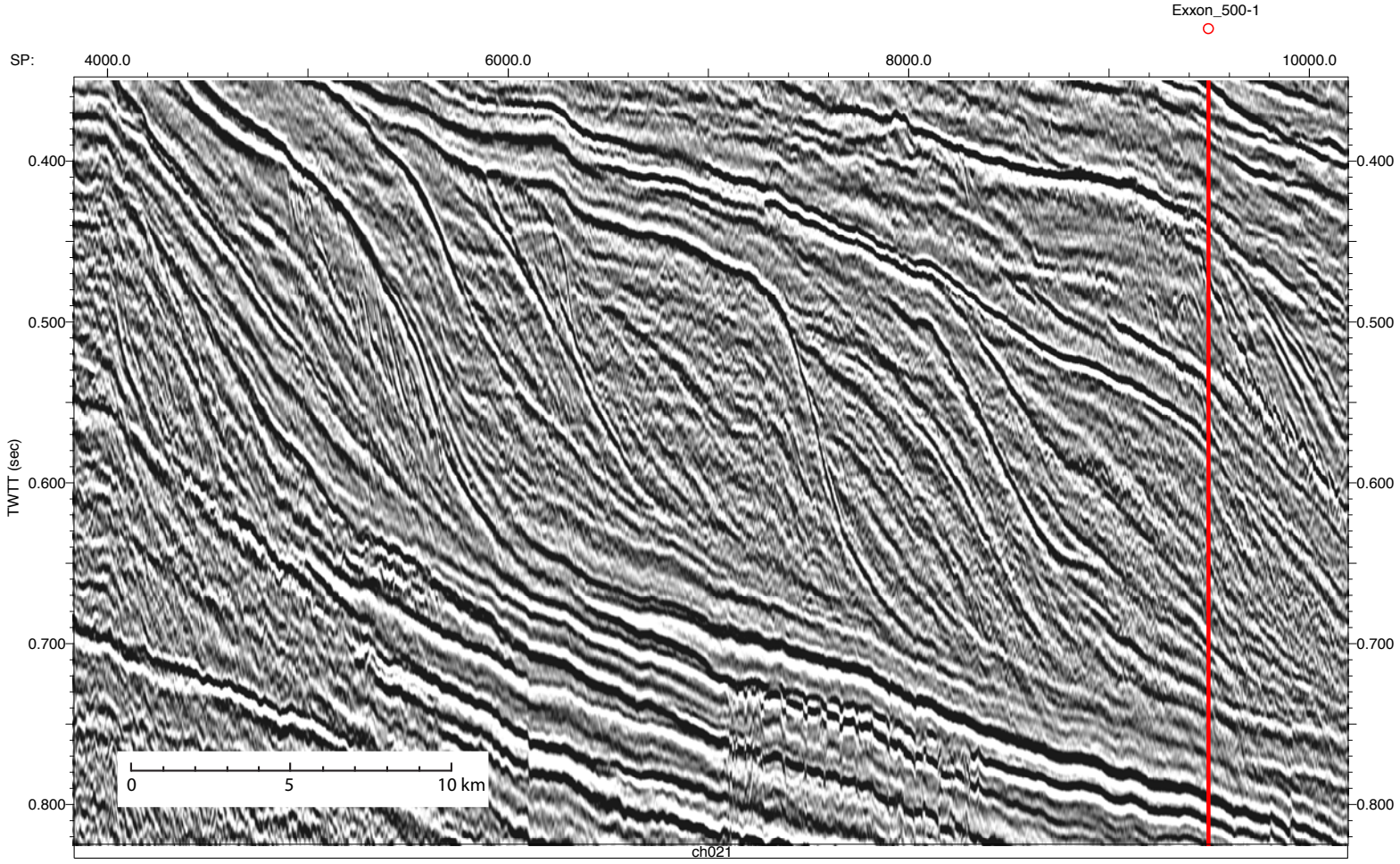
Exxon_500-1
SP:
4000.0
6000.0
8000.0
10000.0
0.400
0.500
0.600
0.700
0.800
TWTT (sec)
0
5
10 km
ch021

19B

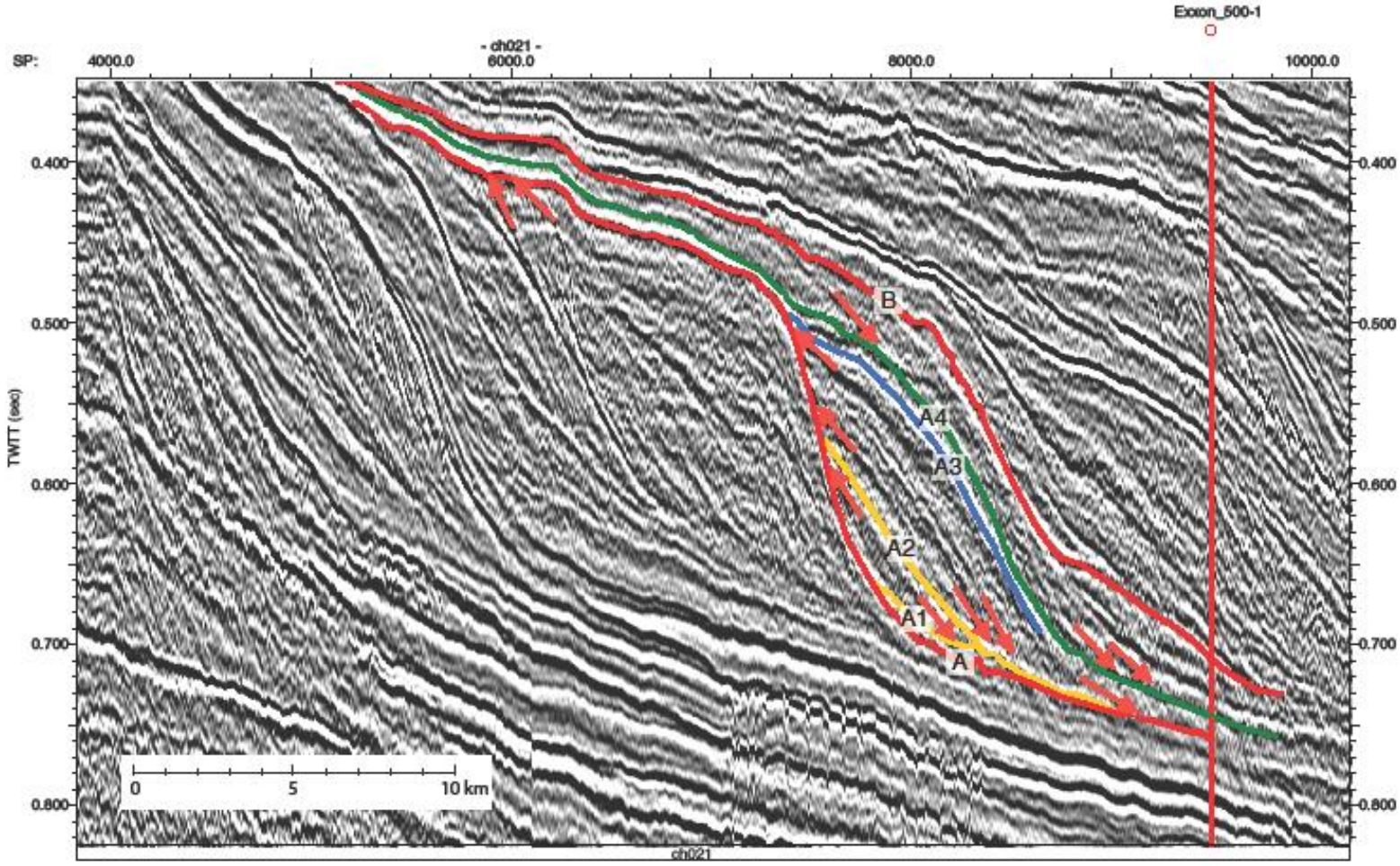
Exxon_500-1
SP:
4000.0
- ch021 -
6000.0
8000.0
10000.0
0.400
0.500
0.600
0.700
0.800
TWTT (sec)
B
A4
A3
A2
A1
A
0
5
10 km
ch021

19C

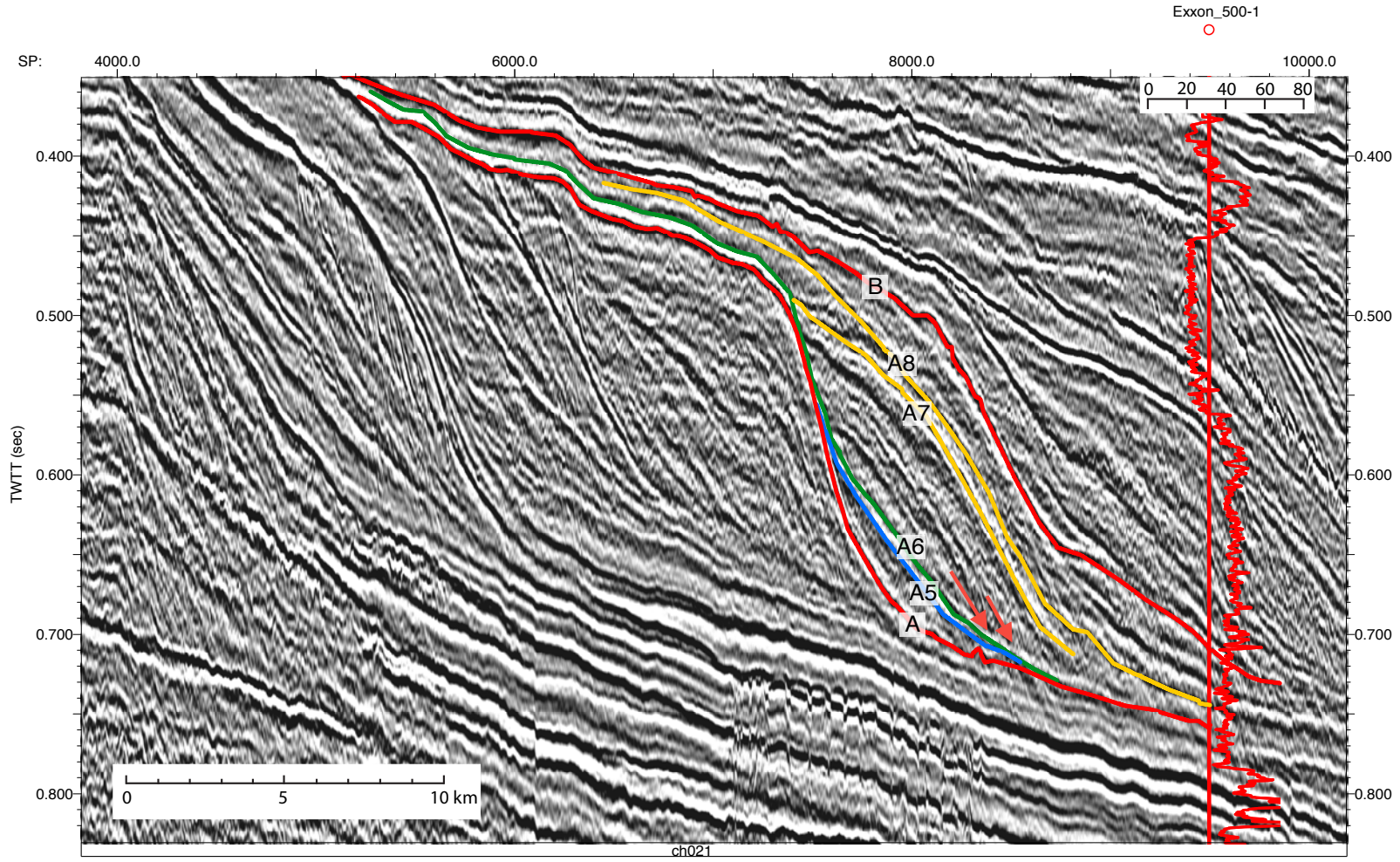

Figure 19. (A) Uninterpreted seismic profile of CH0698 21; (B) Interpreted seismic profile of CH0698 21 with Exxon 500-1 site showing the first interpretation of sequence A (see Figure 16 for location); (C) Interpreted seismic profile of CH0698 21 showing the second interpretation of sequence A (see Figure 16 for location). Red arrows indicate reflection terminations. Vertical red line shows location of the site. Axes are two-way travel time (TWTT) in seconds common-mid point (cmp; labeled incorrectly as "sp" on the axis). Scale is given on lower left in km. Seismic line names are at the bottom of the profile. Reflectors in red indicate sequence boundaries; reflectors in blue indicate the transgressive surfaces (TS); and reflectors in green indicate the maximum flooding surfaces (MFS). Other internal reflections are indicated in shades of yellow.

20A

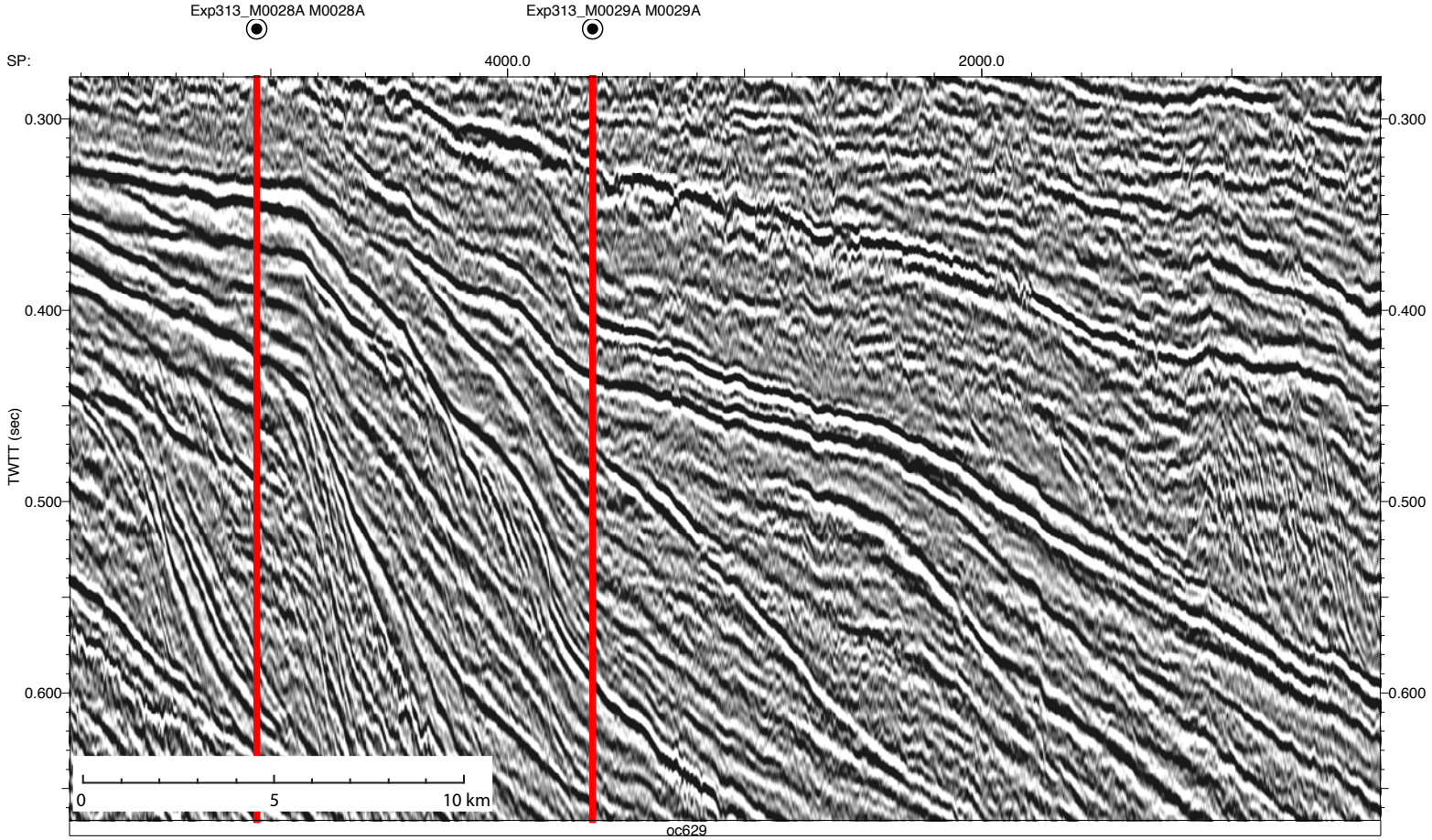
Exp313_M0028A M0028A
Exp313_M0029A M0029A
SP:
4000.0
2000.0
0.300
0.400
0.500
0.600
TWTT (sec)
0
5
10 km
oc629

20B

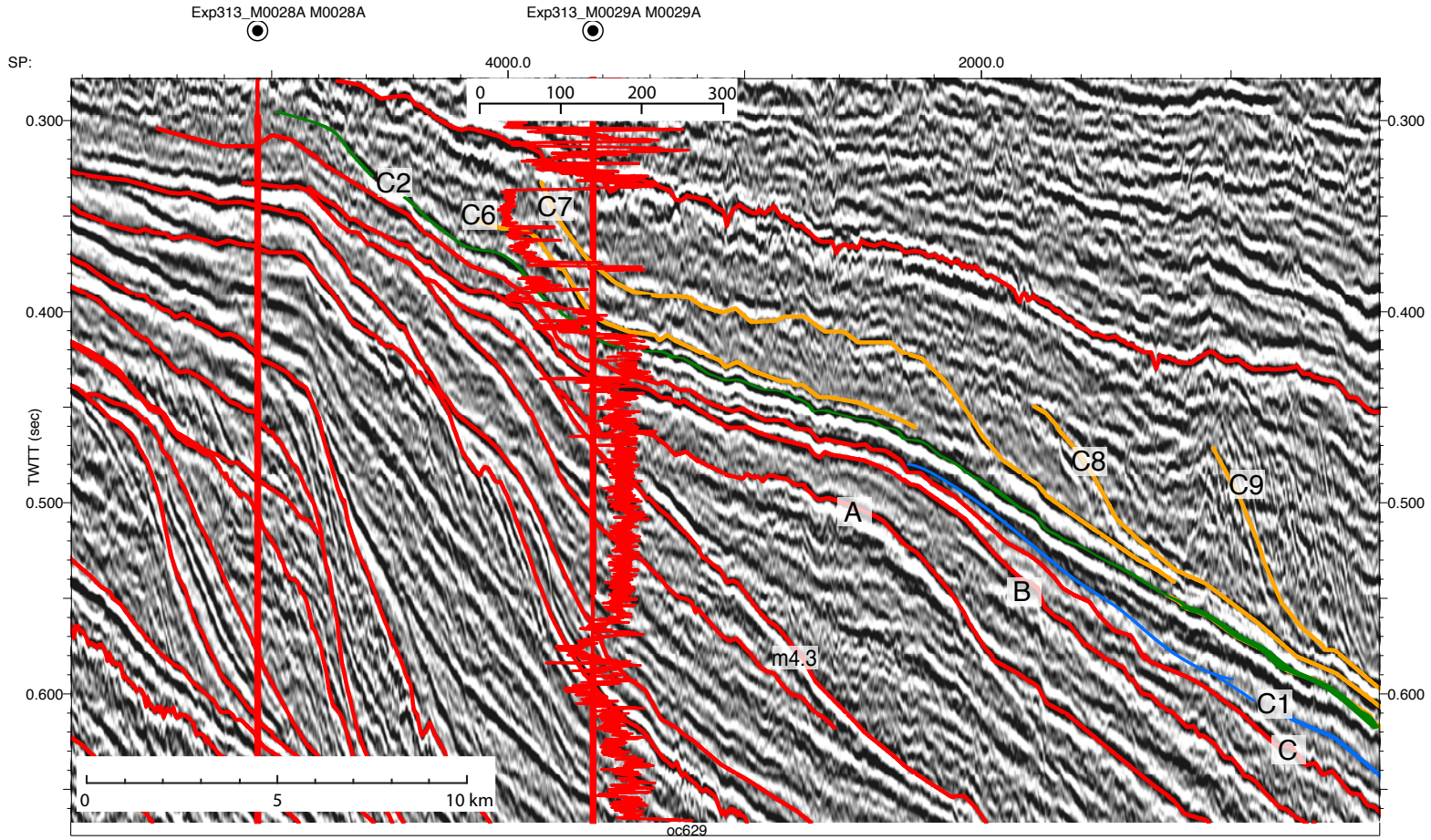

Figure 20. (A) Uninterpreted seismic profile of Oc270 629; (B) Interpreted seismic profile of Oc270 629 with sites M28 and M29 showing sequence boundary A, B, and C (see Figure 16 for location). Gamma-ray log is superimposed on the site M29. Sequence boundary A is associated with a small decrease in log value at 463 msec on the log curve. Sequence boundary B corresponds to a sharp decrease from higher to lower gamma ray values at 435 msec on the gamma-ray log curve. Immediately above the sequence boundary C the highest values in gamma corresponds to the MFS of Sequence C (reflector C2). Caption as in Figure 17B.

21A

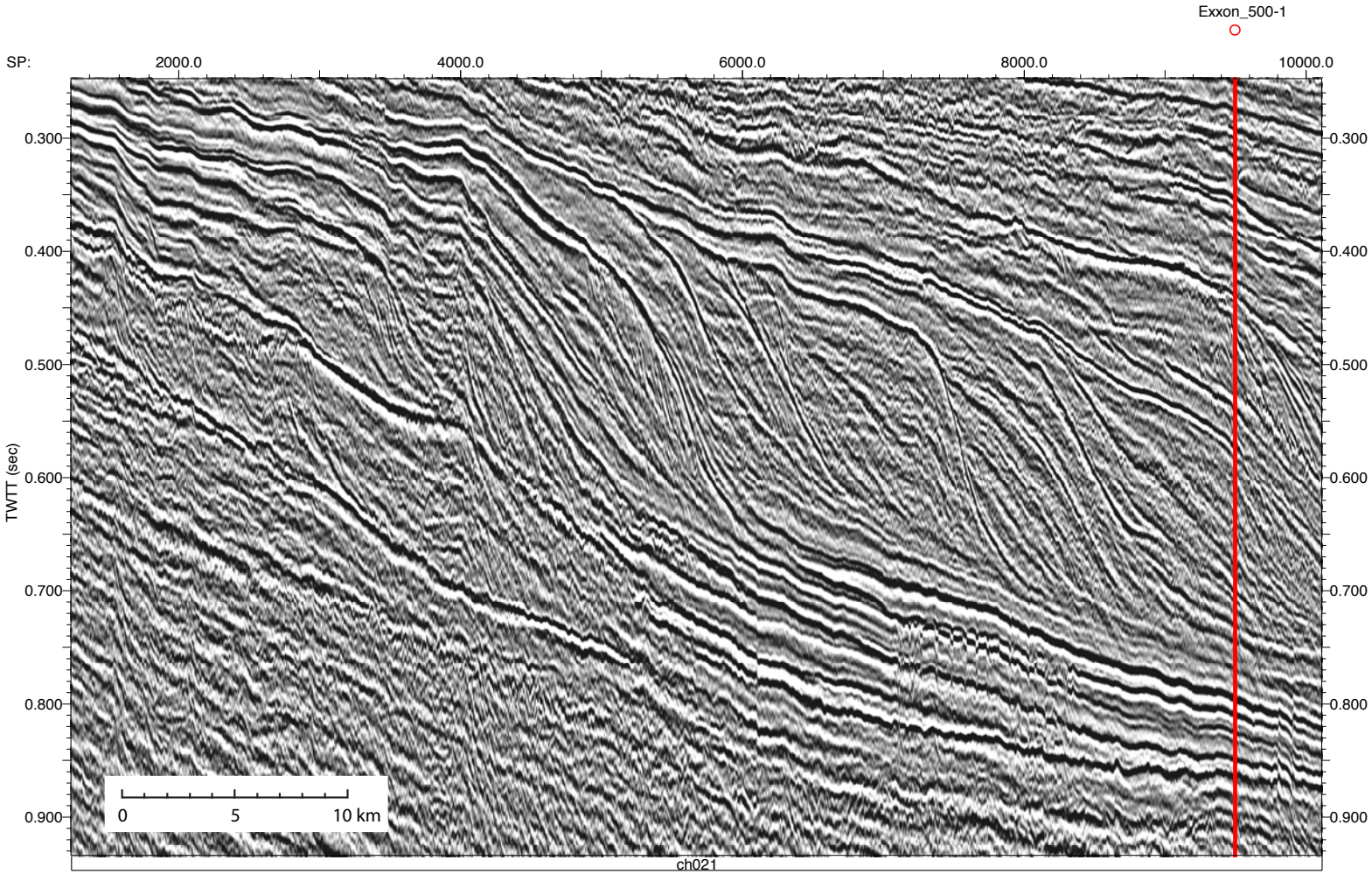
Exxon_500-1
SP:
2000.0
4000.0
6000.0
8000.0
10000.0
0.300
0.400
0.500
0.600
0.700
0.800
0.900
TWTT (sec)
0
5
10 km
ch021

21B

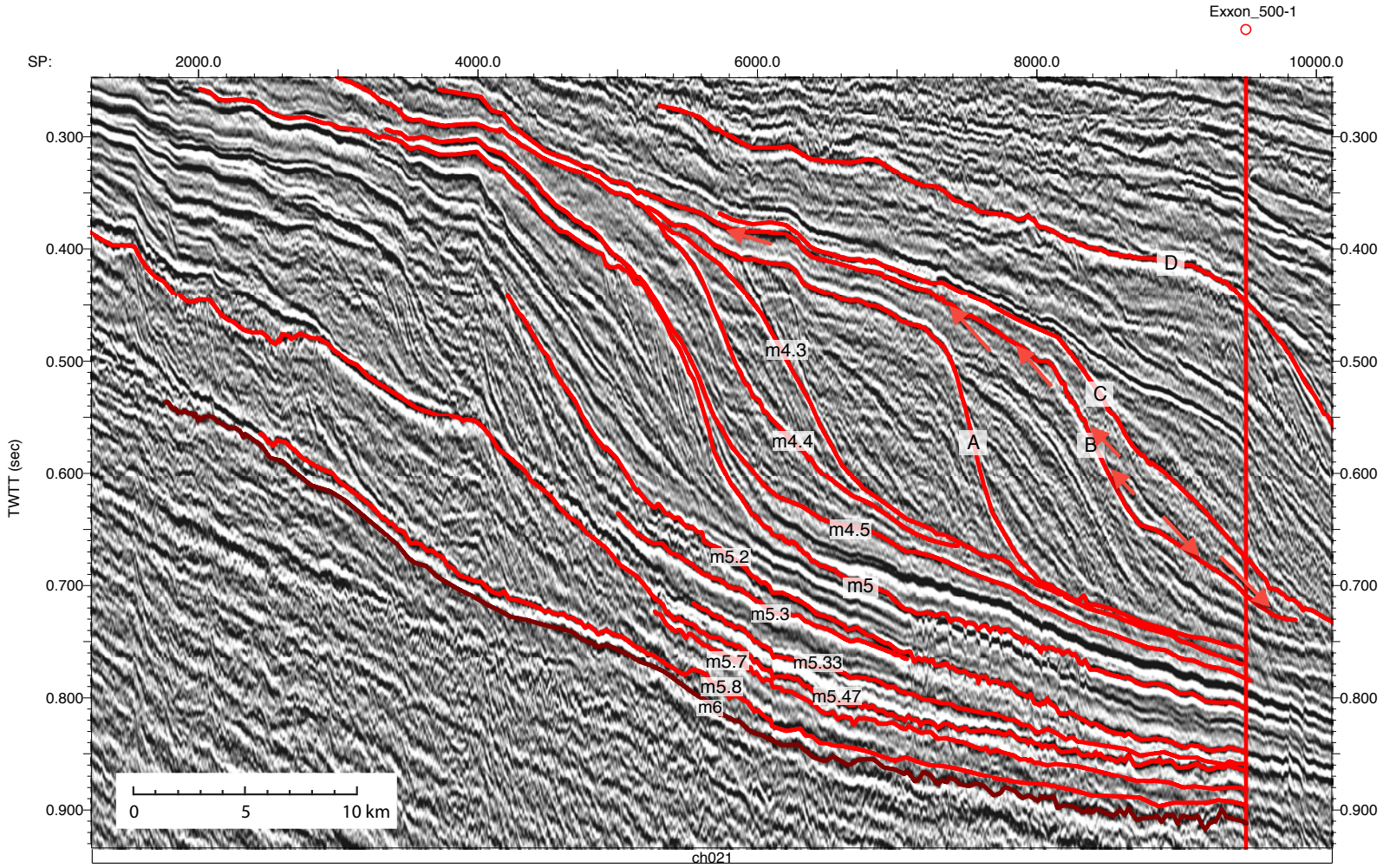

Figure 21. (A) Uninterpreted seismic profile of CH0698 21; (B) Interpreted seismic profile of CH0698 21 with Exxon 500-1 site showing sequence B and reflection terminations associated with sequence boundary B (see Figure 16 for location). Red arrows indicate reflection terminations. Caption as in Figure 18B.

22A

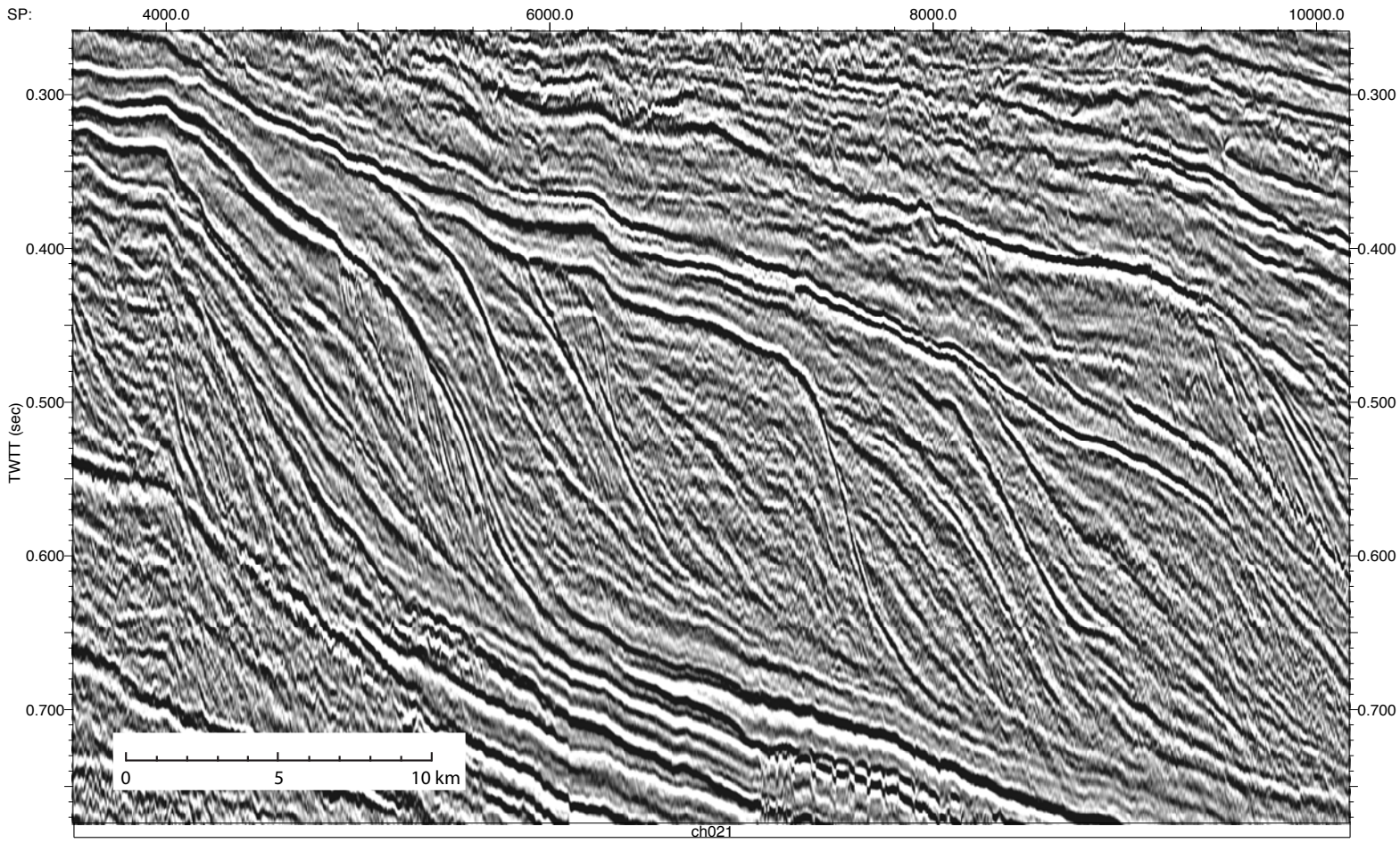
SP:
4000.0
6000.0
8000.0
10000.0
0.300
0.400
0.500
0.600
0.700
TWTT (sec)
0
5
10 km
ch021

22B

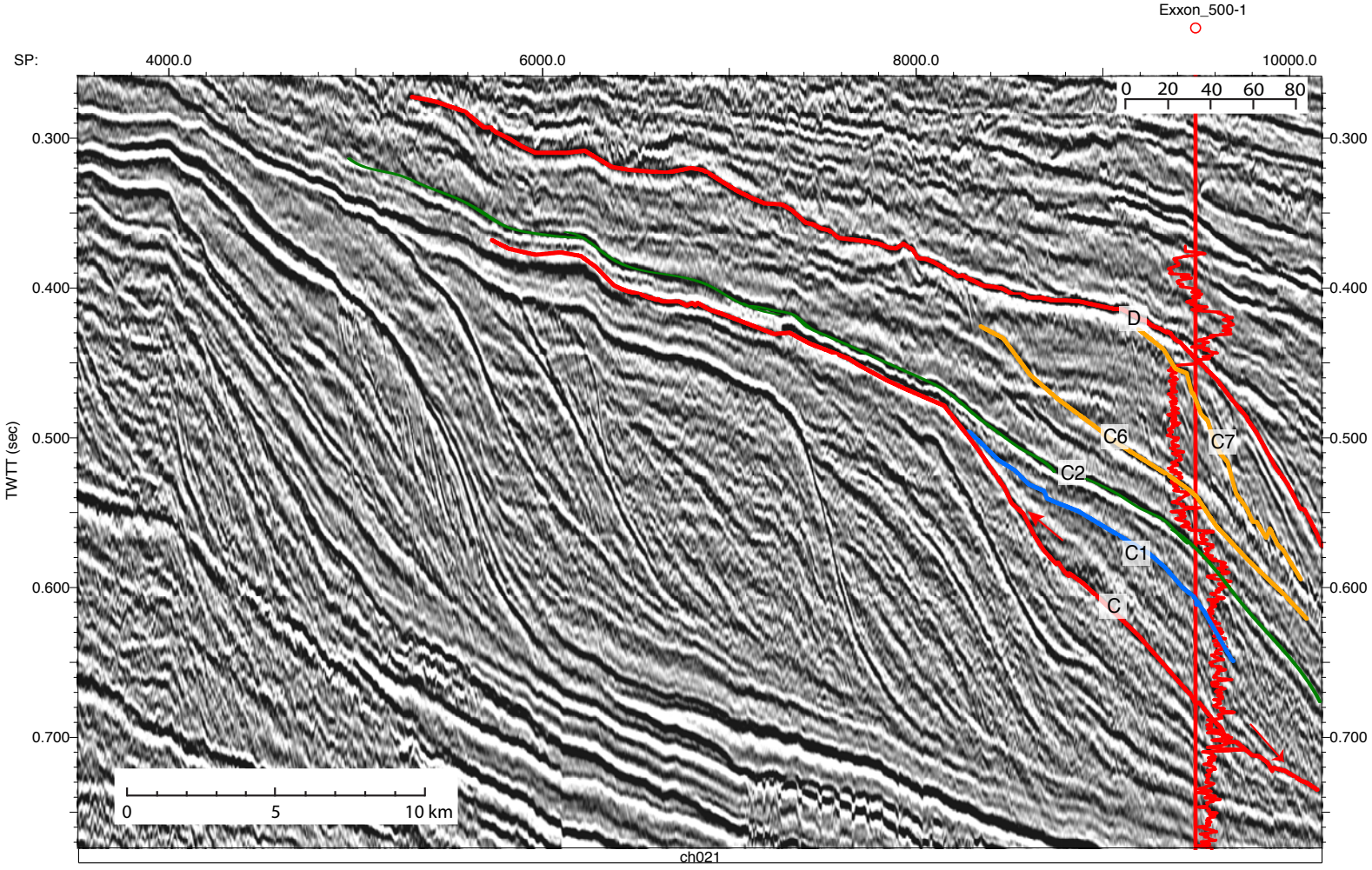

Figure 22. (A) Uninterpreted seismic profile of CH0698 21; (B) Interpreted seismic profile of CH0698 21 with Exxon 500-1 site showing sequence C and reflection terminations associated with sequence boundary C (see Figure 16 for location). Red arrows indicate reflection terminations. Caption as in Figure 19C.

23A

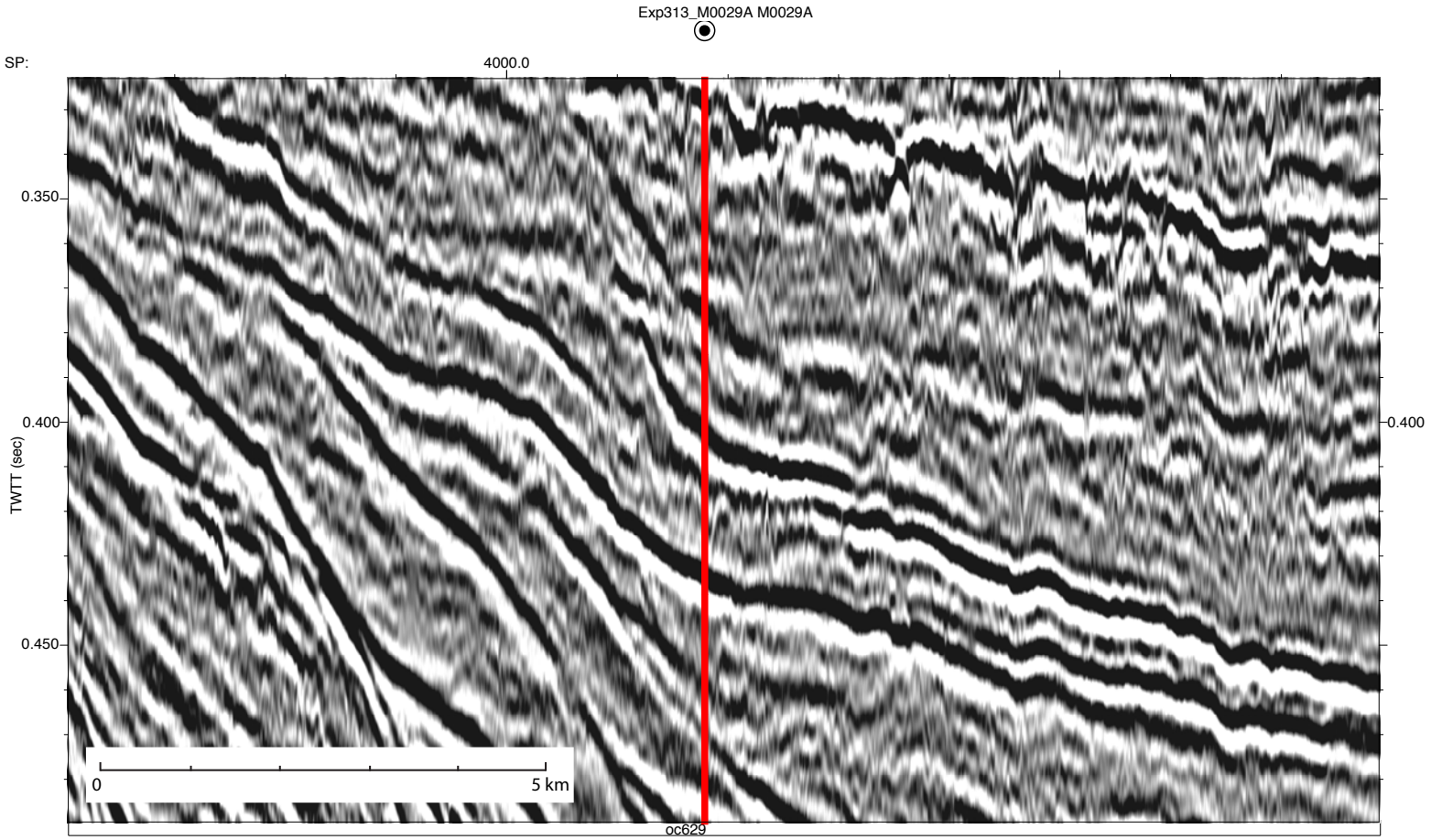
Exp313_M0029A M0029A
SP:
4000.0
0.350
0.400
0.450
TWTT (sec)
0.400
0
5 km
oc629

23B

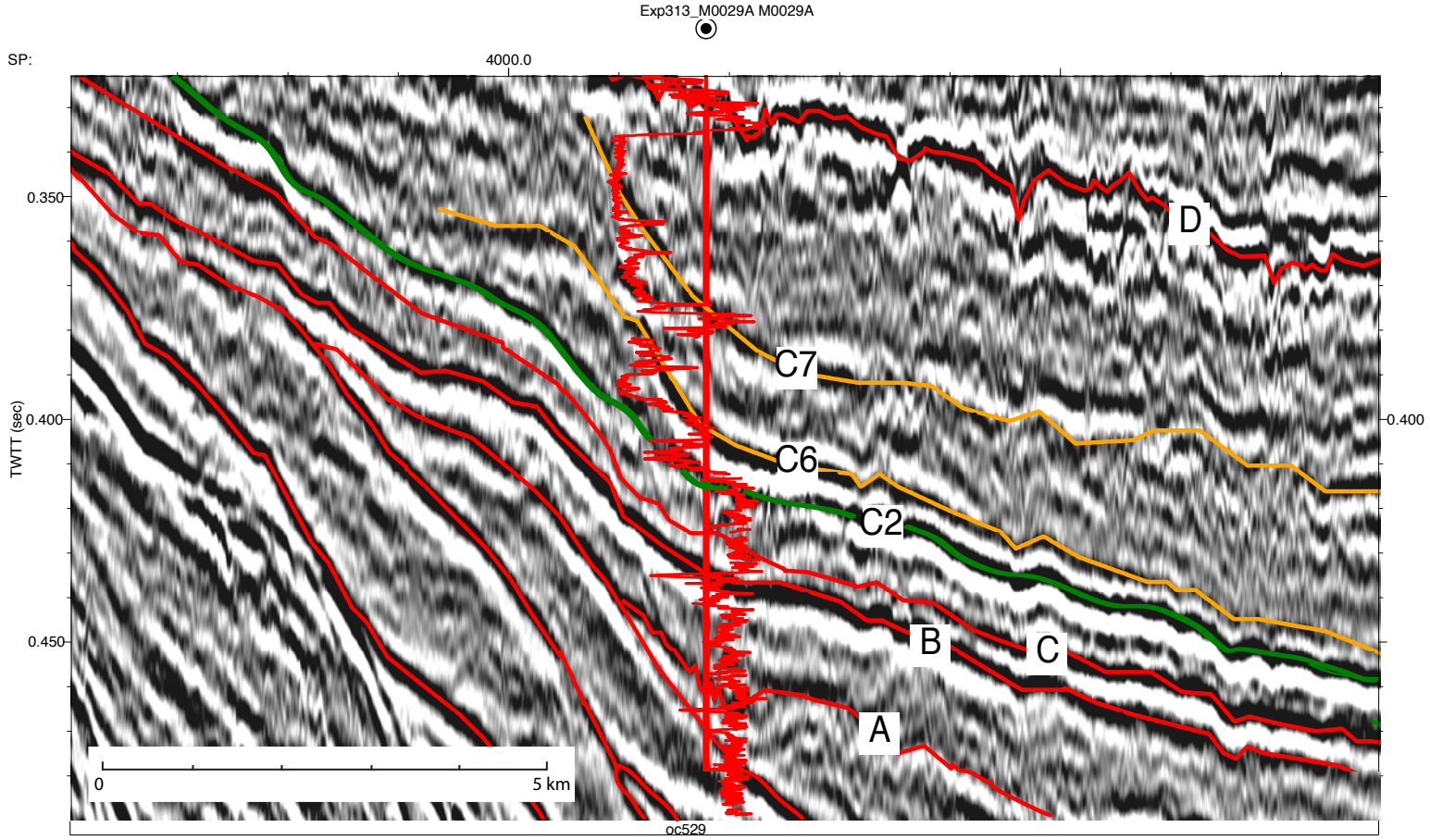
Exp313_M0029A M0029A
SP:
4000.0
0.350
0.400
0.450
TWTT (sec)
0.400
D
C7
C6
C2
B
C
A
0
5 km
oc529

23C

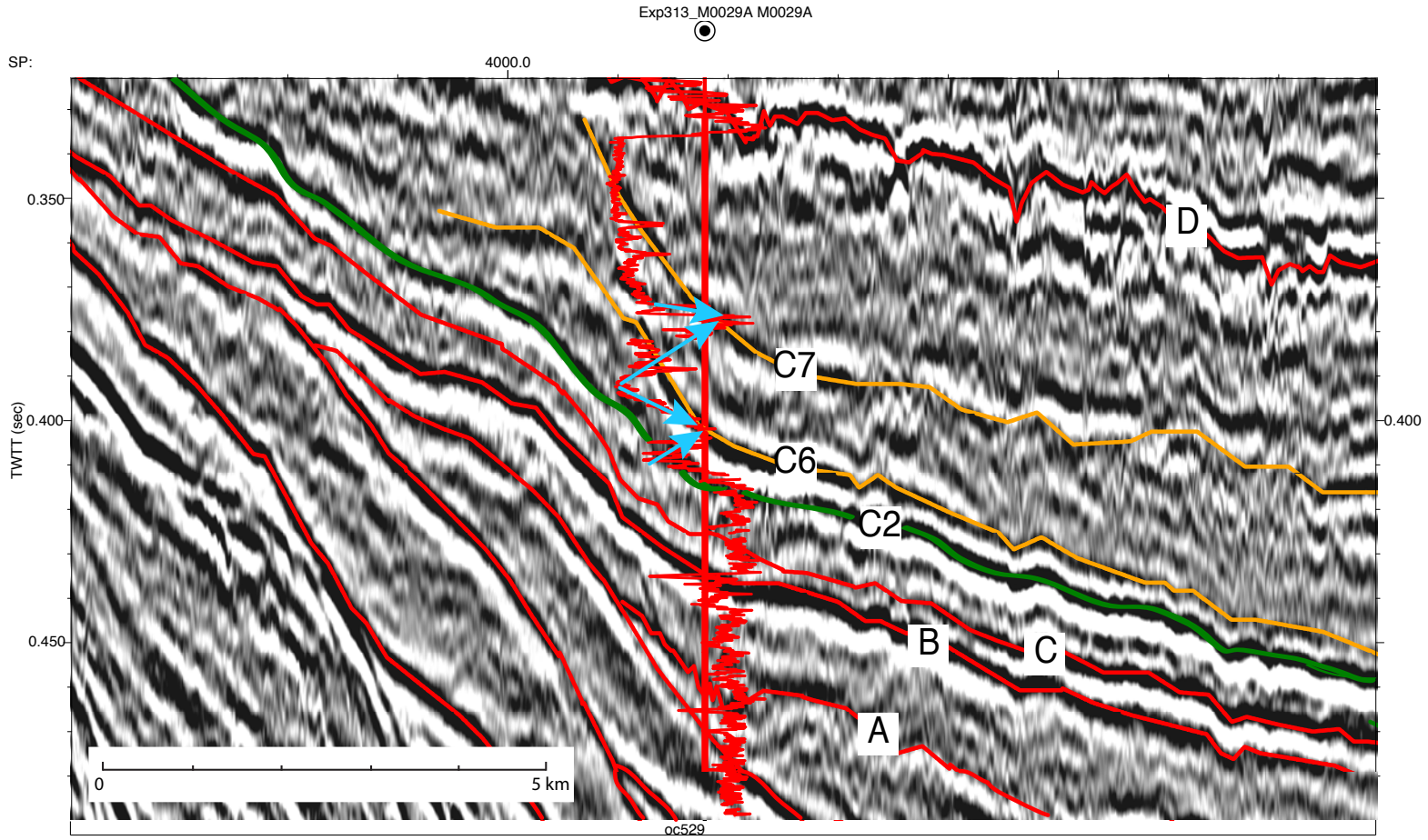

Figure 23. (A) Uninterpreted version of enlargement of sequence C at site M29 on Oc270 629; (B) Interpreted version of enlargement of sequence C at site M29 on Oc270 629; (C) Interpreted gamma-ray log at site M29 showing sequence C. Blue arrows point in inferred fining direction. Converging arrows indicate the two flooding sequences (FS; parasequence boundaries). Caption as in Figure 17B.

24A

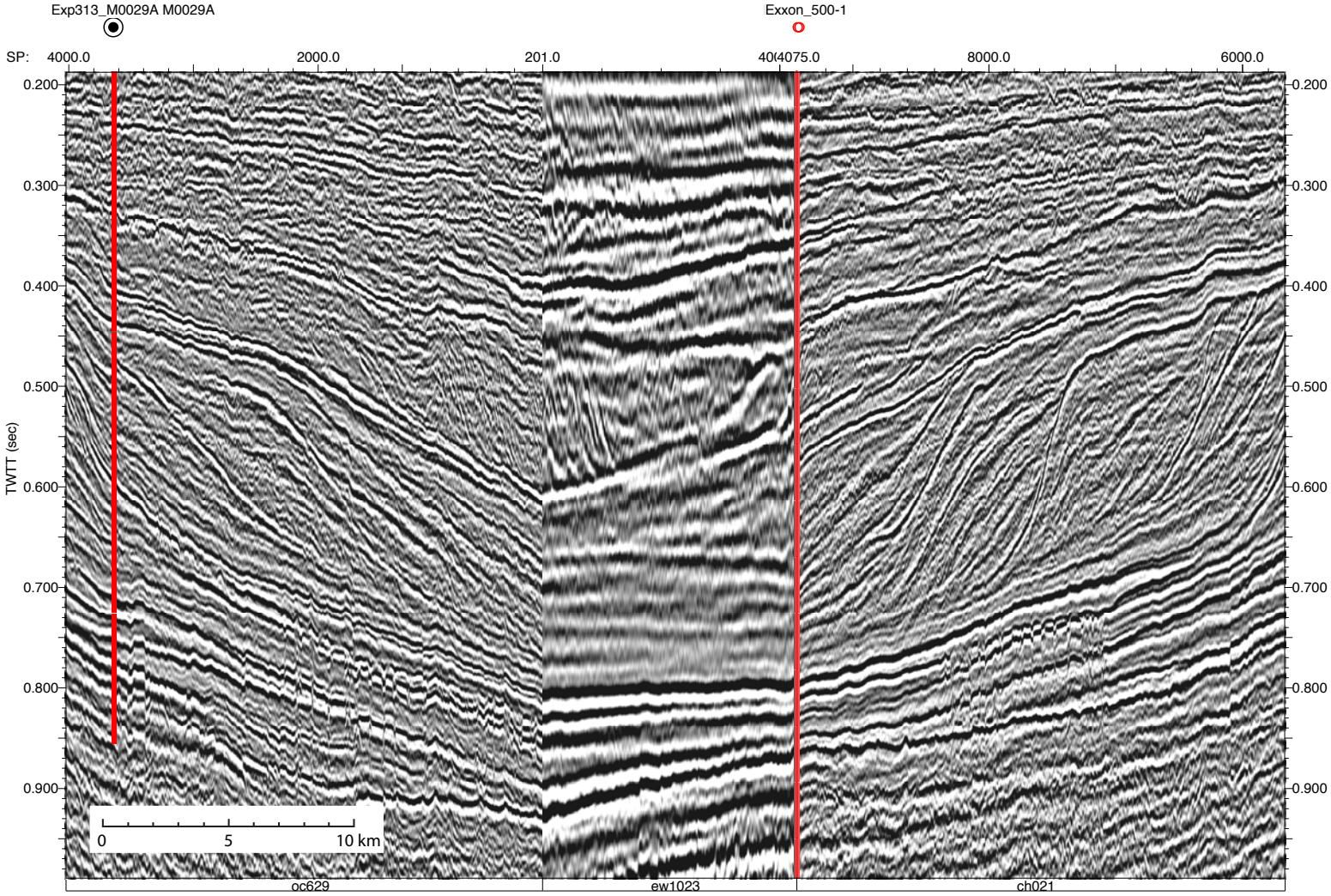
Exp313_M0029A M0029A
Exxon_500-1
SP:
4000.0
2000.0
201.0
40(4075.0
8000.0
6000.0
TWTT (sec)
0.200
0.300
0.400
0.500
0.600
0.700
0.800
0.900
0
5
10 km
oc629
ew1023
ch021

24B

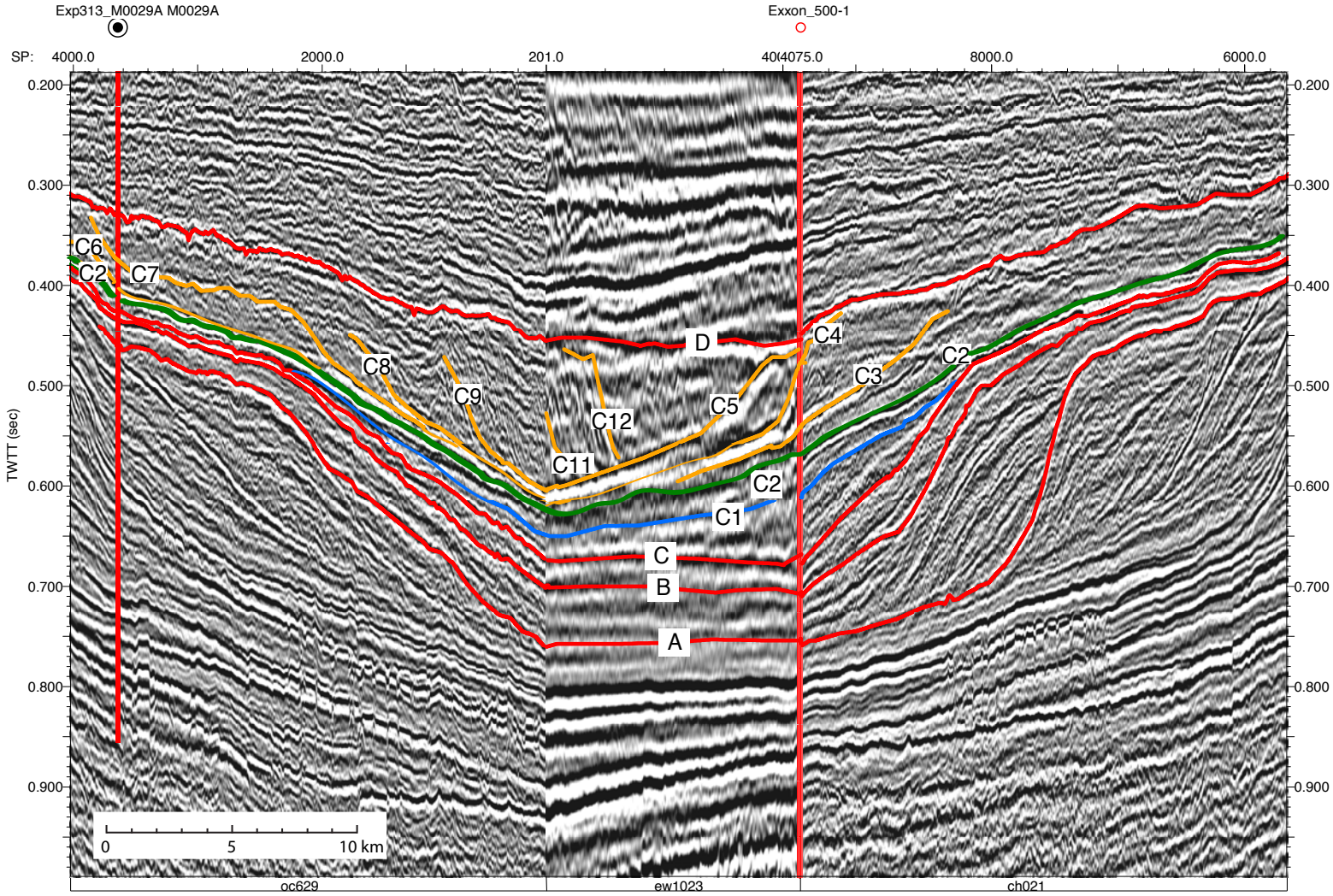

Figure 24. (A) Uninterpreted version of intersection of seismic lines Oc270 629, Ew9009 1023, and CH0698 21; (B) Interpreted version of intersection of seismic lines Oc270 629, Ew9009 1023, and CH0698 21 showing highstand deposits of sequence C (see Figure 16 for location). Sites M29 and Exxon 500-1 are located on this profile. Caption as in Figure 20C.

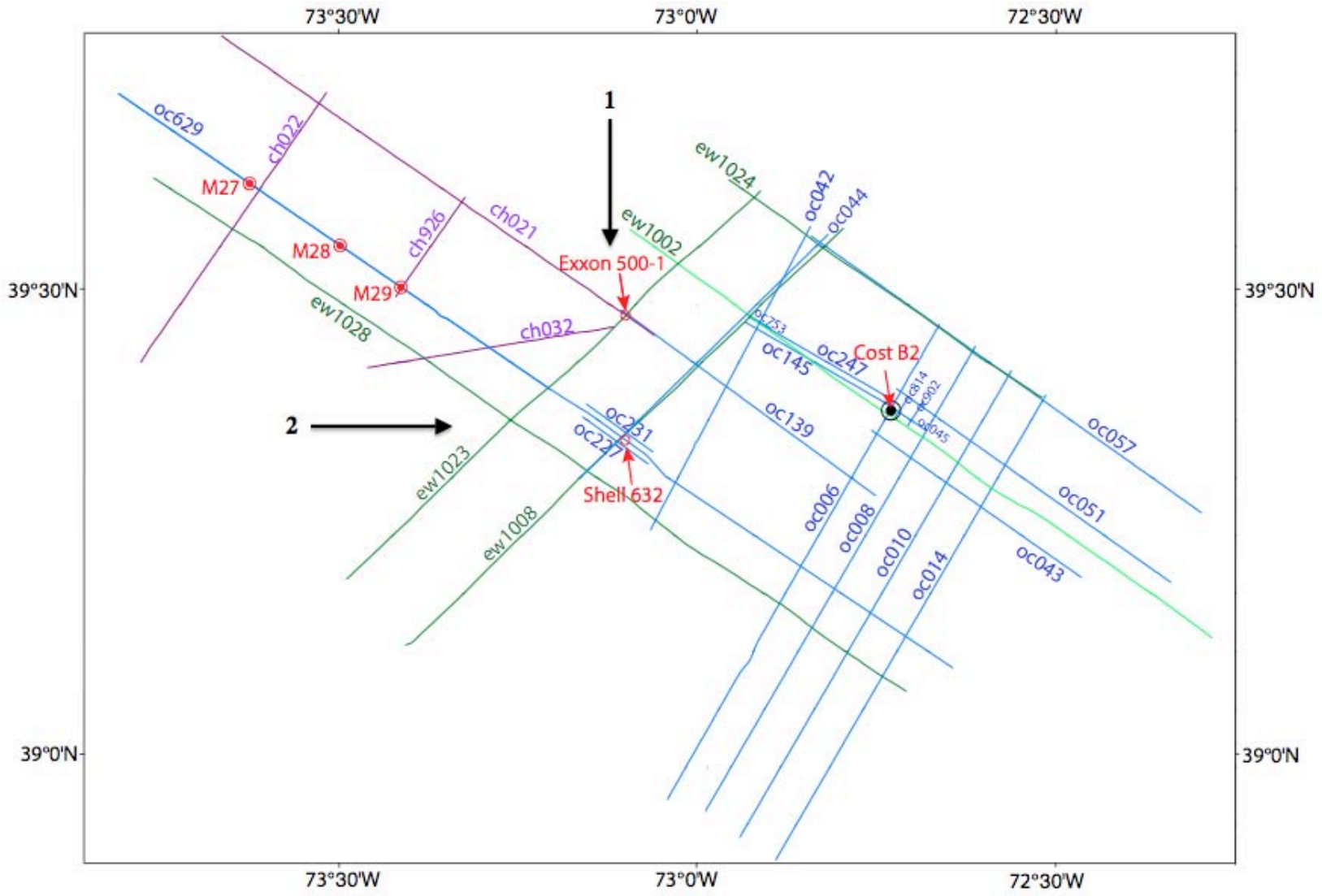

Figure 25. Map showing the direction of the two different sediment supplies of highstand deposits within the sequence C. Numbers 1 and 2 indicate the older and the younger supplies in the given order.

26A

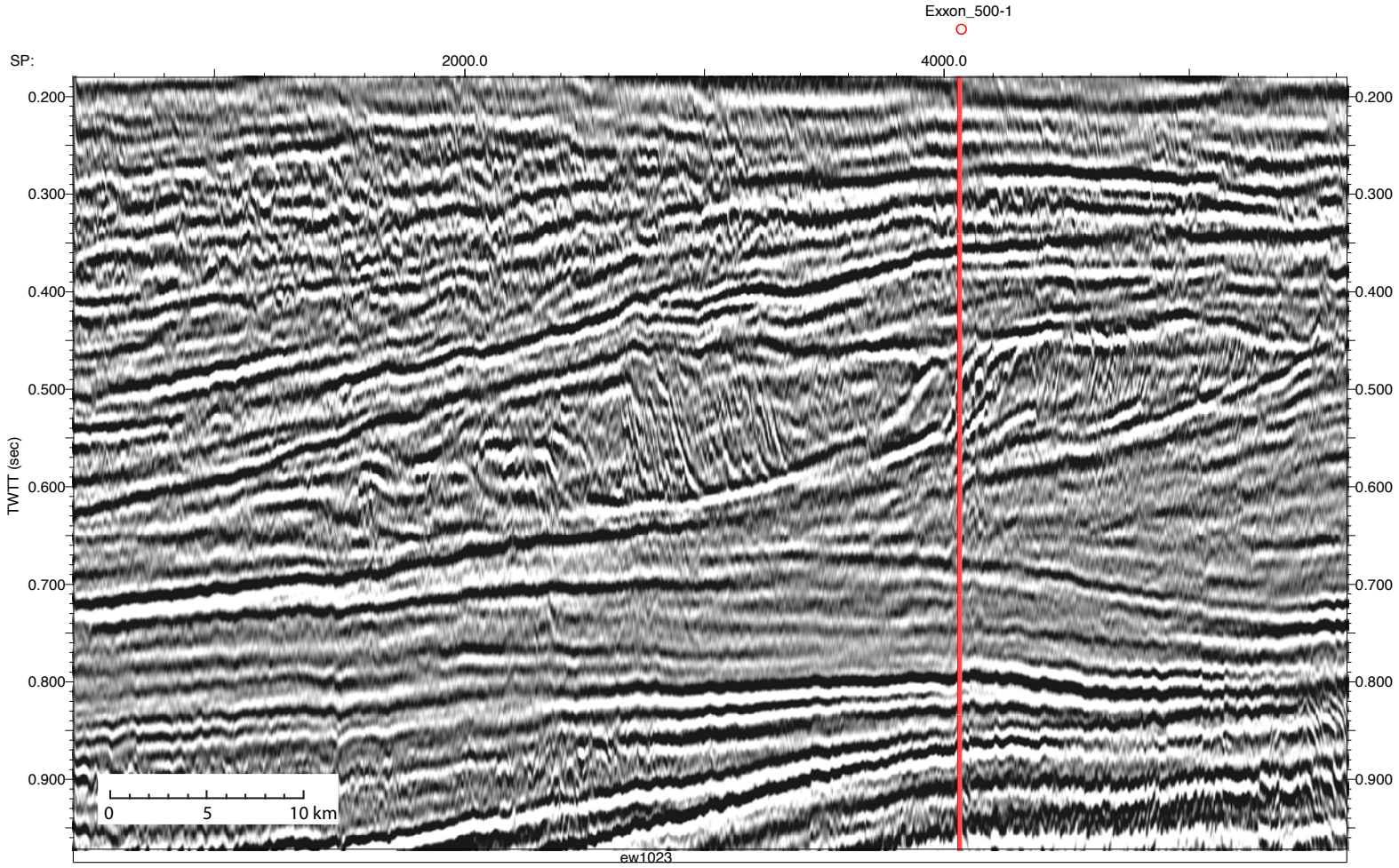
Exxon_500-1
SP:
2000.0
4000.0
0.200
0.300
0.400
0.500
0.600
0.700
0.800
0.900
TWTT (sec)
0
5
10 km
ew1023

26B

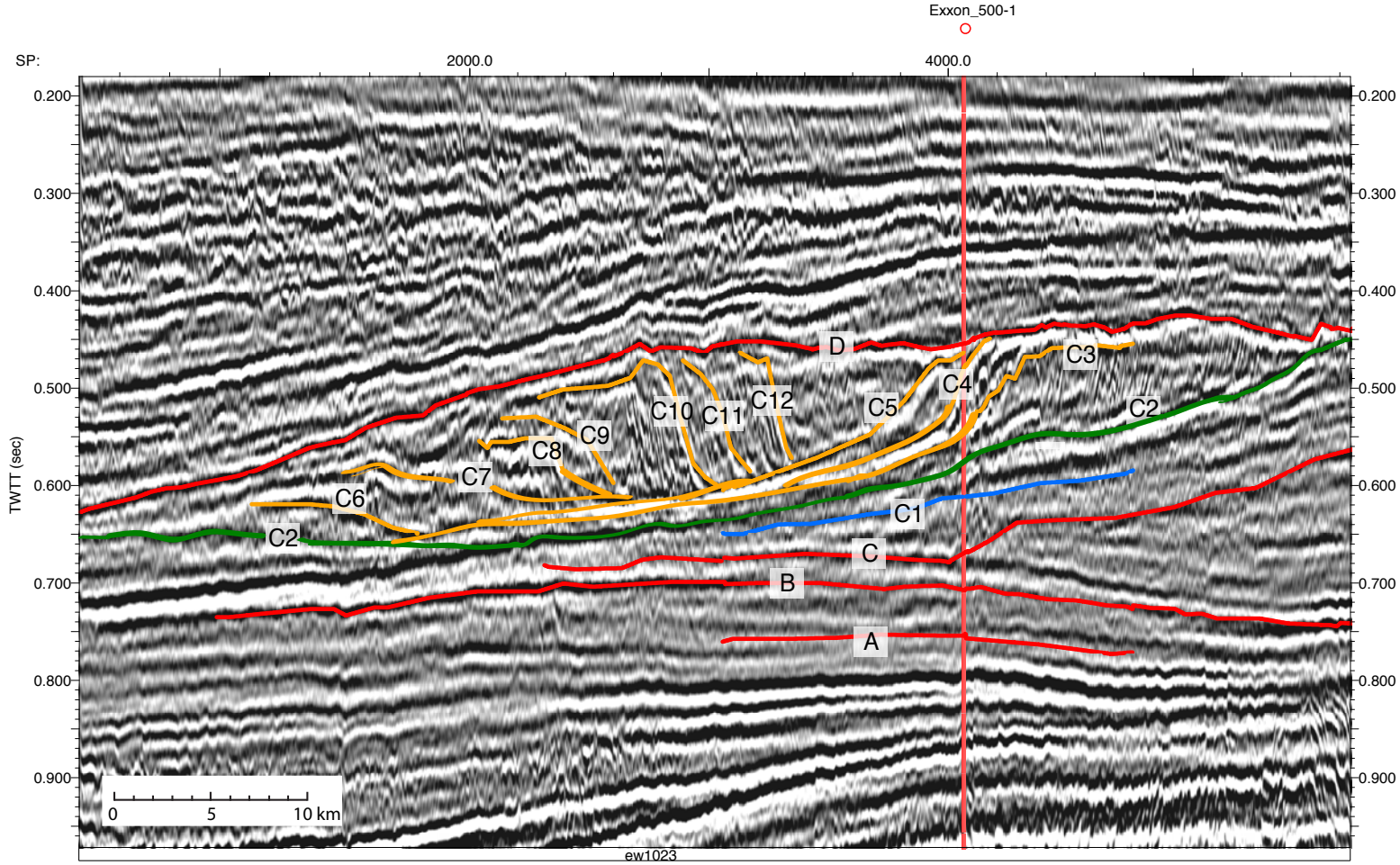

Figure 26. (A) Uninterpreted seismic line Ew9009 1023; (B) Interpreted seismic line Ew9009 1023 showing highstand deposits of sequence C that are deposited by two different sediment supplies (the older deposits are C3-C5 while the younger deposits are C6-C12) are more visible on Ew9009 1023 line.

27A

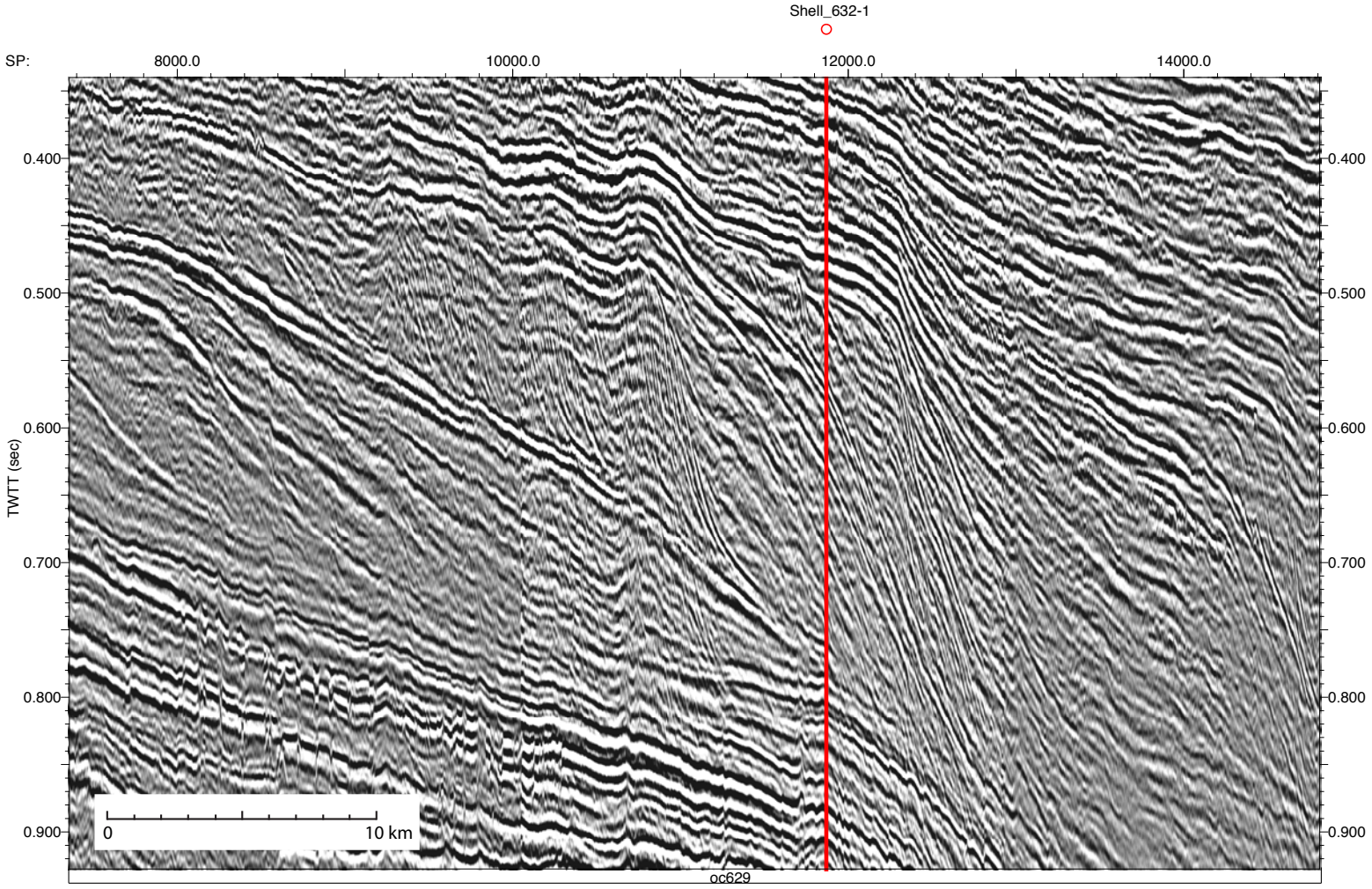
Shell_632-1
SP:
8000.0
10000.0
12000.0
14000.0
0.400
0.500
0.600
0.700
0.800
0.900
TWTT (sec)
0
10 km
oc629

27B

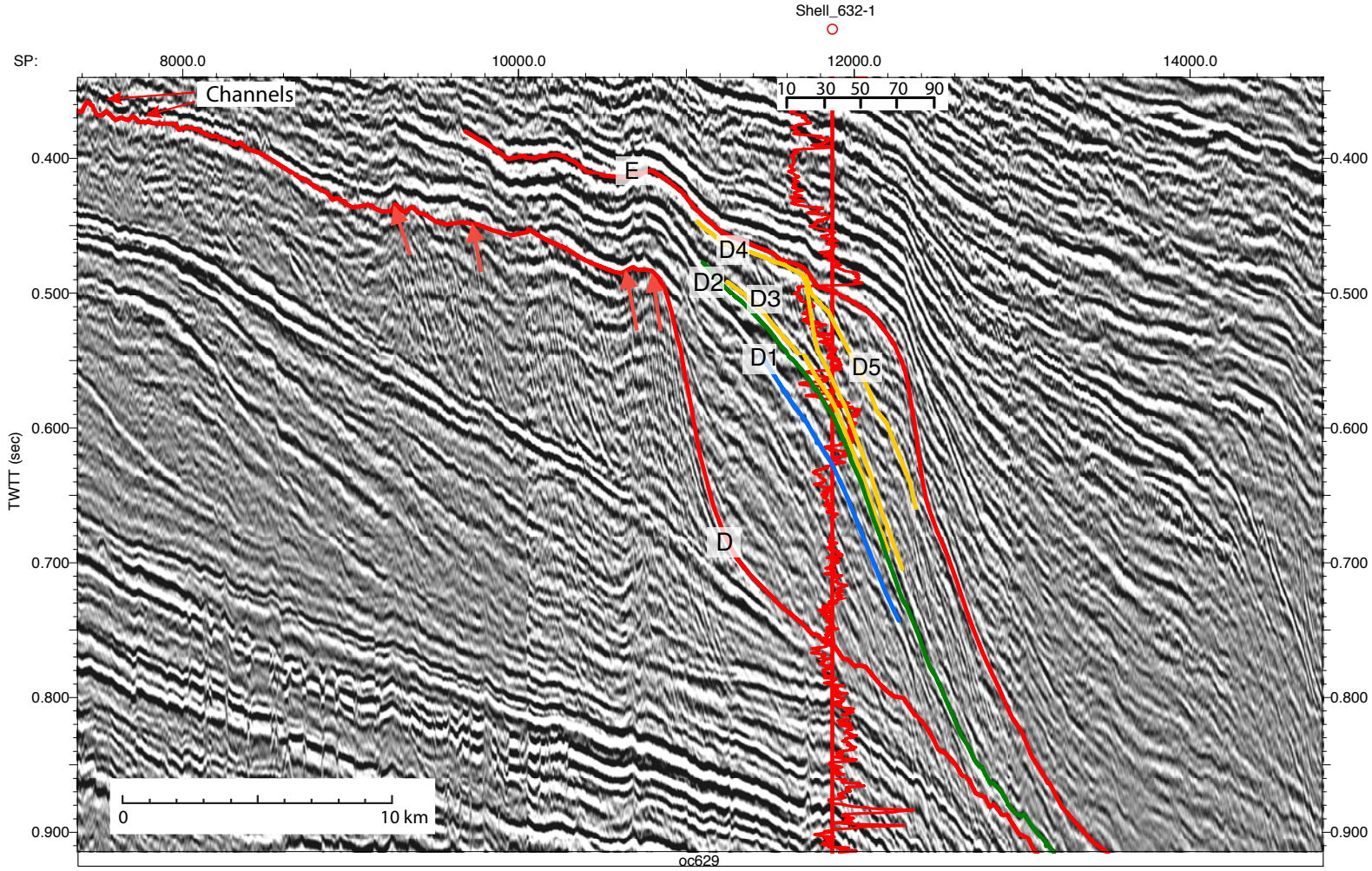

Figure 27. (A) Uninterpreted seismic profile of Oc270 629; (B) Interpreted seismic profile of Oc270 629 with site Shell-632 showing sequence D (see Figure 16 for location). Red arrows indicate reflection terminations. Caption as in Figure 19C. Channels associated with sequence boundary D on the landward part are labeled.

28A

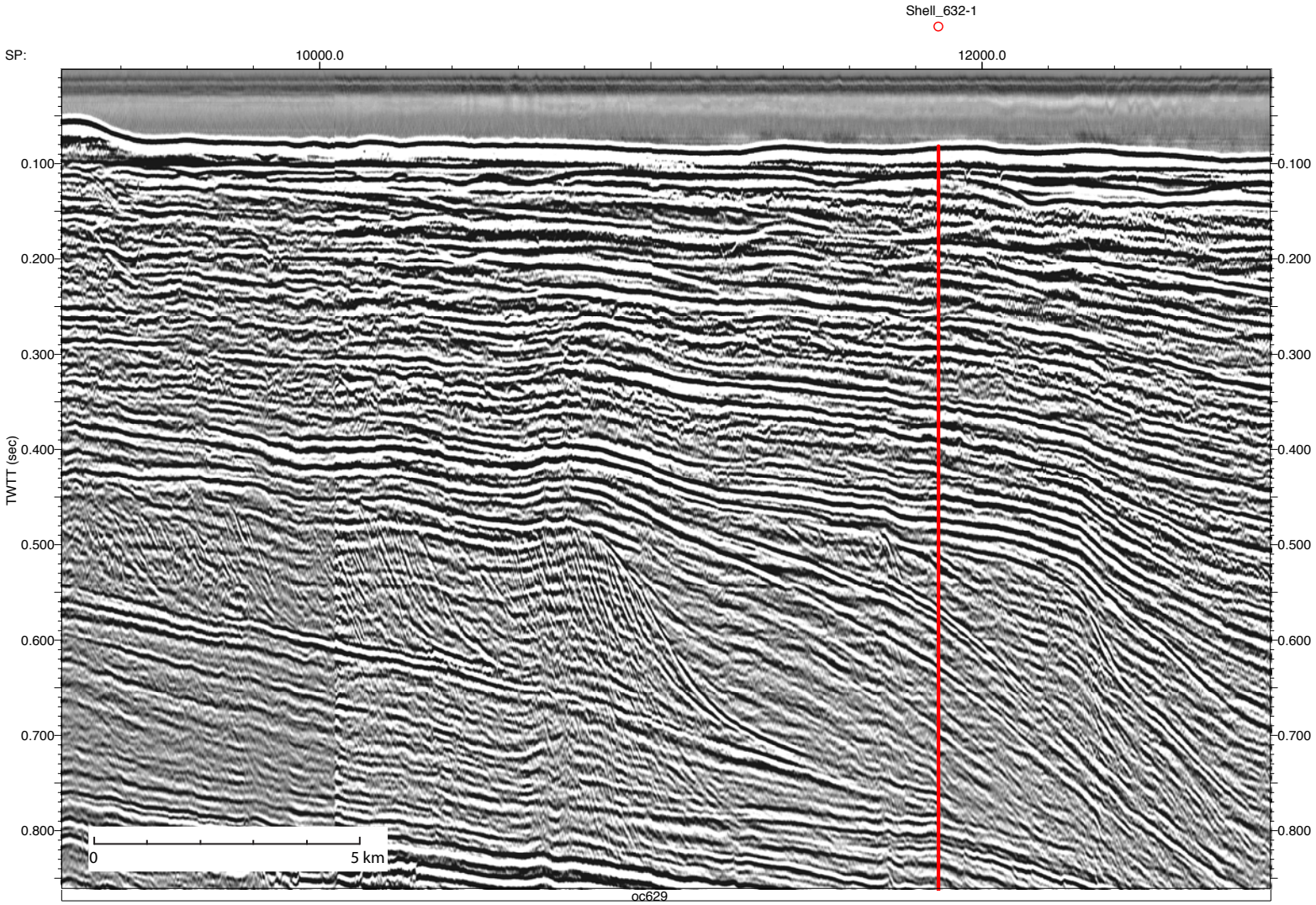
Shell_632-1
SP:
10000.0
12000.0
0.100
0.200
0.300
0.400
0.500
0.600
0.700
0.800
TWTT (sec)
0
5 km
oc629

28B

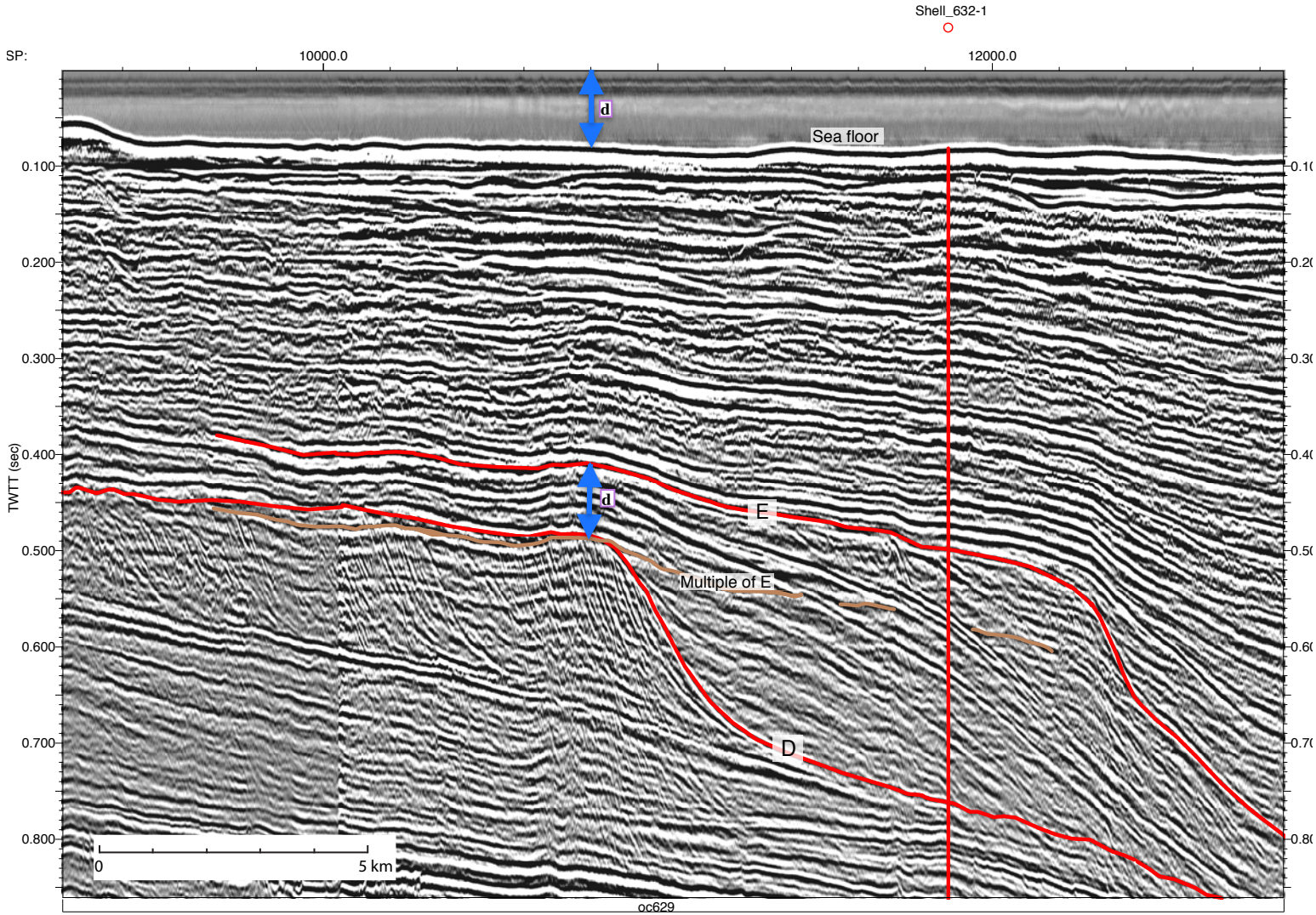

Figure 28. (A) Uninterpreted seismic profile of Oc270 629; (B) Interpreted seismic profile of Oc270 629 with site Shell-632 showing sequence boundary E and its multiple. Two-way travel time difference between sequence boundary E and its multiple is equal to time difference between the sea surface and sea floor, which is corresponding to water depth (d). Vertical red line shows location of the site. Axes are two-way travel time (TWTT) in seconds common-mid point (cmp; labeled incorrectly as "sp" on the axis). Scale is given on lower left in km. Reflectors in red indicate sequence boundaries; reflector in brown indicates the multiple of sequence boundary E.

29A

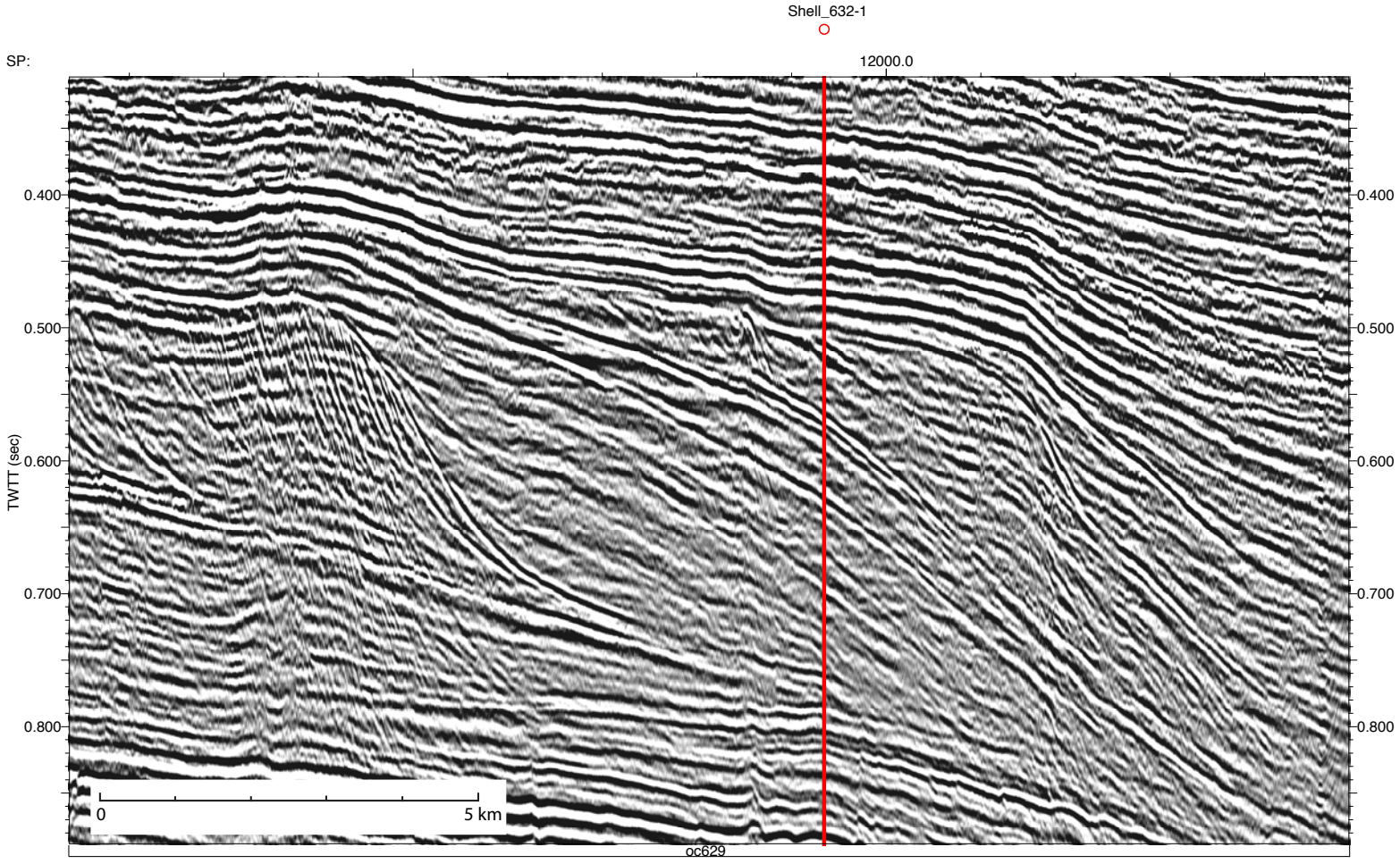
Shell_632-1
SP:
12000.0
0.400
0.500
0.600
0.700
0.800
TWTT (sec)
0
5 km
oc629

29B

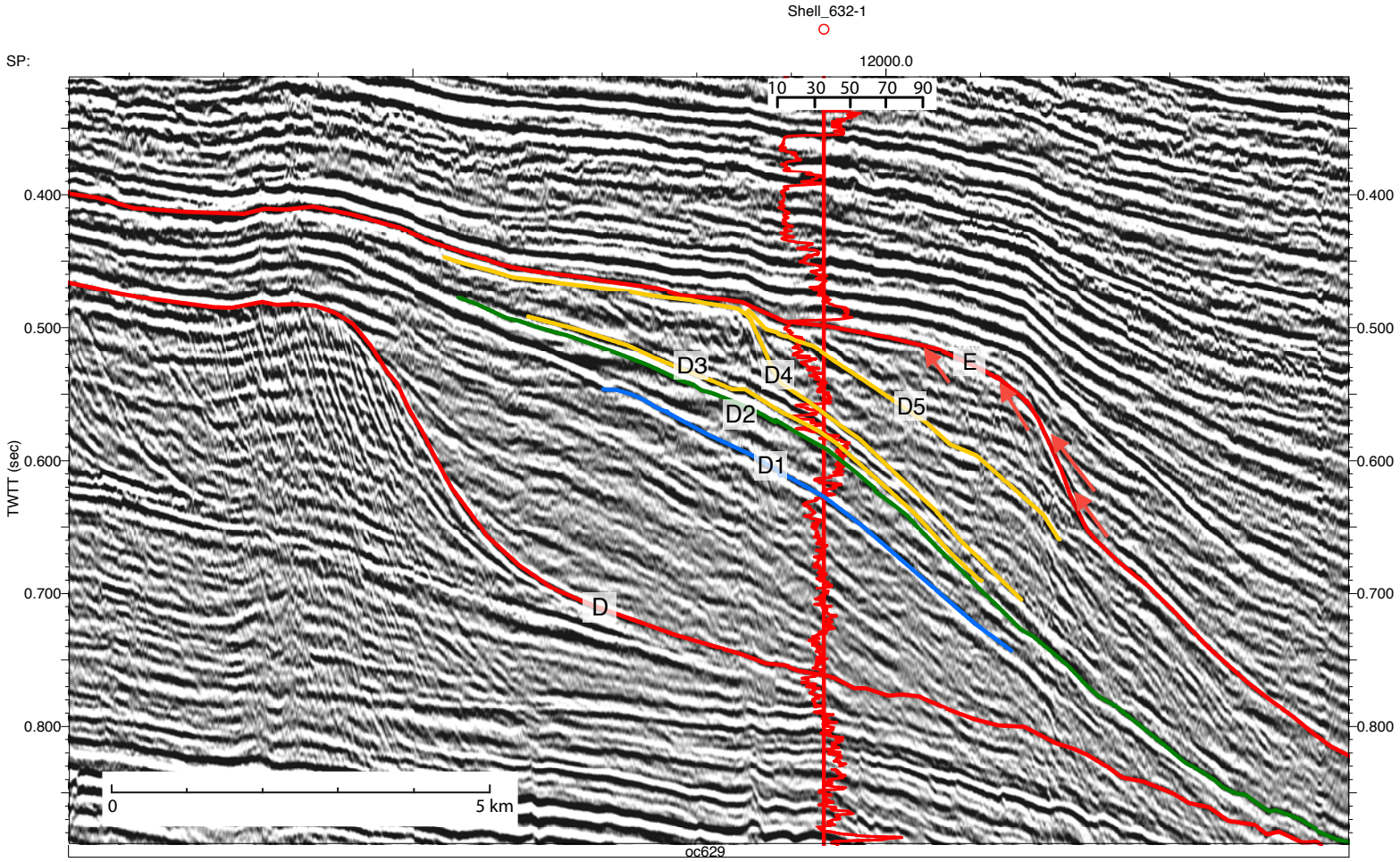

Figure 29. (A) Uninterpreted seismic profile of Oc270 629; (B) Interpreted seismic profile of Oc270 629 with site Shell-632 showing sequence D (see Figure 16 for location) with a different aspect ratio than Figure 27 has. Gamma-ray log is superimposed on the site Shell-632. D1 is the TS of sequence D where it marks the change from a progradational to a retrogradational stacking pattern on the gamma curve. D2 is the MFS where gamma values reach a maximum at approximately 590 msec. Reflection terminations above D4 are interpreted as offlaps, subsequently; deposits above D4 are tentatively interpreted as the FSST. Caption as in Figure 19C.

30A

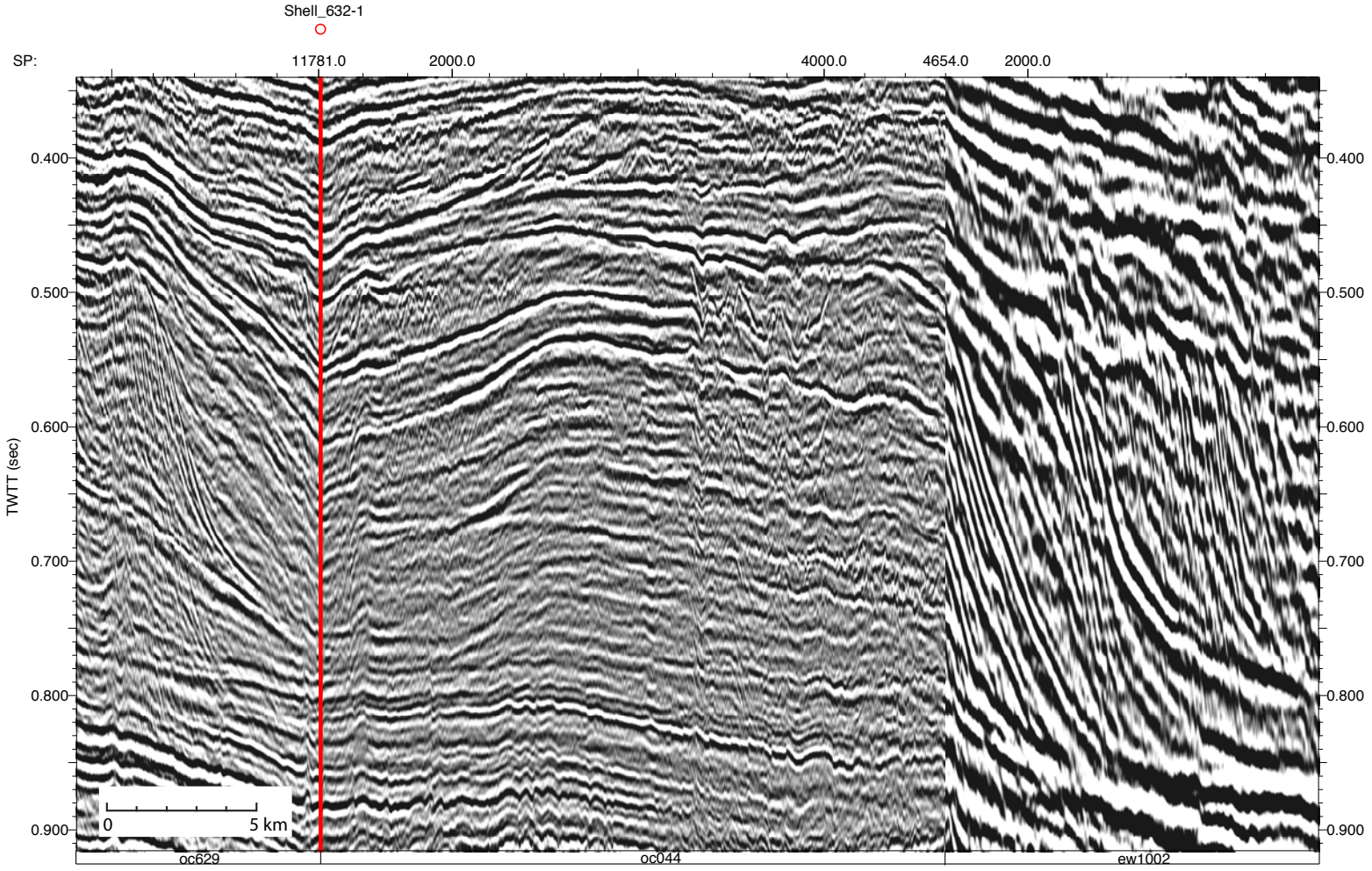
Shell_632-1
SP:
11781.0
2000.0
4000.0
4654.0
2000.0
0.400
0.500
0.600
0.700
0.800
0.900
TWTT (sec)
0
5 km
oc629
oc044
ew1002

30B

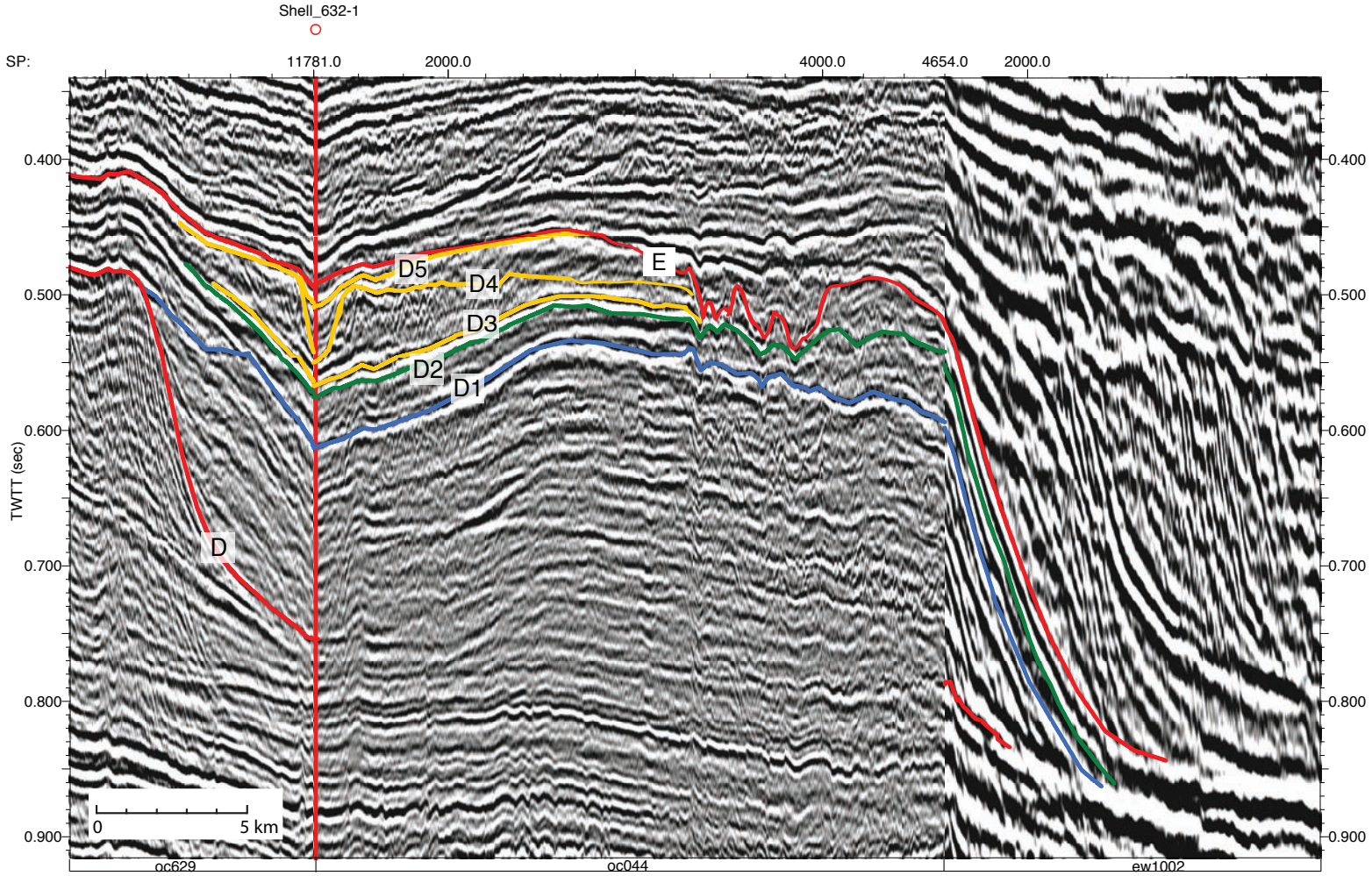

Figure 30. (A) Uninterpreted version of intersection of seismic lines Oc270 629 and 44 and Ew9009 1002; (B) Interpreted version of intersection of seismic lines Oc270 629 and 44, and Ew9009 1002 showing prograding units of sequence D above the MFS (reflector D2) (see Figure 16 for location). Reflector E is associated with a large incised valley at cdps 3650-4000. This incised valley suggests that reflector E is a sequence boundary formed as a result of subaerial exposure. Vertical red line shows location of the site Shell-632 on Oc270 line 629. Axes are two-way travel time (TWTT) in seconds common-mid point (cmp; labeled incorrectly as "sp" on the axis). Scale is given on lower left in km. Seismic line names are at the bottom of the profile. Reflectors in red indicate sequence boundaries; reflectors in blue indicate the transgressive surfaces (TS); and reflectors in green indicate the maximum flooding surfaces (MFS).

31A

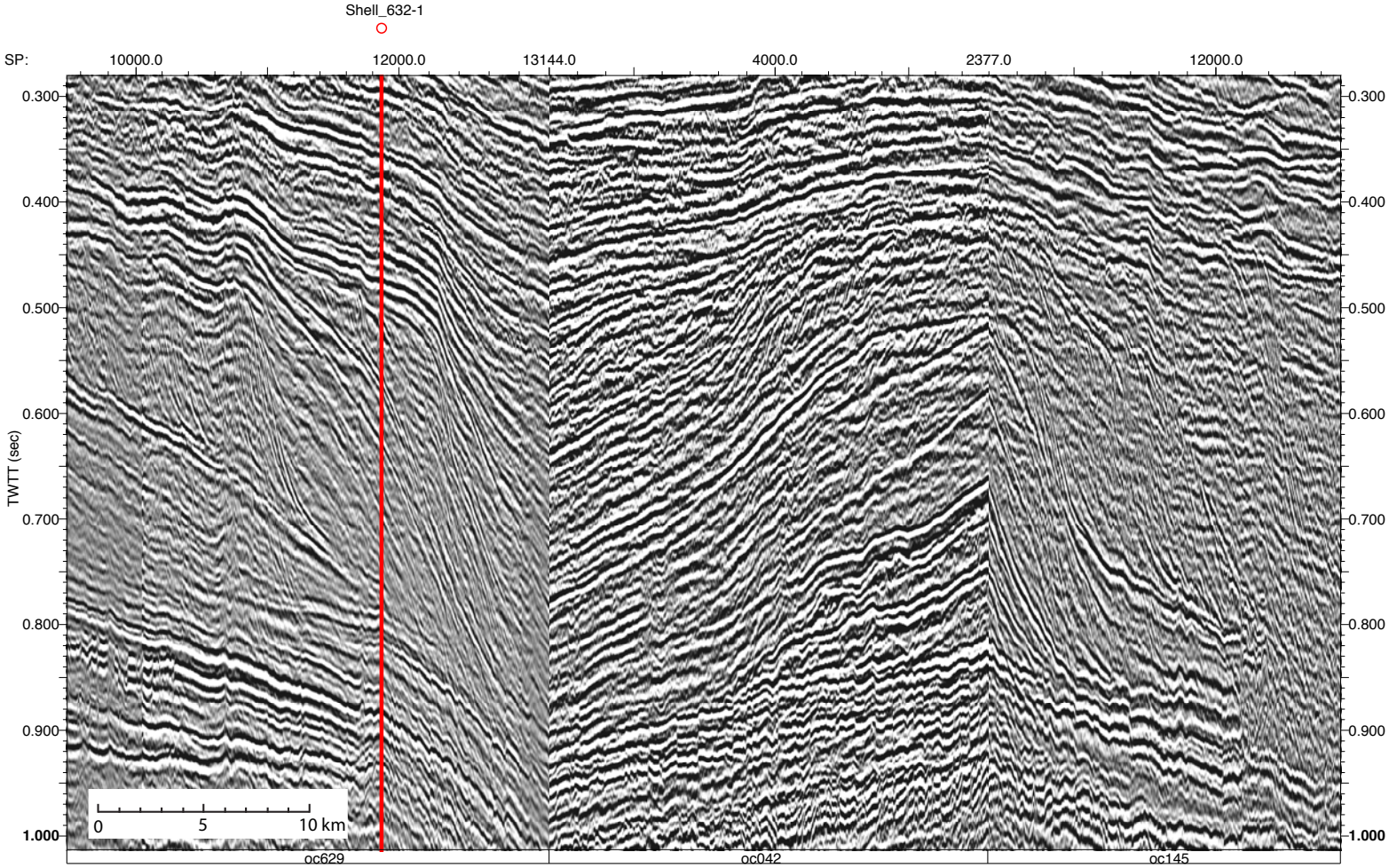
Shell_632-1
SP:
10000.0
12000.0
13144.0
4000.0
2377.0
12000.0
0.300
0.400
0.500
0.600
0.700
0.800
0.900
1.000
TWTT (sec)
0
5
10 km
oc629
oc042
oc145

31B

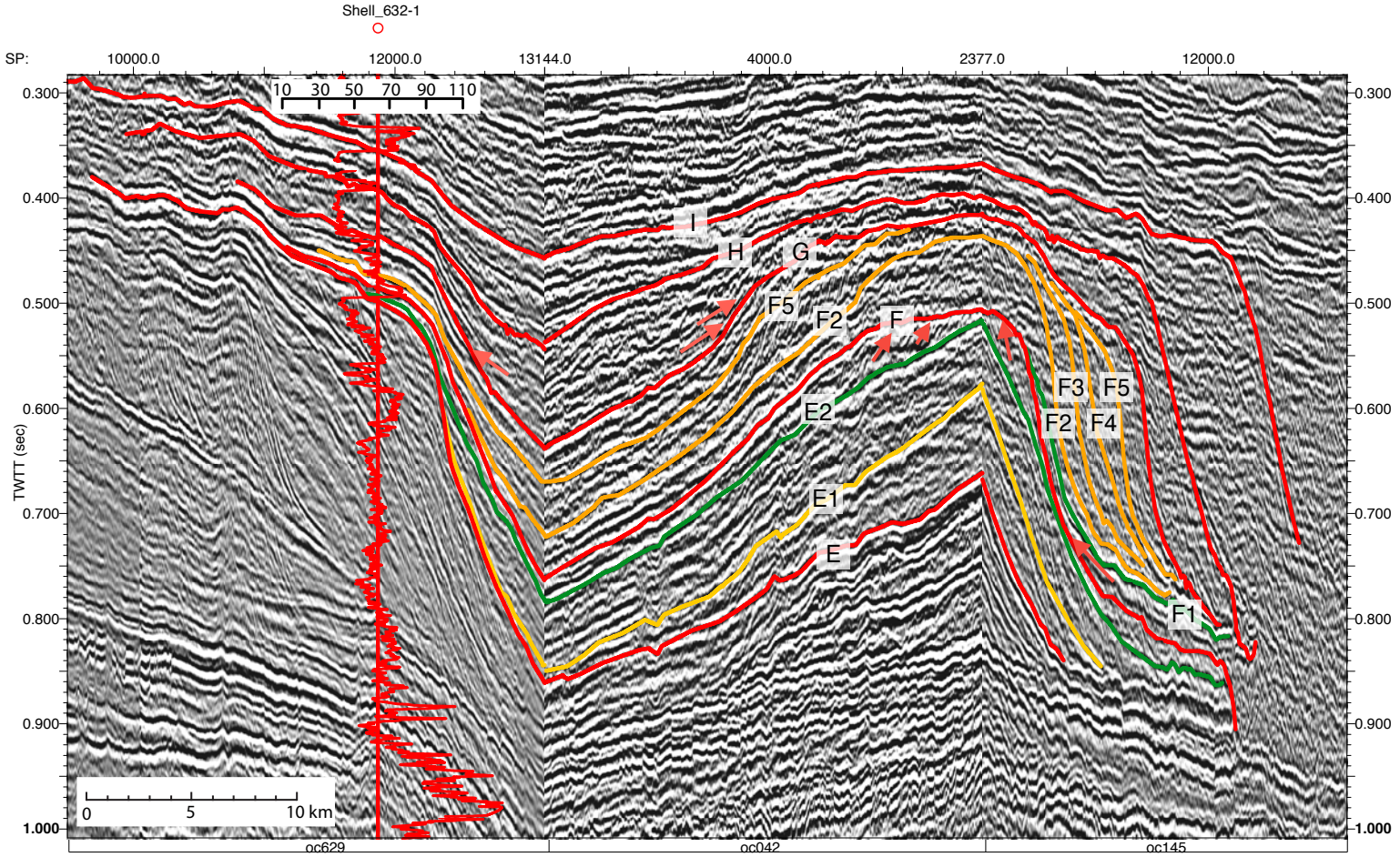

Figure 31. (A) Uninterpreted version of intersection of seismic lines Oc270 629, 42, and 145; (B) Interpreted version of intersection of seismic lines Oc270 629, 42, and 145 with gamma-ray log at site Shell-632 showing sequences E-I (see Figure 16 for location). Caption as in Figure 19C.

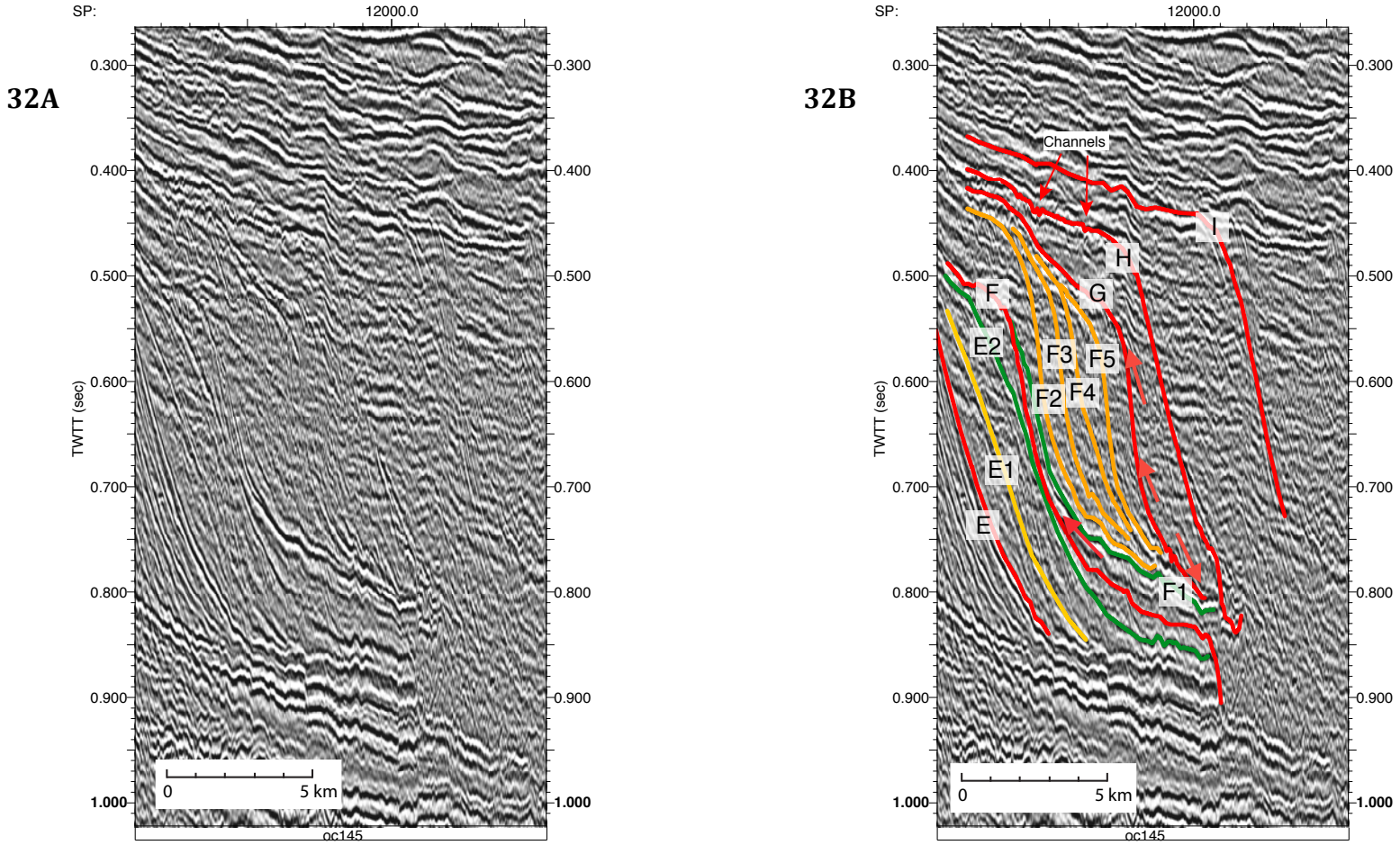

Figure 32. (A) Uninterpreted seismic profile of Oc270 145; (B) Interpreted seismic profile of Oc270 145 showing sequences F-I. Reflector F1 overlies the submarine levees basinward of the clinothem rollover where they onlap onto the sequence boundary F on Oc270 line 145. Five prograding packages (F2-F5) downlap onto the MFS (reflector F1). These packages progressively step down into the basin, and they are interpreted as the FSST of sequence F. Sequence boundary H is an erosional surface with small channels on the landward side of the clinothem rollover (labeled). Red arrows indicate reflection terminations. Caption as in Figure 30B.

33A

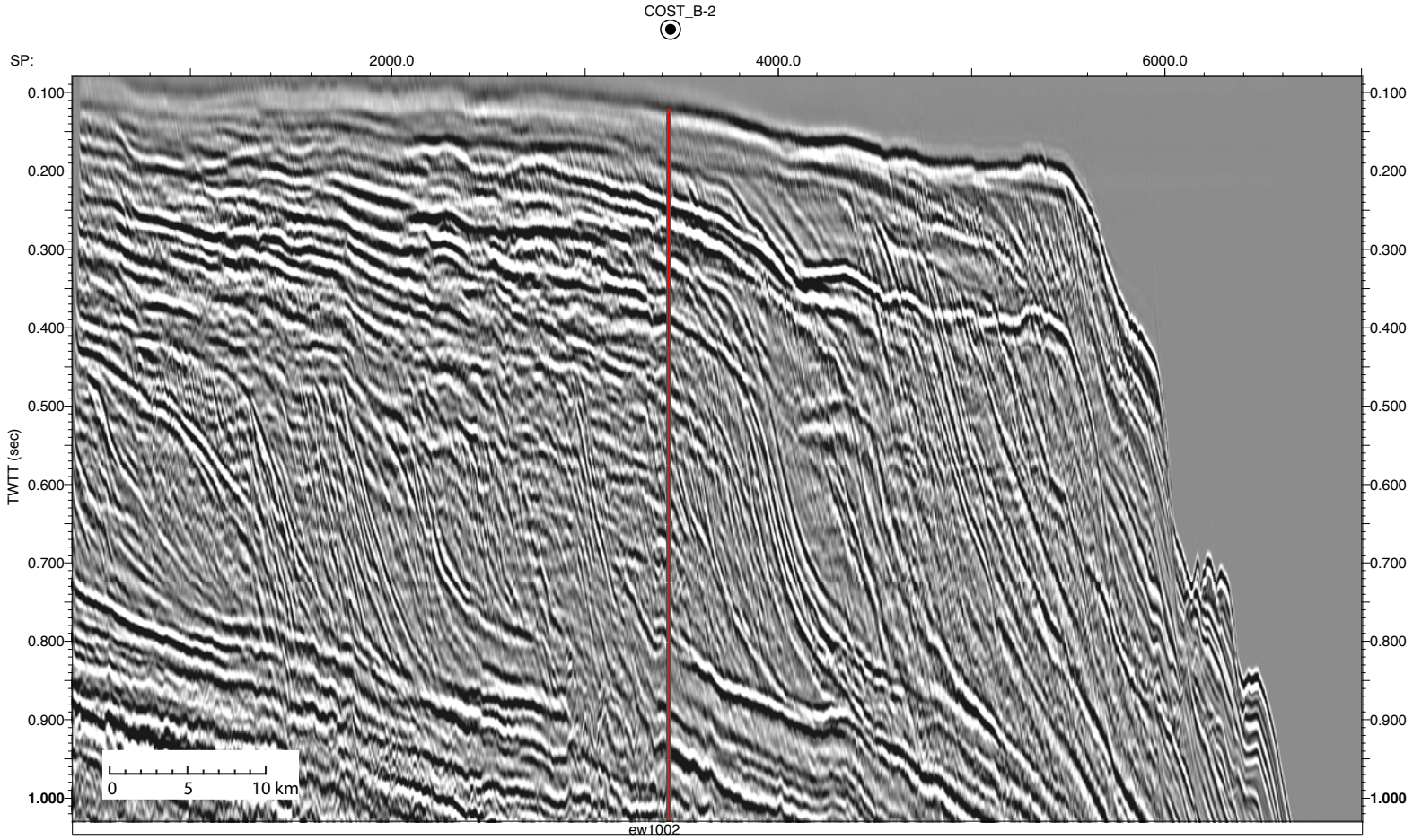
COST_B-2
SP:
2000.0
4000.0
6000.0
0.100
0.200
0.300
0.400
0.500
0.600
0.700
0.800
0.900
1.000
TWTT (sec)
0
5
10 km
ew1002

33B

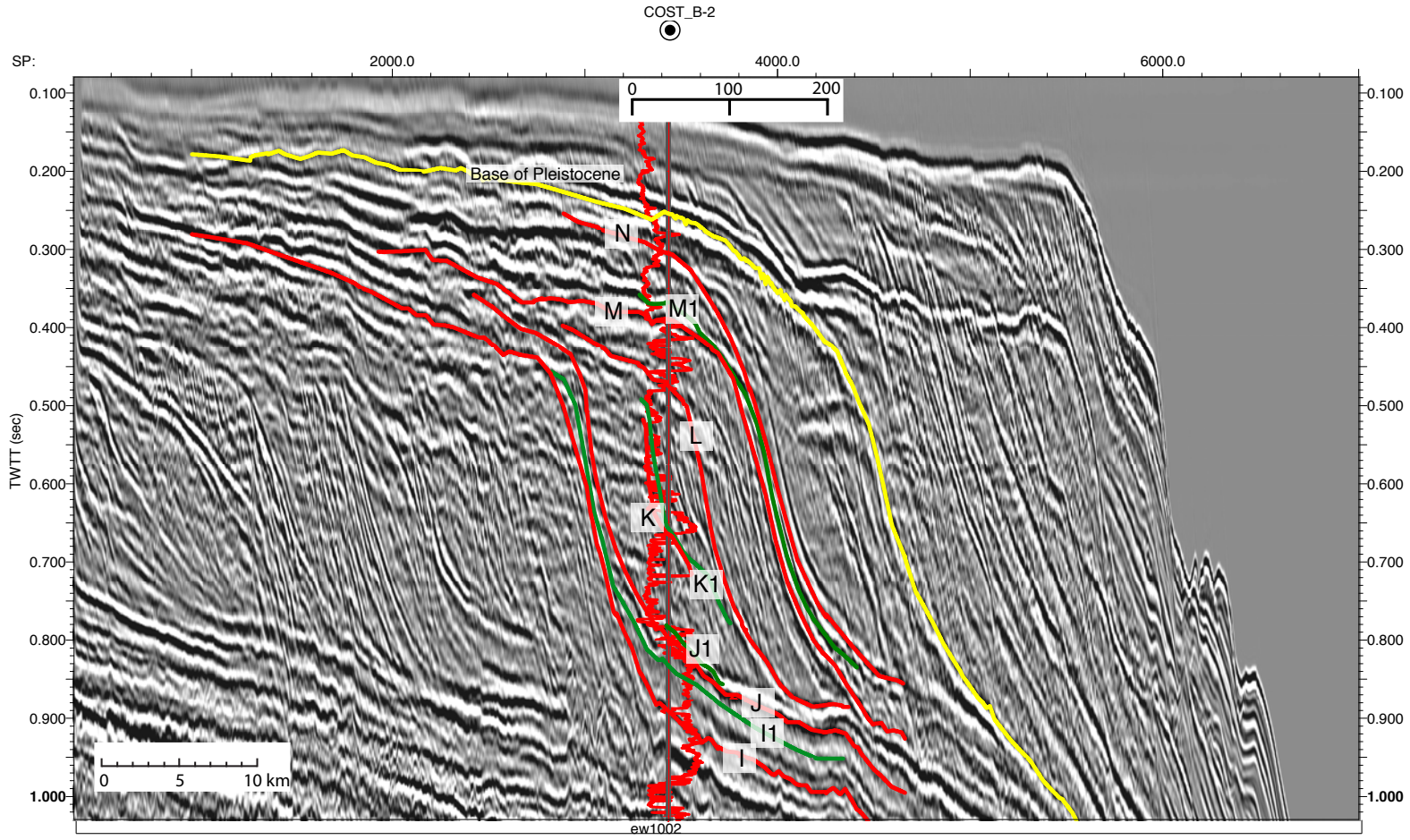
COST_B-2
SP:
2000.0
4000.0
6000.0
0
100
200
Base of Pleistocene
N
M
M1
L
K
K1
J1
J
I1
I
0
5
10 km
TWTT (sec)
0.100
0.200
0.300
0.400
0.500
0.600
0.700
0.800
0.900
1.000
ew1002

33C

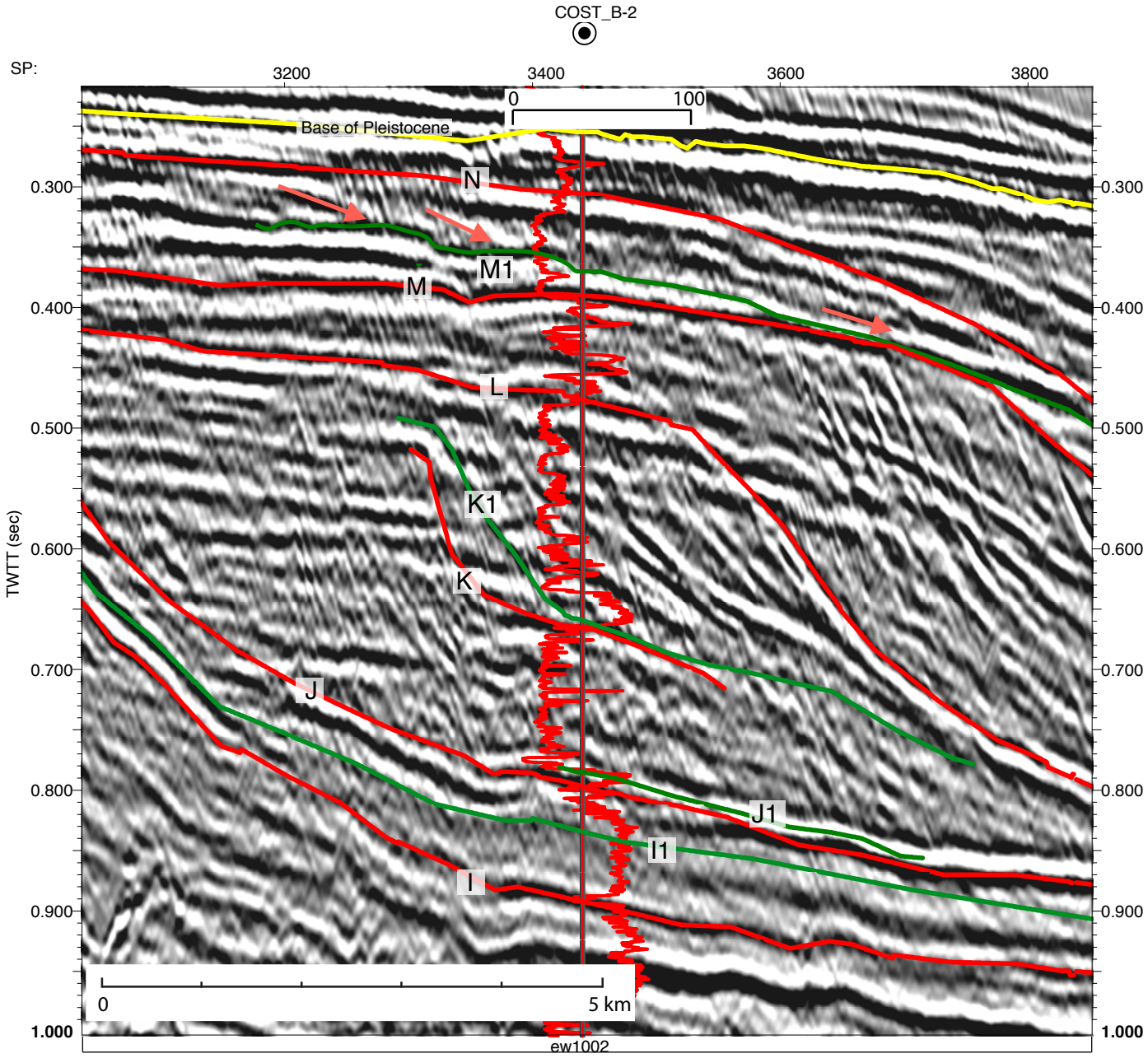
COST_B-2
SP:
3200
3400
3600
3800
0
100
Base of Pleistocene
N
M1
M
L
K1
K
J
J1
I1
I
TWTT (sec)
0.300
0.400
0.500
0.600
0.700
0.800
0.900
1.000
0
5 km
ew1002

33D

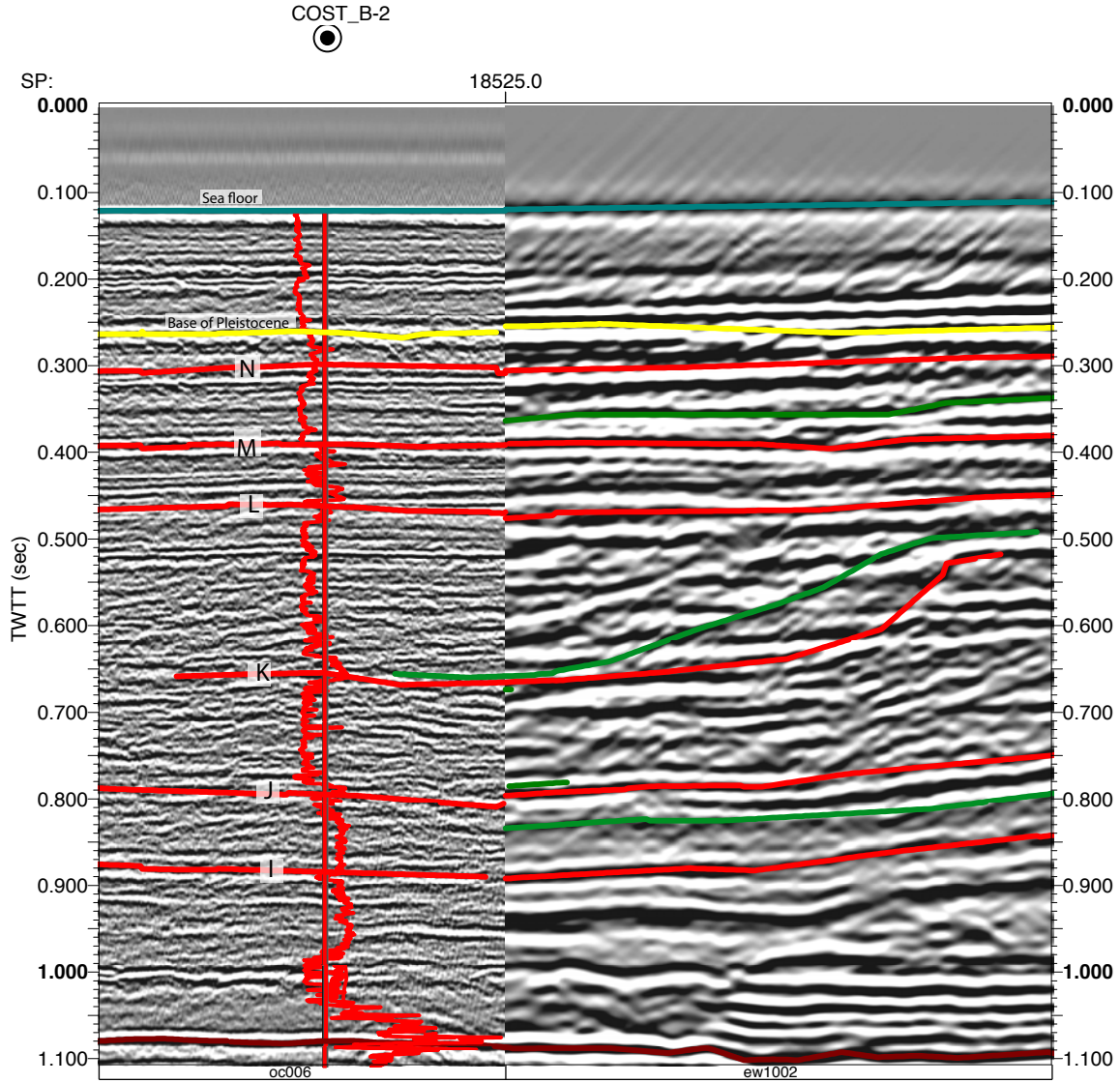

Figure 33. (A) Uninterpreted seismic profile Ew9009 1002; (B) Interpreted seismic profile of Ew9009 1002 with Cost B2 site showing sequences I-N (see Figure 16 for location); (C) Enlargement of sequences I-N at site Cost B2 on Ew9009 line 1002 with a different aspect ratio than Figure 31. Caption as in Figure 17B; (D) Intersection of Oc270 line 6 with Ew9009 line 1002 shows that the COST B-2 projection onto Ew9009 line 1002 is reliable. Scale is different than (C).

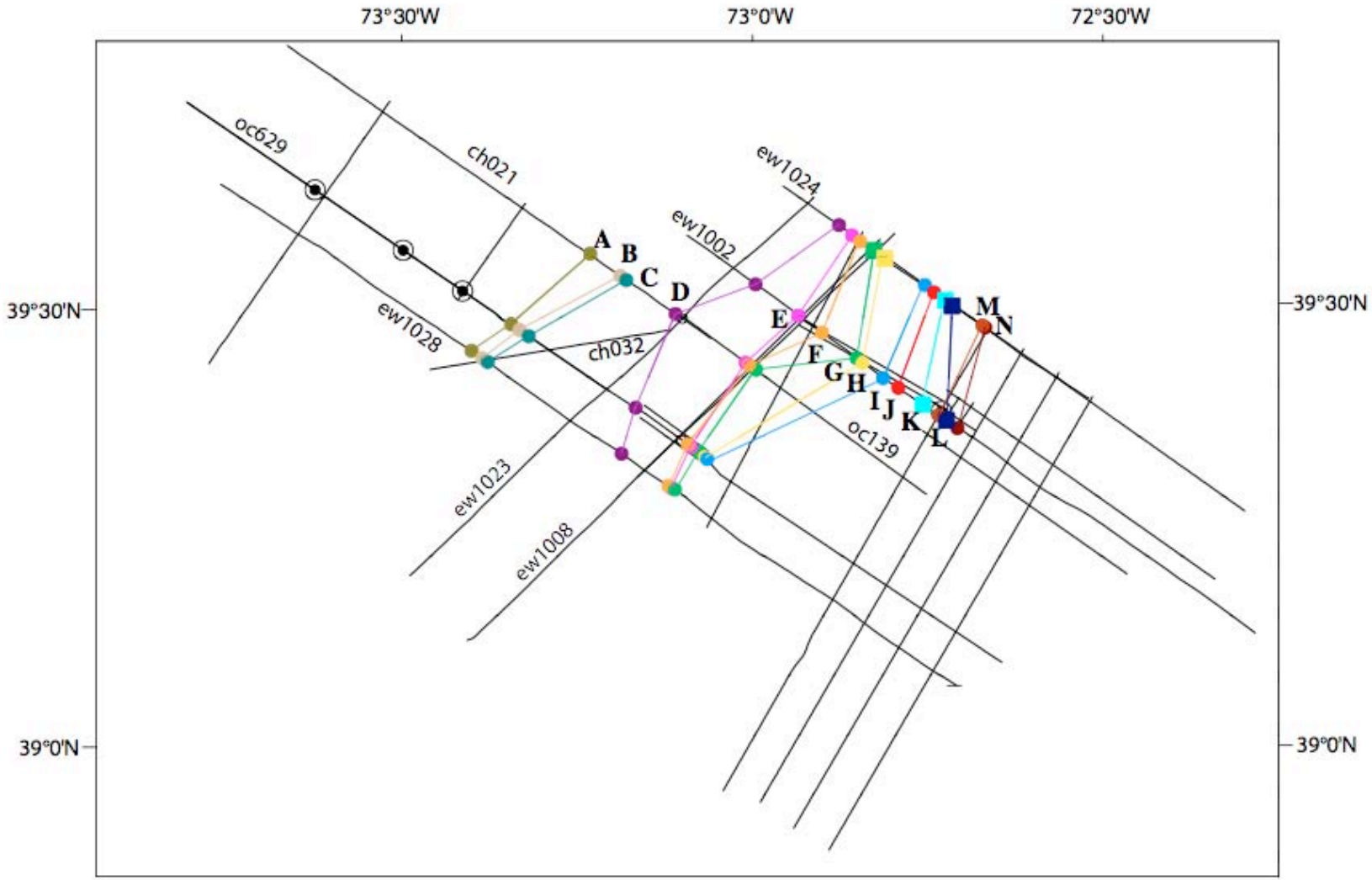

Figure 34. Map of the rollover position of the clinothem above each sequence boundary. Letters represent the names of the sequences. All Miocene sequences in the study area advance basinward (SE) through time.

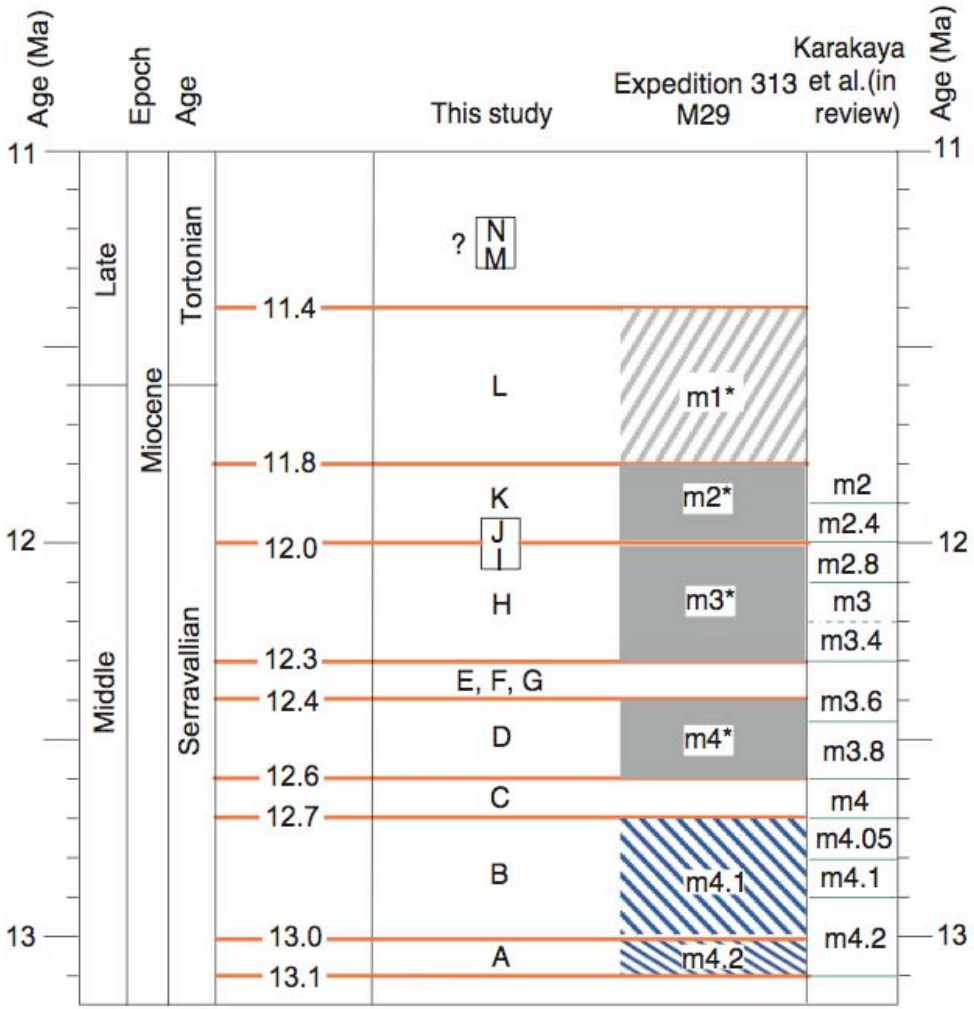

Figure 35. Age estimates of the 14 sequences A-N reported here. Age estimates for sequences m4.2, m4.1, m4, m3, m2, and m1 (Browning et al., 2013) allow correlation to sequences A, B, D, H, K, and L.

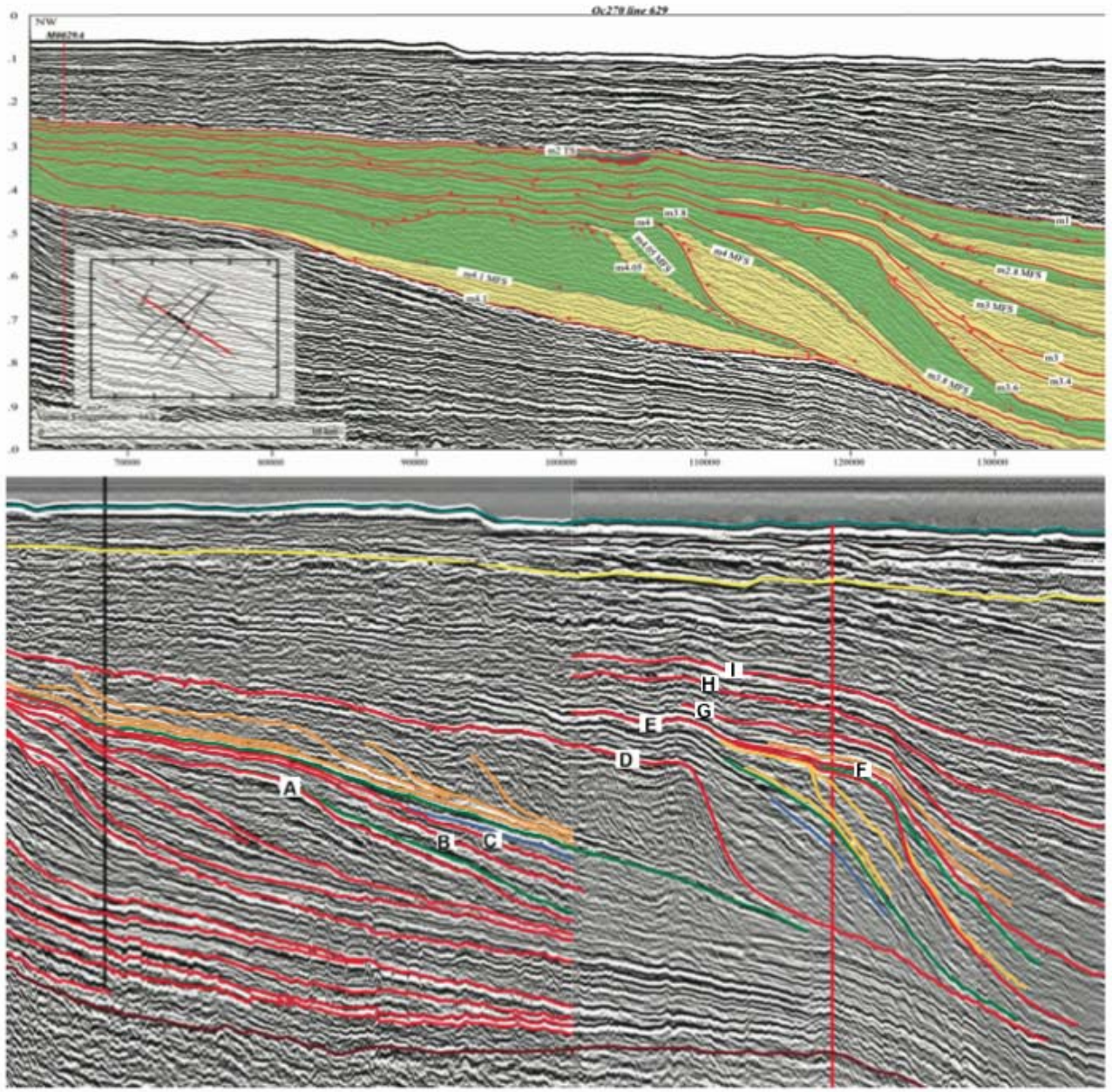

Figure 36. Karakaya (2012)'s sequence boundaries on Oc270 line 629 (the top profile) compared to sequence boundaries in the present paper on the same line (the bottom profile). Note the profiles are displayed at slightly different scales.

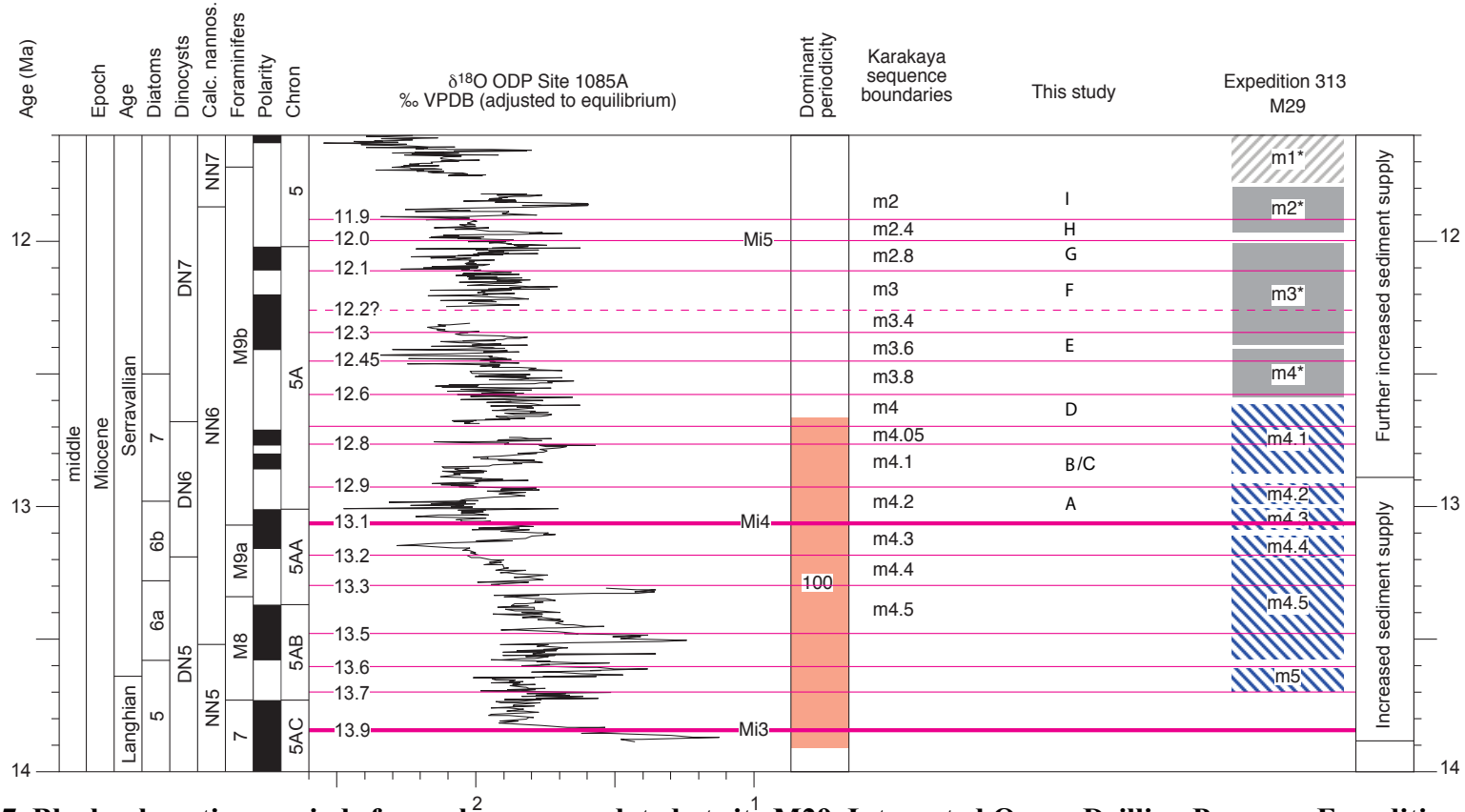

Figure 37. Blocks show time periods for each sequence dated at site M29, Integrated Ocean Drilling Program Expedition 313 (Browning et al., 2013), compared to the global oxygen isotopic record from ODP Site 1085 at the Southwestern African continental margin (Westerhold et al., 2005) (modified from Karakaya et al., in review). Letters indicate sequences in the present study. Blue colored blocks indicate deposition on the clinothem bottomsets. Cross-hachures indicate less certain age tuned to better-dated records at other sites. The asterisk for sequences m4–m1 indicates an updated interpretation versus Miller et al. (1998). Karakaya et al. (in review) sequences are on the left for the comparison. Bold magenta lines indicate the major Miocene events (Mi3, Mi4, Mi5). Time scale of Gradstein et al (2004). Age estimates of sequences K, L, M, N are only constrained to younger than sequence m1 (~ 11.4 Ma) and older than the Pleistocene (P4; Mountain et al., 2007) and are indicated by a question mark.

9 Tables

	High-resolution Multichannel Seismic (MCS) Data (R/V *Oceanus* Oc270 and R/V *Cape Hatteras* CH0698)	**Low-resolution Multichannel Seismic (MCS) Data (R/V *Ewing* Ew9009)**
Frequency (sec) and volume (cubic inch) of seismic source	5; 90	10; 1350
Spacing of the hydrophones (m)	12.5	12.5
Depth that hydrophones towed at (m)	2	6
Sampling rate (msec)	0.5	1
Vertical resolution (m)	5	15

Table 3.1. Comparison of high (R/V *Oceanus* Oc270 and R/V *Cape Hatteras* CH0698) and low-resolution (R/V *Ewing* Ew9009) multichannel seismic data used in this study.

Gamma-ray Logs	Seismic Profile	cdp	Distance to the closest seismic profile (meters)
EXP313-M29	Oc270 line 629	6661	0
Shell 632	Oc270 line 629	11869	0
Exxon 500-1	CH0698 line 21	9508	0
COST B-2	Oc270 line 6	18636	78

Table 3.2.1. Names of the 4 wells that had wireline gamma-ray logs used in this study. Each was tied to the named profile at the cdp shown; the closest distance between the well and the cdp is shown.

Sequence boundaries	Seismic Profile	Criteria
A	CH0698 line 21	O, D, T
B	CH0698 line 21	O, D, T, Log
C	CH0698 line 21	O, D, T
D	Oc270 line 629	O, D, E.T.
E	Oc270 line 629	O, T, Log
F	Oc270 line 629	O, D, T
G	Oc270 line 629	O, D, Log
H	Oc270 line 629	Log
I	Oc270 line 629	Log
J	Ew9009 line 1002	Log
K	Ew9009 line 1002	Log
L	Ew9009 line 1002	T, Log
M	Ew9009 line 1002	T, Log
N	Ew9009 line 1002	T, Log

Table 6.2.1. Sequence boundaries identified in this study (A-N), seismic profiles on which they are identified, and the criteria used to identify them. O—Onlap, D—Downlap, T—Toplap, E.T. —Erosional Truncation, Log—Gamma-ray log.

Sequence boundaries interpreted in this study	Corresponding sequence boundaries from Poulsen et al. (1998)	Corresponding sequence boundaries from Greenlee et al. (1992)	Corresponding sequence boundaries from Expedition 313 (Miller et al., 1996; 2013)	Estimated ages (Ma) of sequences from Browning et al. (2013)	Corresponding sequence boundaries from Karakaya (2012)	Ages of sequence boundaries from Karakaya et al. (in review)
N	Gold?	N.M.	N.M.	N.D	N.M	N.D
M	Blue	Pink-1	N.M	N.D	N.M	N.D
L	Black	Tuscan	m1	11.8-11.4	N.M	N.D
K	Brown	Yellow-2	m2	12.0-11.8	N.M	N.D
J	Gray	N.M.	N.M.	N.D.	m1	N.D.
I	N.M.	N.M.	N.M.	N.D	m2	11.9
H	Red	Blue	m3	12.3-12.0	m2.4	12
G	N.M.	N.M.	N.M.	N.D	m2.8	12.1
F	Green	N.M.	N.M.	N.D	m3	12.2?
					m3.4	12.3
E	Light Blue?	N.M.	N.M.	N.D	m3.6	12.45
					m3.8	12.6
D	Purple	Pink-2	m4	12.6-12.4	m4	12.7
C	N.M.	N.M.	N.M.	N. D.	N.M.	N.D
					m4.05	12.8
B	N.M.	N.M.	m4.1	13.0-12.7	m4.1	12.9
A	N.M.	N.M.	m4.2	13.1-13.0	m4.2	13.1

Table 6.3.1. Correlations of sequences in the present study with the previous studies (Poulsen et al., 1998; Greenlee et al., 1992; Miller et al., 1996; 2013; Karakaya, 2012) and ages estimates from Browning et al. (2013) and Karakaya et al. (in review). Three of the sequences (m4.05, m3.8, m3.4) from Karakaya (2012) that are not mapped in the other studies are left blank on the columns. Uncertain correlations are shown with question marks. N.M.— Not Mapped; N.D.— Not Determined.

10 References

Badley, M. E. (1985). Practical seismic interpretation. International Human Resources Development Corporation, Boston, 266 pp,

Barton, N. 2006. Rock Quality, Seismic Velocity, Attenuation and Anisotropy. 729p. Taylor& Francis, UK & Netherlands.

Browning, J.V., Miller, K.G., McLaughlin, P.P., Kominz, M.A., Sugarman, P.J., Monteverde, D., Feigenson, M.D., and Hernàndez, J.C., 2006, Quantification of the effects of eustasy, subsidence, and sediment supply on Miocene sequences, Mid-Atlantic margin of the United States: Geological Society of America Bulletin, v. 118, p. 567–588, doi:10.1130/B25551.1.

Browning, J.V., Miller, K.G., Sugarman, P.J., Kominz, M.A., McLaughlin, P.P., and Kulpecz, A.A., 2008, 100 Myr record of sequences, sedimentary facies and sea-level change from Ocean Drilling Program onshore coreholes, U.S. Mid-Atlantic coastal plain: Basin Research, v. 20, p. 227–248, doi:10.1111/j.1365 - 2117.2008.00360.x.

Browning, J.V., Miller, K.G., Sugarman, P.J., Barron, J., McCarthy, F., Kulhanek, D., Katz, M.E., and Feigenson, M.D., 2013, Chronology of Eocene-Miocene sequences on the New Jersey shallow shelf: Implications for regional, interregional, and global correlations: Geosphere, v. 9, doi: 10.1130/GES00857.1.

Catuneanu, O., 2002, Sequence stratigraphy of clastic systems: concepts, merits and pitfalls, Journal of African Earth Sciences, v. 35, p. 1-43.

Catuneanu, O., 2006, Principles of sequence stratigraphy: Elsevier, Amsterdam, 375 p.

Catuneanu, O., and 27 others, 2009, Towards the standardization of sequence stratigraphy: Earth-Science Reviews, v. 92, p. 1–33, doi:10.1016/j.earscirev.2008. 10.003.

Christie-Blick, N., Mountain, G.S., and Miller, K.G., 1990, Seismic stratigraphic record of sea level change, in Geo- physics Study Committee, Sea-level change: National Research Council Studies in Geophysics: Washington, D.C., National Academy Press, p. 116–140.

Coe, A.L., ed., 2003, The sedimentary record of sea level change: Cambridge, Cambridge University Press, 288 p.

Emery, D. and Myers, K.,1996, Sequence stratigraphy, Oxford, Blackwell Science, 297p.

Gradstein, F., Ogg, J., and Smith, A., 2004, A geologic time scale 2004: Cambridge, U.K., Cambridge University
Press, 589 p.

Greenlee, S.M., and Moore, T.C., 1988, Recognition and interpretation of depositional sequences and calculation of sea level changes from stratigraphic data—Offshore New Jersey and Alabama Tertiary, in Wilgus, C.K., et al., eds., Sea-level changes: An integrated approach: Society of Economic Paleontologists and Mineralogists Special Publication 42, p. 329–353, doi:10.2110 /pec.88.01.0329.

Greenlee, S.M., Devlin, W.J., Miller, K.G., Mountain, G.S., and Flemings, P.B., 1992, Integrated sequence stratigraphy of Neogene deposits, New Jersey continental shelf and slope: Comparison with the Exxon model: Geological Society of America Bulletin, v. 104, p. 1403–1411, doi:10.1130/0016 7606(1992)104<1403: ISSOND>2.3 .CO;2.

Jones, E.J.W., 1999, Marine geophysics. John Wiley and Sons Ltd: Chichester. ISBN 0-471-98694-1, 466 pp.

Karakaya, S., 2012, Quantitative seismic attribute analysis using artificial neural networks and seismic strati- graphic interpretation of lower to middle Miocene sediments offshore New Jersey [M.S. thesis]: New Brunswick, New Jersey, Rutgers University, 190 p.

Karakaya, S., Miller, K.G., Mountain, G.S., Monteverde, D.E., and Browning, J.V., Eccentricity control of middle Miocene sequences of the middle continental shelf off New Jersey, Geosphere, in review.

Kearey, P., Brooks, M. and Hill, I., 2002, An introduction to geophysical exploration (3rd edition). Blackwell Scientific, Oxford.

Kearey, Philip, Michael Brooks, and Ian Hill. An introduction to geophysical exploration, 2009.

Lanci, L., Kent, D.V., and Miller, K.G., 2002, Detection of Late Cretaceous and Cenozoic sequence boundaries on the Atlantic coastal plain using core log integration of magnetic susceptibility and natural gamma ray measurements at Ancora, New Jersey, Journal of Geophysical Research, v. 107, no. (B10), 2216, doi:10.1029/2000JB000026

Miller, K.G., and Mountain, G.S., 1994, Global sea-level change and the New Jersey margin, in Mountain, G.S., Miller, K.G., and Blum, P., et al., Proceedings of the Ocean Drilling Program, Initial Reports 150: College Station, TX, (Ocean Drilling Program), p. 11-20.

Miller, K.G., Mountain, G.S., Leg 150 Shipboard Party, and Members of the New Jersey Coastal Plain Drilling Project, 1996, Drilling and dating New Jersey Oligocene–

Miocene sequences: Ice volume, global sea level, and Exxon records: Science, v. 271, p. 1092–1095, doi:10.1126/science.271.5252.1092.

Miller, K.G., Mountain, G.S., Browning, J.V., Kominz, M., Sugarman, P.J., Christie-Blick, N., Katz, M.E., and Wright, J.D., 1998, Cenozoic global sea-level, sequences, and the New Jersey transect: Results from coastal plain and slope drilling: Reviews of Geophysics, v. 36, p. 569–601, doi:10.1029/98RG01624.

Miller, K.G., Kominz, M.A., Browning, J.V., Wright, J.D., Mountain, G.S., Katz, M.E., Sugarman, P.J., Cramer, B.S., Christie-Blick, N., and Pekar, S.F., 2005, The Phanerozoic record of global sea-level change: Science, v. 312, p. 1293-1298.

Miller, K.G., Mountain, G.S., Browning, J.V., Katz, M.E., Monteverde, D., Sugarman, P.J., Ando, H., Bassetti, M.A., Bjerrum, C.J., Hodgson, D., Hesselbo, S., Karakaya, S., Proust, J.N., and Rabineau, M., 2013, Testing sequence stratigraphic models by drilling Miocene foresets on the New Jersey shallow shelf, Geosphere, v. 9, no. 5; p. 1–21; doi:10.1130/GES00884.1.

Mitchum, R.M., Jr., Vail, P.R., and Thompson, S., III, 1977, Seismic stratigraphy and global changes of sea level; Part 2, The depositional sequence as a basic unit for stratigraphic analysis, in Payton, C.E., ed., Seismic stratigraphy; applications to hydrocarbon exploration: American Association of Petroleum Geologists Memoir 26, p. 53–62.

Monteverde, D.H., 2008, Sequence stratigraphic analysis of early and middle Miocene shelf progradation along the New Jersey margin [Ph.D. thesis]: New Brunswick, Rutgers University, 247 p.

Monteverde, D.H., Mountain, G.S., and Miller, K.G., 2008, Early Miocene sequence development across the New Jersey margin: Basin Research, v. 20, p. 249–267, doi: 10.1111/j.1365-2117.2008.00351.x.

Mountain, G.S., Burger, R.L., Delius, H., Fulthorpe, C.S., Austin, J.A., Goldberg, D.S., Steckler, M.S., McHugh, C.M., Miller, K.G., Monteverde, D.H., Orange, D.L., and Pratson, L.F., 2007, The long-term stratigraphic record on continental margins, in Nittrouer, C.A., et al., eds., Continental margin sedimentation: From sediment transport to sequence stratigraphy: International Association of Sedimentologists Special Publication 37, p. 381–458.

Mountain, G.S., Proust, J.N., McInroy, D., and Cotterill, C., and the Expedition 313 Scientists, 2010, Proceedings of the International Ocean Drilling Program, Expedition 313: Tokyo, Integrated Ocean Drilling Program Management International, Inc., doi:10.2204/iodp.proc .313.2010.

Neal, J., and Abreu, V., 2009, Sequence stratigraphy hierarchy and the accommodation succession method: Geology, v. 37, p. 779–782, doi:10.1130/G25722A.1.

Nystuen, J.P., 1998, History and development of sequence stratigraphy, in Gradstein,

F.M., Sandvik, K.O., and Milton, N.J., (eds), Sequence stratigraphy–concepts and applications, Norwegian Petroleum Society, Special Publication 8, p.31-116.

Plint, A.G., and Nummedal, D., 2000, The falling stage systems tract: Recognition and importance in sequence stratigraphic analysis, in Hunt, D., and Gawthorpe, R.L., eds., Sedimentary responses to forced regression: Geological Society of London Special Publication 172, p. 1–17, doi:10.1144/GSL.SP.2000.172.01.01.

Poag, C.W., 1984, Neogene stratigraphy of the submerged U.S. Atlantic margin: in Armentrout, J.M., and W.H. Abbott, (eds.), Studies in North American Cenozoic correlations; Palaeogeography, Palaeoclimatology, Palaeoecology, vol. 47, no. 1-2, p. 103-127.

Posamentier, H.W., and Vail, P.R., 1988, Eustatic controls on clastic deposition II—Sequence and systems tract models, in Wilgus, C.K., et al., eds., Sea level changes: An integrated approach: Society of Economic Paleontologists and Mineralogists Special Publication 42, p. 125–154, doi:10.2110/pec.88.01.0125.

Poulsen, C.J., Flemings, P.B., Robinson, R.A.J., and Metzger, J.M., 1998, Three-dimensional stratigraphic evolution of the Miocene Baltimore Canyon region: Implications for eustatic interpretations and the systems tract model: Geological Society of America Bulletin, v. 110, p. 1105–1122, doi:10.1130/0016-7606 (1998)110<1105:TDSEOT>2.3.CO;2.

Rider, M.H., 1990, Gamma-ray log shape used as a facies indicator: critical analysis of an oversimplified methodology: in Hurst, A., Lovell, M.A., and Morton, A.C., editors, Geological applications of wireline logs, Geological Society Special Publications 48, p.27-37.

Sheriff, R. E., & Geldart, L. P. (1983). Exploration seismology Vol. 2: Data-processing and interpretation. Cambridge, Great Britain: Cambridge University Press, 221p.

Vail, P. R., Todd R. G., and Sangree J. B., 1977, Seismic stratigraphy and global changes of sea level, part 5: chronostratigraphic significance of seismic reflections. In: Payton, C. E. (ed.). Seismic Stratigraphy-Applications to Hydrocarbon Exploration. American Association of Petroleum Geologists Memoir 26, p. 99 – 116.

Vail, P.R., 1987, Seismic stratigraphy interpretation using sequence stratigraphy: Part 1. Seismic stratigraphy interpretation procedure, in Bally A.W., ed., Atlas of seismic stratigraphy: American Association of Petroleum Geologists Studies in Geology 27, p. 1–10.

Vail, P. R., and Wornardt Jr, W., 1991, An integrated approach to exploration and development in the 90s: well log-seismic sequence stratigraphy analysis: Transactions- Gulf Coast Association of Geological Societies, v. XLI., p. 329-249.

Van Wagoner, J.C., Mitchum, R.M., Jr., Posamentier, H.W., and Vail, P.R., 1987, Seismic stratigraphy interpretation using sequence stratigraphy: Part 2, Key definitions of sequence stratigraphy, in Bally A.W., ed., Atlas of seismic stratigraphy: American Association of Petroleum Geologists Studies in Geology 27, p. 11–14.

Van Wagoner, J.C., H.W. Posamentier, R.M. Mitchum, P.R. Vail, J.F. Sarg, T.S. Loutit, and J. Hardenbol, 1988, An overview of the fundamentals of sequence stratigraphy and key definitions. In C.K. Wilgus, B.S. Hastings, C.G.St.C. Kendall, H.W. Posamentier, C.A. Ross, J.C. Van Wagoner, eds., Sea-level changes: an integrated approach. Society of Economic Paleontologists and Mineralogists Special Publication No. 42, p. 39-45.

Westerhold, T., Bickert, T., Röhl, U., 2005. Middle to late Miocene oxygen isotope stratigraphy of ODP site 1085 (SE Atlantic): new constraints on Miocene climate variability and sea-level fluctuations. Palaeogeography Palaeoclimatology Palaeoecology 217, 205–222.

Widess, M. B. (1973). How thin is a thin bed?. Geophysics, 38(6), 1176-1180.

Yılmaz, O. (1987). Seismic data processing. Investigations in Geophysics, 2, 526.